Summer 2021

Analysis of the primary volatile compositions in the Oort cloud and Jupiter-family comets towards the goal of understanding their origin and diversity

Mohammad Saki

Department: Physics

ANALYSIS OF THE PRIMARY VOLATILE COMPOSITIONS IN THE OORT CLOUD AND JUPITER-FAMILY COMETS TOWARDS THE GOAL OF UNDERSTANDING THEIR ORIGIN AND DIVERSITY

by

MOHAMMAD SAKI

A DISSERTATION

Presented to the Graduate Faculty of the

MISSOURI UNIVERSITY OF SCIENCE AND TECHNOLOGY

and

UNIVERSITY OF MISSOURI – ST. LOUIS

In Partial Fulfillment of the Requirements for the Degree

DOCTOR OF PHILOSOPHY

in

PHYSICS

2021

Approved by:

Erika Gibb, Advisor
Shun Saito, Co-Advisor
Boncho Bonev
Bruce Wilking
Alexei Yamilov

PUBLICATION DISSERTATION OPTION

This dissertation consists of the following two articles, formatted in the style used by the Missouri University of Science and Technology:

Paper I: Pages 19-52 have been published in the Astronomical Journal (Saki et al., 2020a).

Paper II: Pages 53-90 have been accepted for publication in the Astronomical Journal (Saki et al., 2021)

ABSTRACT

Knowledge of the initial conditions present in the early solar nebula is required to understand the evolution and its current volatile content. Comets were some of the first objects to accrete in the solar nebula. They are among the most pristine (primitive) remnants of the solar system formation, and their present-day volatile composition likely reflects the composition and conditions where (and when) they formed. Therefore, they are fossils of the solar system formation. High-resolution near-infrared spectroscopy is a valuable tool for sampling the parent volatile (i.e., ices subliming directly from the nucleus) composition of comets via analysis of fluorescence emission in cometary comae.

An overall goal of comet volatile composition studies is determining whether comets can be classified based on their volatile content and what this reveals about the history of the early solar system. Early work produced encouraging results, but recent work has left questions regarding whether a compositional taxonomy based on near-infrared measurements is feasible. These include questions such as: Are observed systematic compositional differences between Jupiter-family comets and Oort cloud comets the result of evolutionary effects or reflective of formative conditions? Is temporal variability in coma composition a common phenomenon, and if so, how can present-day measurements be related to natal solar system conditions? Can we place comet volatile compositions in a meaningful context? In this work we examine these questions in the context of near-infrared measurements of Oort cloud comets and Jupiter-family comets, as well as a comparison between our results and extensive results from the Rosetta mission to comet 67P/Churyumov–Gerasimenko.

ACKNOWLEDGMENTS

I would like to sincerely thank my research advisor, Dr. Erika Gibb for teaching me everything: from how to write observing proposals, conduct the observations, reduce near-infrared spectroscopic data, interpret and visualize the results, to how to actively be involved in research and give back to the scientific community. Dr. Gibb, I truly enjoyed every single day of working under your supervision and am looking forward to use this amazing experience as a foundation for my future research path. I would like to thank my my friend and research mate Dr. Nathan Roth for his incredible help in this amazing journey. I also would like to thank my committee members, Drs. Shan Saito, Boncho Bonev, Bruce Wilking, and Alexei Yamilov, for their service and contributions to this work. Working among an outstanding team of comet scientists was a dream come true for me. I would like to sincerely thank Drs. Boncho Bonev, Michael DiSanti, Neil Dello Russo, Ronald Vervack Jr., Hideyo Kawakita, Adam McKay and Younas Khan. You have each taught me many things which contributed to all aspects of my research. I hope we continue to work together after the publication of this dissertation. I would like to thank the professors of the Department of Physics & Astronomy at UMSL, as well as from Missouri S&T, for exceptionally taught graduate courses that I thoroughly enjoyed. My work has been generously supported by National Science Foundation (Grants: AST-1616306, AST-161544, AST-200939, AST-2009910). Finally, I would like to thank my family. My dear wife, Shiva Azizam, who has truly supported me with everything and through all of our ups and downs. My parents Baba Saeid and Maman Soodabeh for their amazing supports, and my close friends Joe & Lynn and Raymond & Edit. I can never thank you enough.

TABLE OF CONTENTS

LIST OF ILLUSTRATIONS

SECTION Page

SECTION

LIST OF TABLES

NOMENCLATURE

Symbol	Description
R_h	Heliocentric Distance
Δ	Geocentric Distance
Δ_{dot}	Geocentric Velocity
β	Phase Angle
Q	Production Rate (molecules s^{-1})

1. INTRODUCTION

1.1. BRIEF HISTORY OF THE SOLAR SYSTEM FORMATION

Our solar system originated as a dense clump in a giant molecular cloud. These clouds are enourmous (~20-200 parsec), such that thousands of solar systems can form out of them. They eventually undergo gravitational collapse. A star is born at the center of a dense clump when the local density becomes sufficiently high enough and the temperature raised to a certain level to ignite thermonuclear fusion, while the outer materials have flatten out into an accretion disk of gas and dust surrounding the central young star. All of the planets, asteroids, moons, and comets of a stellar system will accrete from this "protoplanetary disk" of gas and dust over the next several million years. The protoplanetary disk that formed our solar system is known as the solar (or protosolar) nebula.

Understanding the sequence of events and processes in the history and evolution of the solar system, from the formation of the planets to the source(s) of water and organic matter on Earth, requires knowledge of the initial composition and conditions present in the solar nebula. Comets are some of the smallest (few km in size) objects in the solar system and were among the first objects to accrete out of the solar nebula. Owing to their small size, comets lack a known mechanism for internal self-heating; thus, it is likely that the interior compositions of comets have not been significantly modified and should reflect the composition and the conditions where (and when) they formed.

1.2. COMETS: PRESENT-DAY RESERVOIRS AND ORIGINS

Comets that become available for studying can be placed into one of two dynamical groups: 1- Short period comets, such as the Jupiter-family comets (JFCs) and Encke type comets, which originate from the scattered Kuiper belt and have small orbital inclinations, and 2- Nearly isotropic Oort cloud comets (OCCs), which originate from the Oort cloud (outer reaches of the solar system) with random orbital inclinations.

The dynamical reservoir of a given comet can be identified using the Tisserand parameter, T_J, which measures Jupiter's gravitational influence on a comet's orbital path. Comets with $T_J < 2$ originate from the Oort cloud, a spherical distribution of comets in the outer solar system extending up to tens of thousands of Astronomical Units (AU) from the sun and possibly all the way to the next solar system. This includes dynamically new comets which are entering the inner solar system for the first time (e.g., comet ISON). Oort cloud comets have long orbital periods (hundreds to hundreds of thousands of years, such as comet ER61 with period of ~7600 years), and are often ejected from the solar system by Jupiter following a passage through the inner solar system. Comets with $2 < T_J < 3$ are the JFCs, which reside in the Kuiper belt beyond the orbit of Neptune (30-50 AU). These comets have considerably shorter periods (several to tens of years) and thus offer the opportunity to study and learn about their composition more than once while we are alive. We can also study the effects of multiple close perihelion passages on their volatile composition. Comets with $T_J > 3$ are subdivided into two groups depending on the semi-major axis of their orbit: comets with a semi-major axis interior to that of Jupiter are Encke-type comets, whereas those with a semi-major axis exterior to that of Jupiter and interior to Neptune are Chiron-type comets. The term "ecliptic comets" is also used

interchangeably to describe the JFCs, Encke, and Chiron-type comets, as they lie in or near the ecliptic plane of the solar system.

Historically, OCCs were thought to form at heliocentric distances (R_h) between 5-30 AU from the Sun before getting scattered to their current reservior (Oort cloud), whereas ecliptic comets formed separately at even larger heliocentric distances. IR coma studies indicate that Jupiter-family comets (JFCs; originate from the Kuiper belt and have short orbital periods) are in general depleted relative to Oort cloud comets (OCCs; originate from the Oort cloud and have long orbital periods) in the hypervolatiles CO and CH_4, which may reflect the effects of repeated close perihelion passages on their volatile content (Roth et al., 2020; Saki et al., 2020b; Dello Russo et al., 2016a). On the other hand, large optical surveys of product species found no correlation in depleted chemistry and dynamical age in JFCs, suggesting that compositional differences may instead be primordial and indicative of differences in formation histories for Jupiter-family comets compared to Oort cloud comets (A'Hearn et al., 1995). However, the detection of crystalline silicates in some comets, e.g., 1P/Halley (Bregman et al., 1987), 9P/Tempel 1 (via remote observations of material ejected during the Deep Impact mission (Harker et al., 2005)), and 81P/Wild 2 (in grains returned by the Stardust mission (Zolensky et al., 2006)) implies that material in their nuclei was processed at small R_h and mixed over ranges of distances in the solar nebula. Additionally, dynamical modeling (e.g., Gomes et al., 2005; Levison et al., 2011; Morbidelli et al., 2005) suggests that scattering processes and large-scale mixing of materials in the early solar nebula have complicated the distinction between comet-forming regions (Bockelée-Morvan et al., 2000, 2016; Gomes et al., 2005; Zolensky et al., 2006; Dello Russo et al., 2016b). Therefore, both the Oort cloud and Kuiper belt could contain

comets that represent varying (or, at the other extreme, largely overlapping) formation regions in the solar nebula. The Rosetta mission to comet 67P/Churyumov–Gerasimenko (hereafter 67P) revealed a heterogeneous nucleus, adding more complexity to these scenarios (Rickman et al., 2015; Le Roy et al., 2015; A'Hearn 2017). However, this evidence suggests that comet formation was instead a more "spatially mixed" process.

Since their emplacement in the deep freeze of the outer solar system (either the Oort cloud or the Kuiper belt), the interior compositions of cometary nuclei have remained (at least to a large degree) unprocessed. Most processes that can change the properties of comet nuclei only affect a thin layer (a few meters deep) from the surface, which is thought to be excavated over the course of a perihelion passage into the inner solar system (Stern et al., 2003; Le Roy et al., 2015; Gronoff et al., 2020; Saki et al., 2020a). Some comets exhibit a sudden eruption of materials, referred to as an outburst, close to their perihelion passage. Outbursts are known to start with the sudden appearance and steep brightening of an unresolved plume of material and are often described by brightness magnitude (Sekanina 2010, 2017). Comets that outburst represent additional opportunities to probe the likely more pristine material below a comet's topmost surface layers.

1.3. COMETS TAXONOMIES

To fully characterize comet population, knowledge of present-day dynamical reservoir is required. However, given the complex scattering processes which placed comets in their current orbits and the "spatially mixed" process of comet formation, the volatile compositions of cometary nuclei may represent widely varying formation regions in the protosolar nebula. Thus, a taxonomy based on the volatile composition among the

comet populations is required for a more meaningful understanding of comets formation regions and conditions in the solar nebula. Certain primary volatiles — C_2H_2, CO, CH_4, and OCS — are under-represented in studies of comets as a whole, thus making this task even more challenging (see Saki et al., 2020a; Dello Russo et al., 2016a for more details).

1.3.1. Compositional Taxonomies Measured at the Optical and Radio Wavelengths. Comets have been observed and characterized at optical wavelengths for over thirty years, leading to large databases of photometric and spectroscopic observations and the development of a taxonomy based on composition (e.g., see A'Hearn et al., 1995; Cochran et al., 2012 and references therein). Fragment (daughter) species (e.g., CN, C_2, C_3, CS, NH, OH) formed by the photodissociation of bigger molecules in the coma. These species have emission features at optical wavelengths. Based on the fragment species, comets are classified as either "normal" or "carbon-chain depleted", with several sub-classes of the depleted type (seven distinct taxonomic subgroupings; Cochran et al., 2015; Schleicher and Bair, 2014). However, relating mixing ratios of fragment species to those of their parents is a difficult task, owing to possibly multiple parent volatiles for each fragment.

Some primary volatiles, including complex molecules such as ethylene glycol ($C_2H_6O_2$), emit in the radio wavelength via rotational transitions. As of the time of writing this dissertation, there is no agreement on the existence of comet taxonomic classes based on their composition measured at radio wavelengths (Crovisier et al., 2009; Mumma and Charnley, 2011).

1.3.2. Compositional Taxonomies as Measured at the Near-Infrared Wavelength. Parent (primary) volatiles (i.e., ices subliming directly from the nucleus) emit via ro-vibrational transitions at near-infrared wavelengths. Using modern near-infrared spectrographs such as CSHELL and iSHELL at the 3 m NASA Infrared Telescope Facility and NIRSPEC at the 10 m W. M. Keck Observatory, fundamental transitions of OCS, CO, H_2CO, CH_3OH, C_2H_6, CH_4, HCN, C_2H_2, and NH_3, along with transitions of H_2O can be sampled from the ground in sufficiently bright comets. The outputs of these studies include best-fit rotational temperatures, molecular production rates, molecular abundances ("mixing ratios") relative to both H_2O (the dominant ice in most comets studied) and C_2H_6, and 2D maps of molecular column density along the slit, known as emission spatial distributions or profiles.

Figure 1.1 shows spatial profiles of emissions for many volatiles and dust grains in OCC C/2015 ER61 (PanSTARRS). These spatial profiles show that the emission intensity of volatiles peaks at the position of the nucleus and falls off with increasing nucleocentric distance (ρ) as $1/\rho$, consistent with ices subliming directly from the nucleus with constant outflow speed. This suggests that these volatiles are "primary". Thus, the hypothesis in our near-infrared measurements of comets is that once sublimation of H_2O (the most abundant ice in most comets) is fully activated, the mixing ratios of primary volatiles in comet comae should remain relatively constant (assuming compositional homogeneity) and we can refer to those as the native compositions of the nucleus. Comets observed in the near-infrared to date suggest that this is true in general, although some primary volatiles (NH_3, H_2CO, and C_2H_2) and fragment species (CN and NH_2) show a trend towards enhanced production at

heliocentric distance (R_h) < 0.8 AU (possibly due to release from grains; e.g., see Dello Russo et al., 2016a).

It is a complex task to classify comets based on their primary volatiles in the current sample of the comet population. As of the time of writing this dissertation, there have been about 40 comets sampled in the near-infrared (~25 OCCs and ~15 JFCs). Early near-infrared spectroscopic studies of the primary volatile compositions of comets 1P/Halley (Mumma et al., 1986), C/1996 B2 (Hyakutake) (Dello Russo et al., 2002b; DiSanti et al., 2003; Magee-Sauer et al., 2002b; Mumma et al., 1996) and C/1995 O1 (Hale-Bopp) (Dello Russo et al., 2001, 2000; DiSanti et al., 2001; Magee-Sauer et al., 1999) revealed that they were chemically similar objects (Mumma et al., 2003). Subsequent observations of comet D/1999 S4 (LINEAR) prior to its complete disruption (Mumma et al., 2001) and of the split comet 73P/Schwassman-Wachmann 3B (Dello Russo et al., 2007; Villanueva et al., 2006) showed two comets that were highly depleted in virtually all trace primary volatiles relative to water. At the other extreme, comets C/2001 A2 (LINEAR) (Magee-Sauer et al., 2008) and later C/2007 W1 (Boattini) (Villanueva et al., 2011a) were enriched in the sampled trace primary volatiles. These results formed the basis for a proposed three-tiered taxonomy based on primary volatile abundance ratios, with comets classified as organics-enriched, organics-normal, or organics-depleted (e.g., Mumma and Charnley (2011) and references therein).

However, recent work has suggested that the three-fold classification scheme is incomplete and comet taxonomy in the near-infrared is probably more complex (see Dello Russo et al., 2016a for a recent review of comet taxonomies based on near-infrared spectroscopy). For example, the primary volatile compositions of comets 8P/Tuttle,

C/2007 N3 (Lulin), and 2P/Encke (Bonev et al., 2008b; Gibb et al., 2012; Radeva et al., 2013; Roth et al., 2018) show no systematic enrichment, depletion, or similarity to the mean value. These three comets all had high CH_3OH abundances while being depleted in certain other molecules, for example C_2H_2, and "normal" in others, such as C_2H_6. Long period OCC C/2015 ER61 (a comet included in this work; see Section 3) was also enriched in CH_3OH, normal in OCS, and close to depleted in the rest of the volatiles. This suggests that the chemical diversity among comets is more complex than the simple organics-enriched, organics-normal, and organics-depleted framework.

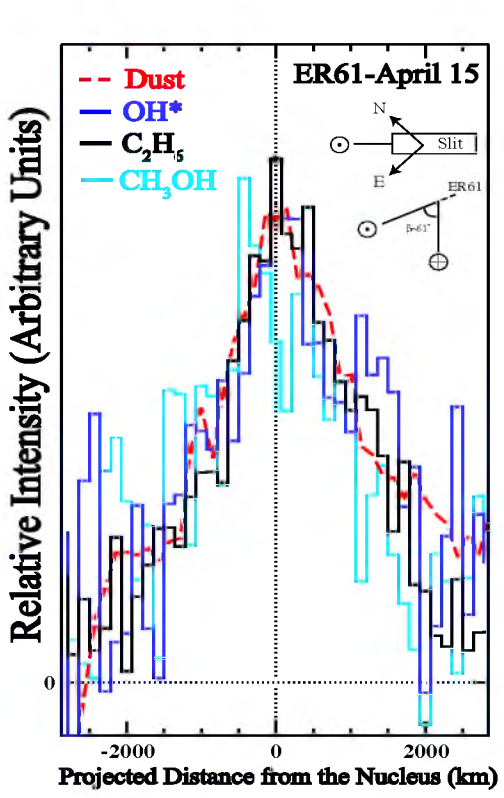

Figure 1.1 Spatial profile of multiple volatiles simultaneously measured with dust in comet ER61 on UT 2017 April 15. The slit was oriented along the projected Sun-comet line (position angle ~ 252°), with the Sun-facing direction to the left as indicated. The Sun-comet-Earth angle (phase angle, β) was ~ 61° on April 15.

1.4. NATAL CONDITIONS, HETEROGENEITY AND VARIABILITY IN COMETS

Considerable compositional diversity exists in the comet population at all wavelengths. Jupiter-family comets are on average depleted in certain primary volatiles (e.g., CH_4, CO) compared with Oort cloud comets. If these compositional differences are truly indicative of natal conditions (natal to comet formation regions), they would imply that JFCs formed in a compositionally distinct region in the protosolar nebula compared with OCCs.

On the other hand, these compositional differences could be due to multiple close encounters of these comets with the Sun, which could affect their volatile composition. Most processes that might alter the properties of the nucleus are expected to affect a thin layer near the surface (few meters deep) over the course of a typical perihelion passage. Short period (ecliptic) comets experiencing many perihelion passages into the inner parts of solar system may suffer more processing compared to dynamically young or new Oort cloud comets. In order to draw conclusions, place the results of present-day observations into a meaningful context, and interpret the clues of our solar system formation, we have to understand potential evolutionary effects, including any systematic differences between short period comets and OCCs. There are few facilities which are capable of performing these types of near-infrared measurements and acquiring observing time is difficult. Moreover near-infrared studies of primary volatile composition have largely been "snapshots" (observations over a single apparition and often near ~ 1 AU). Thus, overcoming the observational biases are important in interpreting the results of volatile compositional studies.

Owing to the lack of spectral coverage, sensitivity and observational limitations, certain primary volatiles such as OCS, CO, CH_4, and C_2H_2 are underrepresented in studies of comets as a whole. Fundamental ro-vibrational bands of CH_4 and CO, are heavily populated in Earth's atmosphere, resulting in highly opaque telluric counterparts. Thus, detection or stringent upper limits of these volatiles require that comets have sufficiently large geocentric velocities (Δ_{dot}) to Doppler-shift corresponding cometary emissions away from their highly opaque telluric counterparts to a region of adequate atmospheric transmittance. JFCs are generally dim, and most observations take place near their closest approach to Earth which is where they have the smallest Δ_{dot}. This precludes the measurements of CO and CH_4. This has resulted in a significant paucity of detections of CO and CH_4 in ecliptic comets. Improving the number of secure measurements of these species especially carbonyl sulfide (OCS), which is severely under-represented in comet studies, is one of the primary goals of this work (see Sections 2-4 for more details).

Some volatiles show asymmetries around perihelion. For instance, the Rosetta mission to comet 67P/C-G, found that mixing ratios of CO and CO_2 in the coma varied due to seasonal effects on the nucleus (Le Roy et al., 2015; Hässig et al., 2015). In these seasonal effects, different portions of the nucleus receive seasonal illumination during different portions of an orbit due to the comet's orientation with respect to the Sun, leading to distinct sources on the nucleus dominating outgassing at different times. In OCC C/2009 P1 (Garradd), H_2O production rates traced the predicted heliocentric dependence, rising and then falling near perihelion. However, CO production increased monotonically throughout the apparition, continuing to rise long after perihelion, perhaps due to seasonal effects on the nucleus.

Some comets have shown variation in volatile mixing ratios on smaller time scales due to diurnal effects (over the course of the rotation of the nucleus, see Bockelée-Morvan et al., 2016; Fink et al., 2016; Luspay-Kuti et al., 2015). For instance, non-uniform mixing ratios of CO/H_2O were observed in OCC C/2009 P1 (Garradd) by both ground-based studies (McKay et al., 2015) and spaced-based studies from the High-Resolution Instrument Infrared Spectrometer aboard the Deep Impact Flyby spacecraft (Feaga et al., 2014). Similar long- and short-term variability in primary volatiles abundances and production rates in OCC C/2015 ER61 (PanSTARRS) were observed during its 2017 apparition (perhaps due to diurnal and seasonal effects).

Some primary volatiles such as NH_3, H_2CO, C_2H_2 display enhanced production at small R_h ($< \sim 0.8$ AU), perhaps due to grain sources (Dello Russo et al., 2016a). This emphasizes the need of primary volatile measurements over a large range of R_h. Determining to what extent these phenomena occur in the comet population is crucial to interpreting the results of volatile composition studies and placing them in a meaningful context.

1.5. A BRIEF OVERVIEW OF OBSERVATIONS AND DATA REDUCTION

This section will provide an overview of the techniques used for the near-infrared spectroscopic observations and procedures used for data reduction and analysis reported in this work (for more details see Section 3 in Saki et al., 2020b, 2021).

1.5.1. Observation. To address these pressing matters in cometary science, this study includes near-infrared spectroscopic measurements of the primary volatile compositions of four comets: the dynamically young, long period OCC C/2015 ER61

(PanSTARRS), the OCC C/2002 T7 (LINEAR), the JFCs 21P/Giacobini-Zinner and 46P/Wirtanen. These comets were measured using the state-of-the-art near-infrared spectrographs at ground-based observatories such as NASA Infrared Telescope Facility (IRTF). Comets presented in this work were observed and their spectra were acquired with the newly commissioned iSHELL spectrograph (Rayner et al., 2012, 2016) and CSHELL (the predecessor to iSHELL) at the 3m NASA Infrared Telescope Facility (IRTF). A brief overview of our observational techniques and data reduction precedures is given here, and a comprehensive description is provided in Section 2 and 3 in this dissertation (see Section 3 in Saki et al., 2020, 2021).

Observations were performed using a standard ABBA nod pattern, with A and B beams symmetrically placed about the midpoint of the slit and separated by half its length (on-chip nodding). In the case of 21P/Giacobini-Zinner, some of the data were acquired using off-chip nodding, in which the A beam is placed at the midpoint of the slit whereas the B beam is placed perpendicular to the slit to the blank sky. Combining spectra of the nodded beams as A-B-B+A cancelled emissions from thermal background, instrumental biases, and "sky" emission (lines and continuum). The data were dark-subtracted, flat-fielded, and cleaned of cosmic ray hits and "hot" (high dark current) pixels. Flux calibration was performed using appropriately placed bright IR flux standards on each date.

1.5.2. Data Reduction. The data reduction procedures that we used are described extensively in the refereed literature (Dello Russo et al., 1998; Bonev, 2005; DiSanti et al., 2006, 2014; Radeva et al., 2010; Villanueva et al., 2009). Their application to unique aspects of iSHELL spectra is detailed in §3.2 of DiSanti et al. (2017). Contributions from continuum and gaseous emissions were determined in the comet spectra as previously

described (e.g. DiSanti et al., 2016). This procedure is illustrated in Figure 1.2. The fully resolved transmittance function was convolved to the resolving power of the data ($\lambda/\Delta\lambda$ ~25,000 for CSHELL and ~40,000 for iSHELL) and scaled to the level of the comet continuum. The modeled continuum was then subtracted to isolate cometary emission lines.

Nucleocentric (or "nucleus-centered") production rates (Q_{NC}) were determined using a well-documented formalism (Bonev, 2005; Dello Russo et al., 1998; DiSanti et al., 2001; Villanueva et al., 2011a); see Section 3.2.2 of DiSanti et al., (2016) for further details. The nucleocentric production rates were multiplied by an appropriate growth factor (GF), which was determined using the well-established Q-curve methodology (e.g. Dello Russo et al., 1998; Bonev (2005); DiSanti et al., 2001; Gibb et al., 2012) to establish a total (or global) production rate, Q. This GF corrects for atmospheric seeing, which suppresses signals along lines of sight passing close to the nucleus due to the use of a narrow slit, as well as potential drift of the comet during an exposure sequence.

1.5.3. Molecular Fluorescence Analysis. Synthetic models of fluorescence emission for each targeted species were compared to observed line intensities, after correcting each modeled line intensity (g-factor) for the monochromatic atmospheric transmittance at its Doppler-shifted wavelength (according to the geocentric velocity, Δ_{dot}, of the comet at the time of the observations). The g-factors used in synthetic fluorescence emission models in this study were generated with quantum mechanical models developed for each molecule. These models include CH_4 (Gibb et al., 2003), C_2H_6 (Villanueva et al., 2011b), H_2O (Villanueva et al., 2012b), CH_3OH (DiSanti et al., 2013; Villanueva et al., 2012a), HCN (Lippi et al., 2013; Villanueva et al., 2011a), H_2CO (DiSanti et al., 2006),

OH* (Bonev et al., 2006), C_2H_2 (Villanueva et al., 2011a), CO (Paganini et al., 2013), and NH_3 (Villanueva et al., 2013).

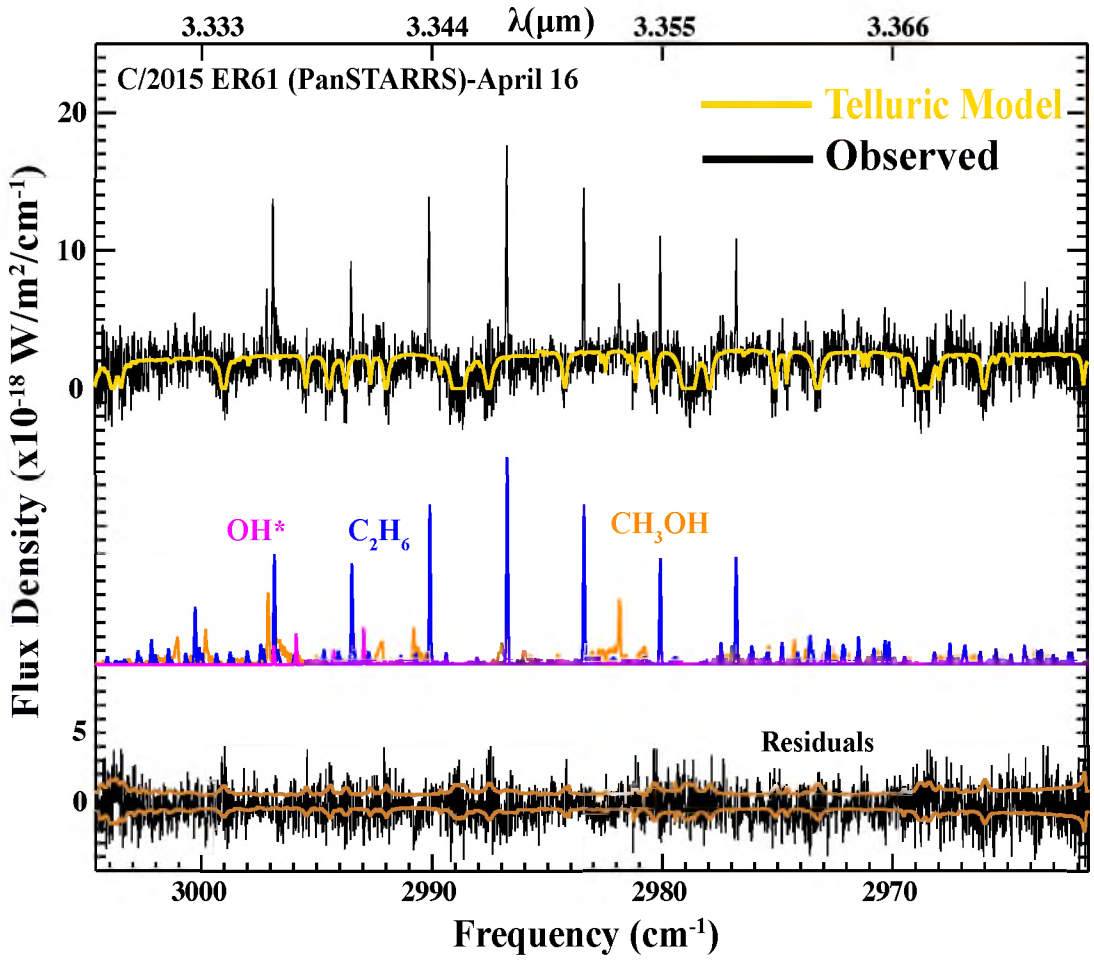

Figure 1.2. Fluorescence emission of OH*, C_2H_6, and CH_3OH in comet ER61 on UT 2017 April 16. The yellow trace overplotted on the uppermost cometary spectra is the telluric absorption model (convolved to the instrumental resolution). Individual fluorescence emission models (color-coded by species for clarity) are plotted below. At the bottom of the panel is the residual spectrum (after subtracting the telluric absorption model and all relevant fluorescent emission models) with the 1σ uncertainty envelope overplotted in bronze.

A line by line analysis and a Levenberg-Marquardt nonlinear minimization technique (Villanueva et al., 2008) was used to fit fluorescence emission from all species simultaneously in each echelle order, allowing for high-precision results, even in spectrally crowded regions containing many spectral lines within a single instrumental resolution element. Production rates for each sampled species were determined from the appropriate fluorescence model at the rotational temperature of each molecule.

1.5.4. Determination of Rotational Temperature. Rotational temperatures were determined using correlation and excitation analyses as described in Bonev (2005); Bonev et al., (2008a); DiSanti et al., (2006); Villanueva et al., (2008). In general, well-constrained rotational temperatures can be determined for individual species with intrinsically bright lines and for which a broad range of excitation energies is sampled. These conditions were satisfied for H_2O in at least one setting in each data set.

1.6. UNCERTAINTIES IN MEASUREMENTS.

This section has been adopted from Bonev Ph.D. dissertation (Bonev, 2005) and Roth Ph.D. dissertation (Roth, 2019) and will provide the main sources of uncertainties for quantities measured or retrieved in this work (please see Roth, 2019 for more details). These quantities include molecular production rates (determined as the weighted mean of individual production rates for each measured line of a given species; Q_{line}), rotational temperatures (determined as the temperature which produces a zero-slope best-fit line when relating F/g vs. E_{up} for each line of a given species), and growth factors (see Roth, 2019 and Bonev, 2005 for details). The reduction algorithms employed in this work calculate two sources of uncertainty for each quantity: stochastic error and standard error.

The stochastic error is a measure of the signal-to-noise ratio (SNR) of each of the lines. For all but the brightest comets, the signal from emission lines in the coma is weaker than the background signal introduced by the sky, including continuum and emission lines from telluric species – hence the dominant source of noise in the measured flux of each cometary line originates from thermal background noise (Bonev, 2005). The standard error is a measure of how quantities derived from the lines (e.g., Qi, Fi/gi) are spread about the weighted mean or about the best-fit line. In contrast to the stochastic error, the standard error is indicative of uncertainties introduced by modeled quantities (such as the g-factors): for instance, the flux of a C_2H_6 line may be measured with very high signal-to-noise, yet the production rate derived from the line may be in poor agreement with those derived from other C_2H_6 lines if its g-factor is poorly modeled.

In the case of global production rates and growth factors, these uncertainties are the stochastic and standard errors in the weighted means used to calculate each quantity. In the case of rotational temperatures derived with excitation analysis, the uncertainties are the stochastic and standard errors in a linear best fit. It is important to note that in most cases, the standard error is found to dominate over the stochastic error when using the instruments, models, and reduction algorithms employed in this work. The followings will examine how these quantities are incorporated into: (a) Uncertainties in molecular production rates introduced by uncertainties in rotational temperatures, uncertainties in growth factors, uncertainties in the telluric absorption model, and uncertainties in flux calibration. (b) Uncertainties in the abundance ratios, including for molecules whose transitions are in separate instrumental settings (i.e., abundance ratios between molecules that are not observed simultaneously).

1.6.1. Uncertainties in Molecular Production Rate. The molecular production rates reported in this dissertation are the weighted averages of the production rates calculated for each line of an individual species (e.g., Disanti et al., 2005; Dello Russo et al., 1998; Bonev, 2005). The uncertainty associated with production rates for individual lines, Q_i, is the stochastic error. When calculating the overall production rate using the weighted average of these quantities, both the stochastic error and the standard error of the average are calculated, and the larger of the two is taken to be the overall uncertainty. However, calculating this average production rate requires additional quantities, including the rotational temperature, the transmittance predicted by the telluric absorption model at the frequency of each line, the growth factor of each molecule, and the flux calibration determined for each spectral order.

In the case of the rotational temperature, uncertainties can be introduced in the slope of the best-fit line of F/g vs. E_{up} by uncertainties in the measured flux of each line, whether due to low signal-to-noise in the measured flux, uncertainties in modeling of the transmittance function (and hence the correction for telluric absorption) at the frequency of the line, or uncertainties in the applied flux calibration. Additional uncertainty can be introduced by the modeled g-factor, or the predicted intensity of the lines. Each of these will contribute to a greater spread in the derived F/g of individual lines about the best-fit line and are accounted for by the standard error calculation. In general, the possible spread in production rates due to uncertainty in rotational temperature is found to be well within the uncertainty limits given by the standard error of the weighted average production rates reported in this work.

In the calculation of the growth factor, uncertainties are introduced by the spread of the production rates calculated at successive intervals along the slit about the "terminal" production rate value. The production rates at each position along the slit inside the terminal region are incorporated into a weighted average, and the standard and stochastic error are calculated, with the greater being taken as the overall uncertainty. Errors in the growth factor, especially when the growth factor of H_2O is assumed for weaker trace species, are systematic: while they introduce uncertainties in the production rates, they do not affect the uncertainties in calculated mixing ratios.

Finally, uncertainty in flux calibration can introduce uncertainties in the derived production rates. Similar to the growth factor, these uncertainties are systematic within a given instrumental setting and will affect the production rates but not the derived mixing ratios. The algorithms employed in this work incorporate a 10% uncertainty due to flux calibration in the reported measurements.

1.6.2. Uncertainties in Abundance Ratios. Once the production rates have been calculated, the final task is to derive mixing ratios, or relative abundances. In this case, the standard errors of the weighted average production rates of each species are added in quadrature, which gives the uncertainty in their abundance ratio. However, for molecules whose transitions are not observed simultaneously (e.g., if the mixing ratio CH_4/H_2O was calculated using $Q(CH_4)$ from the iSHELL Lp1 setting and $Q(H_2O)$ from the M2 setting), an additional source of uncertainty is introduced due to the variable nature of the coma and the considerable amount of time required to take measurements in two separate settings (on the order of several hours). The uncertainty introduced in such measurements is estimated to be 10%, which is added to the uncertainty in the calculated mixing ratios.

PAPER

I. CARBONYL SULFIE (OCS): DETECTIONS IN COMETS C/2002 T7 (LINEAR), C/2015 ER61 (PANSTARRS), AND 21P/GIACOBINI–ZINNER AND STRINGENT UPPER-LIMITS IN 46P/WIRTANEN

ABSTRACT

Carbonyl sulfide (OCS) is one of the sulfur-bearing molecules detected in different astronomical environments, including comets. The present-day sulfur chemistry in comets may reveal much about the origin of these ices and their subsequent processing history. Cometary sulfur molecules such as H_2S, H_2CS, SO_2, SO, CS, CS_2, S_2, and NS have been detected in many comets. However, OCS, the only sulfur-bearing species with fluorescence emission lines at infrared wavelengths, is under-represented in comet volatile studies, having been reported in only six comets so far. We targeted OCS at the NASA Infrared Telescope Facility (IRTF), in comets 46P/Wirtanen, 21P/Giacobini–Zinner, and C/2015 ER61 (PanSTARRS) in 2017-2018 using the high resolution iSHELL spectrograph, and in C/2002 T7 (LINEAR) in 2004 using the heritage CSHELL spectrograph. In comet C/2015 ER61, the OCS abundance was similar to those measured in bright comets such as comets C/2012 S1 (ISON) and C/1996 B2 (Hyakutake), while in C/2002 T7 it was relatively depleted. Our OCS measurement in 21P/Giacobini–Zinner is the first definitive detection of this molecule in a Jupiter Family comet from a ground-based facility and is close to the average OCS abundance determined in comet 67P/Churyumov-Gerasimenko by the Rosetta mission. Our 3σ upper limit for comet 46P/Wirtanen is the lowest reported OCS

abundance in any comet. We present production rates and mixing ratios (with respect to H_2O) for these comets and place our results in the context of comets measured to date.

1. INTRODUCTION

Comets are volatile rich small bodies that are among the most primitive remnants of the early solar system. They were some of the first bodies that formed in the protosolar nebula in the giant planet region between 5 – 30 au (or more) from the Sun. Subsequent giant planet migration ejected them into their current dynamical reservoir of either the Oort cloud (Vokrouhlický et al., 2019) or the Kuiper belt (Nesvorný et al., 2017). As comets enter the inner solar system (heliocentric distance < 3 au) increasing solar radiation causes their ices to sublime, creating a freely expanding atmosphere known as the coma, along with a dust tail and an ion tail. The chemical composition of nucleus ices should provide insights into the initial conditions and subsequent evolution of the early solar system. Most processes that may change the properties of comet nuclei only affect a thin layer (a few meters deep) from the surface, which is excavated over the course of a perihelion passage into the inner solar system (Stern et al., 2003; Gronoff et al., 2020). Because of their small size, comets lack a known mechanism for internal self-heating; thus, it is likely that the interior compositions of comets have not been significantly modified and should reflect the composition and the conditions where (and when) they formed (Mumma and Charnley 2011; Bockelée-Morvan et al., 2004).

High resolution infrared (IR) spectroscopy is a valuable way to characterize the primary volatile composition of the nucleus through analysis of fluorescent emissions in

the coma. Coupled with protoplanetary disk models, the nucleus composition inferred from these studies may place observational constraints on the nascent disk mid-plane where comets formed. With about 40 comets characterized in the IR and radio and more than 200 comets cataloged at optical wavelengths, a large number of molecules have been identified in cometary atmospheres, both from ground- and space-based observations (Cochran et al., 2015; Le Roy et al., 2015; Biver et al., 2015a; Dello Russo et al., 2016b; Roth et al., 2018).

Certain primary volatiles like C_2H_2, CO, CH_4, and OCS are under-represented in studies of comets as a whole. IR coma studies indicate that Jupiter-family comets (relative to Oort cloud comets) are in general depleted in the hypervolatiles CO, CH_4, and C_2H_6, which may reflect the effects of repeated close perihelion passages on their volatile content. On the other hand, large optical studies of product species found no correlation between dynamical family and carbon-chain depletion, suggesting that these differences may instead be primordial and indicative of differences in formation histories for Jupiter-family comets compared to Oort cloud comets (Dello Russo et al., 2016b and references therein). The detection of crystalline silicates in some comets coupled with updates in dynamical models (e.g., Levison et al., 2011) suggests that scattering processes and large-scale mixing of materials in the early solar nebula have complicated the distinction between comet-forming regions (Bockelée-Morvan et al., 2000, 2016; Gomes et al., 2005; Zolensky et al., 2006; Dello Russo et al., 2016b). Therefore, the Oort cloud and Kuiper belt contain comets that may represent varying (or, at the other extreme, largely overlapping) formation regions in the solar nebula. The Rosetta mission to comet 67P/Churyumov–Gerasimenko (hereafter 67P) revealed a heterogeneous nucleus, adding more complexity to these scenarios (Rickman et al., 2015, Le Roy et al., 2015), stimulating fundamental questions concerning

the extent to which abundances measured in cometary comae are representative of the pristine composition of nucleus ices (see A'Hearn 2017 for a discussion of these questions). In this work we address these complex questions by significantly increasing the number of OCS measurements in comets, thereby advancing our understanding of their sulfur chemistry. We report the detection of OCS in two Oort cloud comets, C/2015 ER61 (PanSTARRS) (hereafter ER61) and C/2002 T7 (LINEAR) (hereafter T7), and in one Jupiter-family comet (JFC), 21P/Giacobini–Zinner (hereafter G-Z). We also present a (3σ) upper-limit for OCS in JFC 46P/Wirtanen (hereafter Wirtanen). In Section 2, we discuss the importance of OCS in comets. In Section 3, we discuss our observations and our data reduction methodology. In Section 4, we present our results. In Section 5, we discuss our results and place them in the context of comets characterized to date.

2. OCS IN COMETS

Carbonyl sulfide (OCS) is one of the parent volatiles (native ices) that has been stored for ~ 4.5 billion years in icy grains in the nuclei of comets. The present-day sulfur chemistry in comets may reveal much about the origin of these ices and their subsequent processing history, making the measurement of sulfur-bearing molecules in comets an important piece to the puzzle of cometary origins (Dello Russo et al., 1998). Sulfur species should be present in cometary nuclei since comets were likely formed in the mid-plane of the protoplanetary disk from icy grains, where volatiles (including OCS) could freeze out on the surface of dust grains. OCS serves as a link between sulfur and oxygen bearing-species. It is extremely under-represented in the current sample of measurements of

cometary volatiles, and the only known sulfur-bearing species in comets with strong transitions at IR wavelengths; its ν_3 band near 4.85 μm is inherently very strong, being an order of magnitude stronger than the CO ν_1 band near 4.7 μm and rivaling the strength of the CO_2 ν_3 band that renders the region from ~ 4.1 – 4.4 μm totally opaque to ground-based observations. Our OCS measurements are well-suited to address the paucity of OCS detections in comets.

Despite being inherently strong, OCS has been detected in only six comets to date: C/1995 O1 Hale-Bopp (hereafter Hale-Bopp), C/1996 B2 Hyakutake (hereafter Hyakutake), 67P/Churyumov-Gerasimenko (via the Rosetta mission), C/2012 S1 (ISON), C/2014 Q2 (Lovejoy), and 2P/Encke (tentative); see discussion section for more details. The small number of OCS measurements is largely due to limitations in spectral coverage and/or sensitivity in previously available instruments. Owing to its piece-wise continuous nature, targeting OCS with NIRSPEC at Keck requires a second M-band setting in addition to the standard one used to measure H_2O together with the strongest CO lines seen in comets (e.g., see Gibb et al., 2012), while the limited sensitivity and small spectral grasp of the previous facility spectrograph at IRTF (CSHELL; Tokunaga et al., 1990; Greene et al., 1993) limited measuring OCS to bright comets. With iSHELL, the OCS ν_3 band is fully encompassed together with H_2O and CO within a single instrument setting (see Sec. 3) and, unlike NIRSPEC or CSHELL, active guiding is feasible at wavelengths independent of the bandpass used to obtain spectra (specifically, for the observations of C/2015 ER61, 21P, and 46P included in this study, the iSHELL M2 setting; see Section 3).

3. OBSERVATIONS AND DATA REDUCTION

We targeted OCS in comets Wirtanen, G-Z, and ER61 in 2017-2018 using the high-resolution ($\lambda/\Delta\lambda \sim 40{,}000$) IR immersion grating echelle spectrograph iSHELL (Rayner et al., 2012, 2016) at the 3-m NASA Infrared Telescope Facility (IRTF) on Maunakea, HI. The superior IR active guiding capabilities of iSHELL enabled us to achieve observing efficiency of up to 80%. This paper reports results from two iSHELL settings: our custom L-band setting ("Lcustom", covering ~ 2.8 – 3.2 μm) which contains multiple strong transitions of H_2O, sampling a range of excitation energies and enabling robust determination of rotational temperature (T_{rot}), and M2 (covering ~ 4.5 – 5.2 μm) which samples emissions of OCS and H_2O simultaneously. The iSHELL observations were performed with a 0.75" wide (6-pixel wide) slit, oriented along the projected Sun-comet line on all dates.

We also present archival data of comet T7 acquired in 2004 using CSHELL at resolving power $\lambda/\Delta\lambda \sim 25{,}000$ using the 1.0" (5-pixel) wide slit. T7 was a daytime object, which precluded use of the optical guide camera in CSHELL. Instead, images of the comet were taken before and after each sequence of scans to monitor and correct for cometary drift. To correct slight errors in tracking and re-position the comet on the array, the CSHELL slit was set at its default position angle of 270° (east–west on the sky).

To achieve flux calibration, a suitably bright IR flux standard star was observed using a 4" wide slit on each date and for each setting (using a wider slit for the star than was used for the comet helps minimize loss of signal and thereby achieve a truer measure of the stellar continuum; see Bonev 2005; Radeva et al., 2010; Villanueva et al., 2011 for

further details regarding flux calibrations). Table 1 shows the observing log for the data presented in this paper.

Table 1. OCS Observation Log.

Comet	UT Date	Instrument	Time (UT)	R_h (au)	Δ (au)	$d\Delta/dt$ (km s^{-1})	T_{int} (mins)
T7[a]	5-May-2004	CSHELL	15:52- 21:14	0.671	0.631	-65.67	16
	9-May-2004	CSHELL	15:44-21:05	0.713	0.484	-61.37	12
ER61[b]	12-May-2017	iSHELL	14:16-17:16	1.043	1.251	9.25	94
G-Z[c]	25-July-2018	iSHELL	12:02-13:58	1.20	0.64	-13.66	85
	28-July-2018	iSHELL	13:32-15:44	1.18	0.61	-13.39	96
	29-July-2018	iSHELL	13:25- 15:23	1.17	0.61	-13.31	86
46P[d]	14-Dec-2018	iSHELL	09:06-11:59	1.055	0.078	-1.49	122
	19-Dec-2018	iSHELL	05:39-08:03	1.058	0.079	2.00	114

Notes. R_h, dR_h/dt, Δ, $d\Delta/dt$, and T_{int} are heliocentric distance, heliocentric velocity, geocentric distance, geocentric velocity, and total on source integration time, respectively. For comets observed with iSHELL, the slit position angle (PA) was oriented along the projected Sun-comet line on all dates. [a] T7 reached perihelion (0.614 AU) on 2004 April 23 and was closest to Earth (0.266 AU) on 2004 May 19. We targeted OCS on two dates, May 5 and May 9. [b] ER61 reached perihelion (1.042 AU) on 2017 May 10 and was closest to Earth (1.178 AU) on 2017 April 18, shortly after its outburst on April 4 (Saki et al., 2021). We observed ER61 and targeted the OCS spectral region on 2017 May 12. [c] G-Z reached perihelion (1.010 AU) on 2018 September 10 and was closest to Earth (0.077 AU) on the same day. [d]Wirtanen reached perihelion (1.055 AU) on 2018 December 12 and was closest to Earth (0.077 AU) on 2018 December 16. We targeted the OCS spectral region on December 14 and 19.

All observations were performed using a standard ABBA nod pattern (sequence of four scans) where the A and B beams were placed symmetrically about the midpoint along the 15" (for iSHELL) or 30" (for CSHELL) long slit and separated by half its length. Thus, the comet was present in both beams, thereby providing increased signal-to-noise (by a factor of up to $\sqrt{2}$ compared with nodding to blank sky). Combining the frames as A-B-B+A (comet-sky-sky+comet) canceled out background thermal continuum, sky emission

(lines and continuum), and instrumental biases to second order in airmass (see Figure 2 of DiSanti et al., 2001). The data were then dark-subtracted (to account for high dark-current pixels), flat-fielded (using an internal continuum lamp), cleaned of cosmic ray hits and hot pixels, and rectified to produce two-dimensional (spatial-spectral) frames, where each row corresponds to a constant (and unique) spatial position along the slit, and each column to a unique wavelength. We found that spatially resampling using a third-order polynomial more completely removed the curvature in the spatial dimension from iSHELL frames and so employed this in place of previously used second-order polynomials (DiSanti et al., 2017; Roth et al., 2018). The spectral frames were spatially registered, and spectra were then extracted by summing signal over 15 rows (approximately 2.5"), seven rows to each side of the nucleus, defined as the peak of dust emission in a given spectral order. Our observational procedures and data reduction algorithms have been rigorously tested and well documented in peer-reviewed literature (Bonev 2005; Dello Russo et al., 1998; DiSanti et al., 2001, 2006, 2014, 2017; Villanueva et al., 2009; Radeva et al., 2010).

The Planetary Spectrum Generator (Villanueva et al. 2018) was used to generate atmospheric models, to assign a wavelength scale to the spectra, and to establish absolute column burdens of the component absorbing species in the terrestrial atmosphere. We convolved the fully resolved atmospheric transmittance function to the resolving power of the data and scaled it to the level of the comet continuum. We then subtracted the modeled continuum to isolate cometary emission lines as previously described (e.g., DiSanti et al., 2016). The procedure is illustrated in Figure 1. Synthetic models of fluorescent emission for our targeted species were compared to observed line intensities, after correcting each modeled line intensity for the monochromatic atmospheric transmittance at its Doppler-

shifted wavelength (according to the geocentric velocity of the comet at the time of the observation). The g-factors used in synthetic fluorescent emission models in this study were generated with quantum mechanical models for OCS, CN (Paganini and Mumma, 2016), and H_2O (Villanueva et al., 2012b).

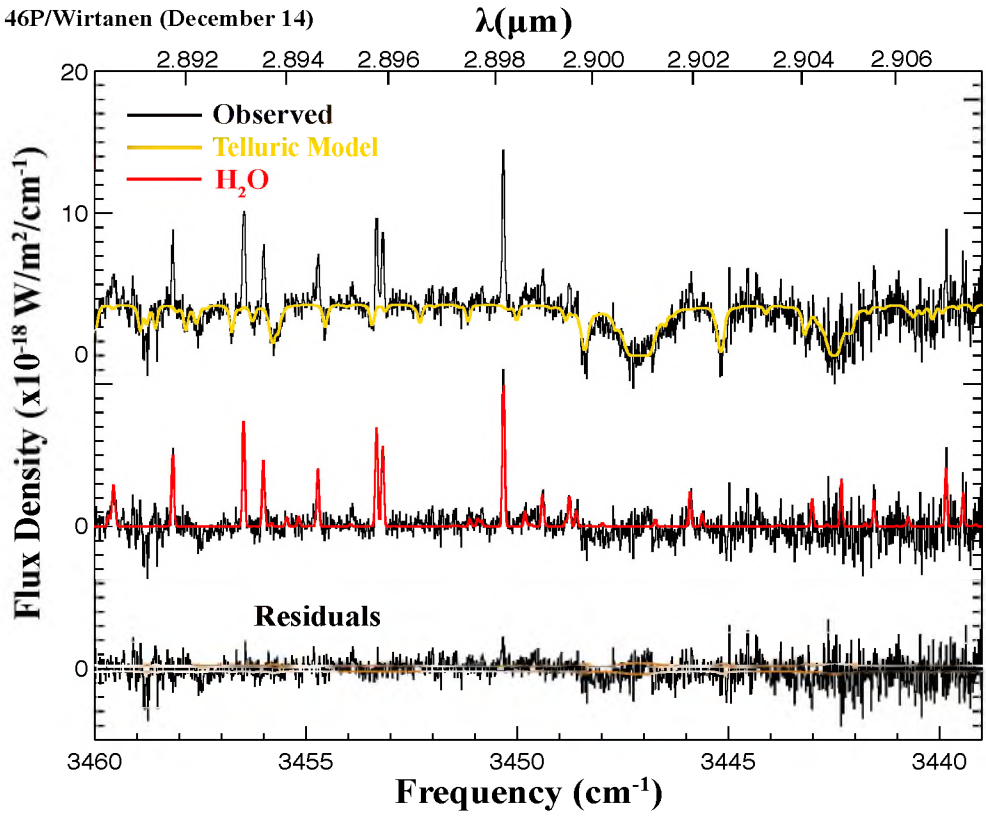

Figure 1. Extracted spectra showing clear detections of H_2O in comet Wirtanen. The yellow trace overplotted on the uppermost cometary spectrum is the best-fit telluric transmittance model (convolved to the instrumental resolution). Directly below is the residual spectrum (after subtracting the telluric absorption model), with the H_2O fluorescence emission model overplotted in red. At the bottom of the panel is the residual spectrum (after subtracting the telluric absorption model and H_2O fluorescence model), with the 1σ uncertainty envelope overplotted in bronze.

4. RESULTS

We determined water rotational temperatures (T_{rot}), OCS and H_2O production rates (Qs), and the abundance (or "mixing") ratio Q_{OCS}/Q_{H2O} (expressed in **%**) for all comets in this paper. We found consistent results and excellent fits to the comet spectra (both for telluric absorptions and for cometary emission features).

4.1. SPATIAL PROFILE AS DIAGNOSTIC FOR OCS OUTGASSING SOURCE

In comet T7 the OCS emissions were sufficiently strong when coadded on both dates (May 5 and May 9) to determine the spatial profile along the slit (see Figure 2). The H_2O production rate and the relative OCS abundances were consistent on both dates, thus we coadded the lines for both molecules to increase the SNR. Figure 2 suggests that the spatial distribution of OCS in T7 followed that of H_2O as well as the dust within measurement uncertainties. Owing to limited S/N along the slit, we were unable to extract meaningful emission spatial profiles for OCS in the other comets presented here. Most high-resolution infrared observations of comets permit investigations of processes in the inner coma, where both nucleus and extended sources (i.e., release from one or more sources in the coma) may contribute to the production and spatial distribution of a particular volatile. Analysis of spatial profiles for coma molecules can indicate whether their distribution differs from that expected for direct sublimation from the nucleus, as opposed to release from extended sources in the coma (Dello Russo et al., 1998, 2016a; DiSanti et al., 2001; Brooke et al., 2003). The spatial profile for molecules produced by direct sublimation peak in intensity at (or at least near) the position of the nucleus before

falling off with increasing nucleocentric distance (ρ) as ρ^{-1}, whereas molecules having an extended source display a flatter distribution, falling off more slowly with ρ (e.g., see Figure 3 in Dello Russo et al., 1998). In our OCS study, the OCS spatial distribution is formally consistent with H_2O; however, the low SNR does not allow for a definitive conclusion on the presence (or absence) of a distributed OCS source in the coma of comet T7 (see Figure 2), but the spatial profiles of H_2O and OCS are consistent with common outgassing sources seen in other comets (e.g., Hale-Bopp, ISON).

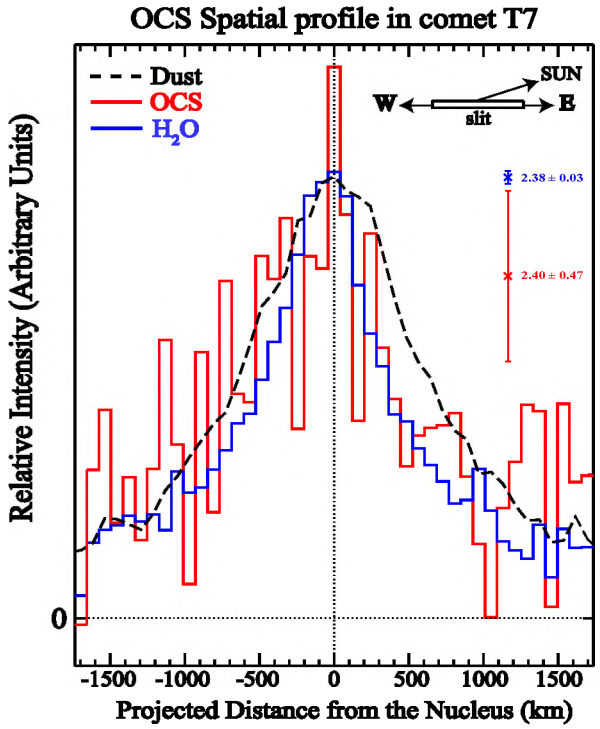

Figure 2. Spatial profiles of OCS simultaneously measured with dust and H_2O in comet T7 on UT 2004 May 5 and May 9 combined. The slit was oriented in its default position (East-West) with the Sun-facing direction to the right as indicated. The combined growth factor and its ±1σ uncertainty measured from each profile are indicated at right.

Evidence for the existence of OCS extended sources has been identified in bright comets Hale-Bopp near R_h = 1 au, and in ISON at R_h = 0.46 au. In comet Hale-Bopp near perihelion, the long-slit infrared observations suggested OCS originated substantially or even predominantly from extended sources (~ 70%; see Dello Russo et al., 1998 for further details). The broad and flat spatial distribution of OCS in comet ISON also suggested that a significant fraction may have come from an extended source (Dello Russo et al., 2016a).

4.2. ROTATIONAL TEMPERATURE

Rotational temperatures (T_{rot}) were determined using correlation and excitation analyses that have been extensively described in the literature (e.g., Bonev 2005, Bonev et al., 2008a, DiSanti et al., 2006, Villanueva et al., 2008). In general, well-constrained rotational temperatures can be determined for individual species with intrinsically bright lines and for which a sufficiently broad range of excitation energies is sampled. These conditions are met for strong H_2O lines centered near 3452 cm^{-1} in CSHELL spectra, and in Lcustom order 179 with iSHELL spanning ~ 3437.8 – 3465.8 cm^{-1} and are augmented by including H_2O lines in additional iSHELL orders (see Figure 1 and Table 2).

For T7 the T_{rot} for H_2O on May 5 (104^{+6}_{-10} K) was consistent with that from May 9 (106^{+4}_{-5} K). The H_2O rotational temperature for ER61 was measured as 60^{+6}_{-5} K on May 12. For our G-Z analysis, we calculated production rates and mixing ratios at T_{rot} = 48 K and 64 K, consistent with rotational temperatures derived from CO (64^{+15}_{-11} K) and H_2O (48^{+19}_{-13} K) on July 28 and 29, respectively (Roth et al., 2020). We used three iSHELL settings for Wirtanen on Dec 14 and 19 and were able to retrieve well-

constrained rotational temperatures on both dates. We found the T_{rot} for H_2O as measured from the Lcustom setting (84 ± 3 K) on December 14 was in agreement with that from the M2 setting (83 ± 7 K), thus we used T_{rot} = 84 K when determining production rates and mixing ratios. The H_2O T_{rot} on December 19 was also consistent with that on December 14 (86^{+17}_{-11} K). We were unable to measure rotational temperatures for OCS in any of the observations reported here, so we adopted the rotational temperature of simultaneously measured H_2O within the same setting (M2). Rotational temperatures for different molecules within the same comet and the same instrumental setting are generally found to be consistent even for molecules with different photo-dissociation lifetimes (e.g., see DiSanti et al., 2006; Anderson 2010; Gibb et al., 2012; and DiSanti et al., 2016 supporting this approach).

4.3. PRODUCTION RATES AND MIXING RATIOS

Production rates for sampled species were determined using the appropriate fluorescence model at the measured (or assumed) rotational temperature. Nucleus-centered production rates (Q_{NC}, molecules s^{-1}) were calculated using the well-established formalism relating line flux, fluorescence g-factor, and physical (gas outflow speed, photo-dissociation lifetime) and geometric parameters (R_h, Δ; see Dello Russo et al., 1998; DiSanti et al., 2001, 2006, 2014; Bonev 2005; Villanueva et al., 2011). Q_{NC} is then scaled by a growth factor (GF), which relates molecular production rates in the fraction of the coma along the column described by the beam (of size 0.75" × 2.5" for iSHELL, and 1" × 3" for CSHELL) to the global production rate (Q_{global}). This method

analyzes spatial profiles of emission using the "Q-curve" formalism, dating back to the analysis of OCS in comet Hale-Bopp (Dello Russo et al., 1998). A canonical spherically symmetric outflow velocity, v_{gas} = 800 $R_h^{-0.5}$ m s^{-1}, was assumed in determining our production rates. This velocity is based on velocity-resolved observations of several moderately bright comets at radio wavelengths (Biver et al., 2006, 2011; Cordiner et al., 2014; also see Bonev 2005 supporting this assumption). We were able to explicitly determine that OCS traced the spatial profile of H_2O in comet T7 and the derived OCS GF (combined on both dates) is consistent with the GF derived for H_2O (see Figure 2); therefore, we assumed the GF of simultaneously measured H_2O when calculating OCS production rates (Qs). Global production rates for all the comets targeted in this paper along with OCS mixing ratios relative to water are presented in Table 2.

For comet T7 we measured OCS mixing ratios of 0.036% ± 0.009% and 0.043% ± 0.006% on May 5 and May 9 respectively. Figures 3 A-B show extracted spectra with clear OCS, CN, and H_2O emissions in T7 (with traces and labels as described in Figure 1). In ER61, the OCS mixing ratio was found to be 0.150% ± 0.031%. Figure 3C shows detections of H_2O, CN, and OCS lines in ER61 on May 12. In the case of G-Z, since the H_2O production rate and relative OCS abundances were consistent throughout our July observations, we coadded the spectra on all three dates (July 25, 28, and 29), and found OCS mixing ratios of 0.116% ± 0.022% (assuming T_{rot} = 48 K) and 0.108% ± 0.021% (assuming T_{rot} = 64 K), demonstrating that the abundance of OCS relative to H_2O was not sensitive to the assumed T_{rot}. Figure 3D shows the clear detections of OCS, CN and H_2O in G-Z.

Table 2. OCS abundances.

Molecules	T_{rot} (k)	Growth Factor	Q (molecules s^{-1})	Abundance (%)
		Wirtanen Dec 14 – 2018		
H_2O	84 ± 3	2.32 ± 0.08	$(5.95 \pm 0.23) \times 10^{27}$	100
OCS	(84)	(2.32)	$< 9.38 \times 10^{23}$	<0.016[a]
		Wirtanen Dec 19 – 2018		
H_2O	86^{+17}_{-14}	1.98 ± 0.08	$(6.04 \pm 0.3) \times 10^{27}$	100
OCS	(86)	(1.98)	$< 9.92 \times 10^{23}$	<0.016[a]
		G-Z July 25,28, and 29 (combined)		
H_2O	(48)[b]	1.90 ± 0.04[c]	$(2.63 \pm 0.20) \times 10^{28}$	100
OCS	(48)	(1.9)	$(3.07 \pm 0.41) \times 10^{25}$	0.116 ± 0.022
H_2O	(64)[b]	1.90 ± 0.04[c]	$(2.86 \pm 0.22) \times 10^{28}$	100
OCS	(64)	(1.9)	$(3.10 \pm 0.46) \times 10^{25}$	0.108 ± 0.021
		ER61 May 12 – 2017		
H_2O	60^{+6}_{-5}	2.34 ± 0.36	$(7.04 \pm 0.25) \times 10^{28}$	100
OCS	(60)	(2.34)	$(1.06 \pm 0.19) \times 10^{26}$	0.15 ± 0.031
		T7 May 5 – 2004		
H_2O	104^{+6}_{-10}	2.34 ± 0.03	$(5.39 \pm 0.25) \times 10^{29}$	100
OCS	(104)	(2.34)	$(1.95 \pm 0.47) \times 10^{26}$	0.036 ± 0.009
		T7 May 9 – 2004		
H_2O	106^{+4}_{-5}	2.51 ± 0.05	$(5.08 \pm 0.16) \times 10^{29}$	100
OCS	(106)	(2.51)	$(2.22 \pm 0.21) \times 10^{26}$	0.043 ± 0.006

Note. values in parenthesis are assumed. [a] 3σ upper limit. [b] Temperature from Roth et al., (2020). [c] The average of the growth factors (from Roth et al., 2020).

We were unable to detect any OCS emission lines with SNR greater than 5 for Wirtanen, yet our derived 3σ upper limits on both December 14 and 19 are consistent (being <0.016%). Figure 1 shows the detection of H_2O in comet Wirtanen in Lcustom order 179 on December 14. For the comets analyzed here, we have excluded OCS lines that are blended with CN and/or H_2O. CN emissions in all of these comets were strong, consistent with other comets measured at the similar R_h (see Dello Russo et al., 2016b for more details).

Individual OCS emission lines are not detected in all of the comets in this paper (see Figure 3); however, by combining the flux of all the unblended OCS lines we achieved a sensitive measurement of OCS production rate and its abundance relative to H_2O in comets T7, G-Z, and ER61 and report a stringent upper limit in comet Wirtanen. Centered on the Doppler-shifted line frequency, line flux was measured for a given line by integrating over the spectral range of each line in each comet.

Identical measurements were performed away from the expected line centers ($\nu'_i = \nu_i + \Delta\nu$), with $\Delta\nu$ ranging from −0.3 to +0.3 cm^{-1}. This method has been validated for weak species in other comets measured at IR wavelengths (see Villanueva et al., 2009; Paganini et al., 2017). In the case of sampling noise, the peak flux will occur offset from the Doppler-shifted line center. Instead, the peak composite flux for each comet is found at the expected position (see Figure 4). We performed the same measurement for H_2O and found that OCS composite line has the same shape and width as the H_2O composite line. As an example, we plotted the H_2O composite line for comet G-Z in Figure 4(A).

5. DISCUSSION

5.1. OCS AND OTHER SULFUR-BEARING SPECIES IN COMETS

Roughly 40 comets have been sampled with high-resolution IR spectroscopy and differences in composition have been noted among both OCCs and JFCs. This relatively small sample size has made the development of a chemistry-based classification system difficult.

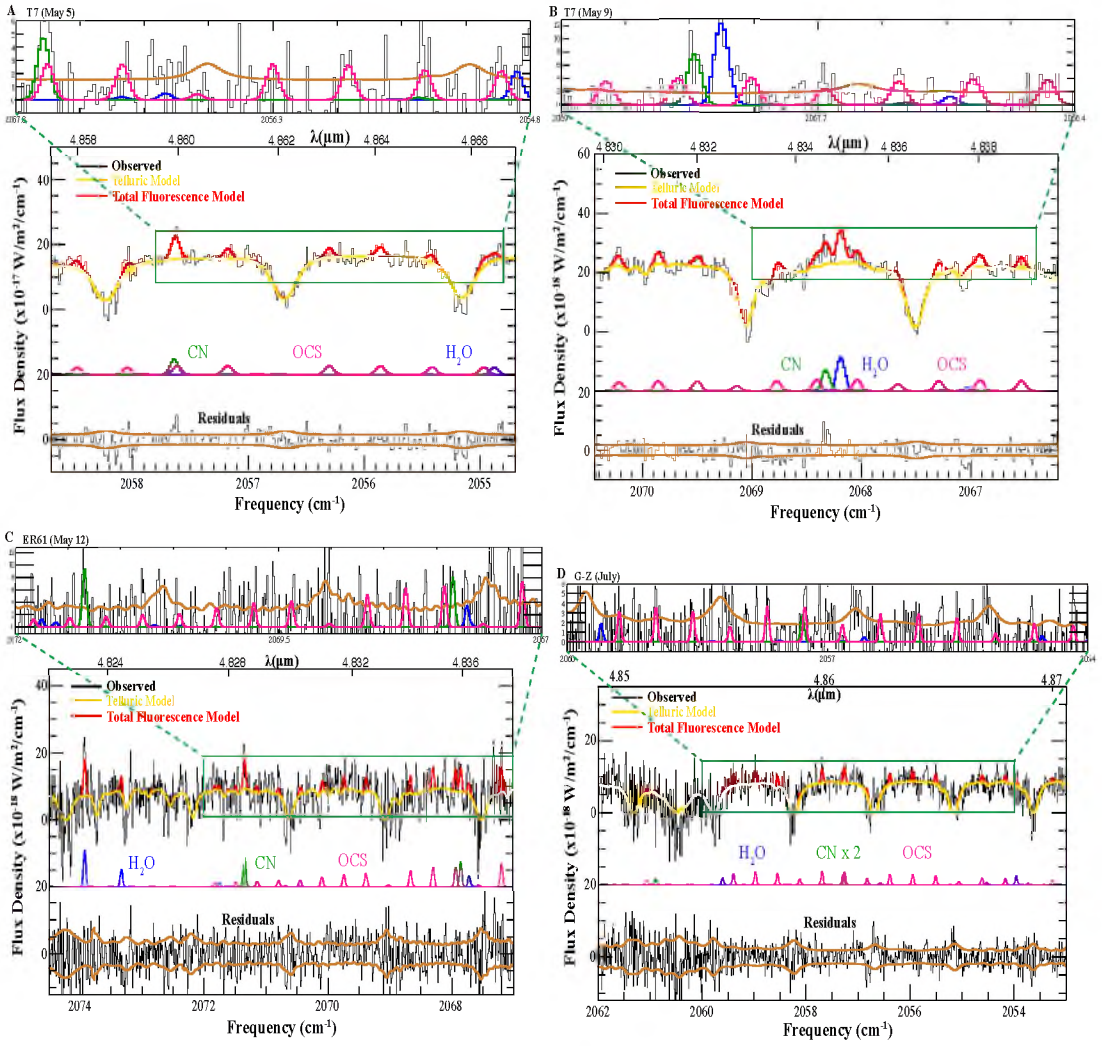

Figure 3. Fluorescence emissions of OCS, CN, and H_2O in comets T7, G-Z, and ER61. The yellow traces overplotted on the uppermost cometary spectra are the telluric absorption models (convolved to the instrumental resolution), while the total modeled fluorescent emissions are overplotted in red. Individual fluorescent emission models (color-coded by species for clarity) are plotted below. At the bottom of each panel is the residual spectrum (after subtracting the telluric absorption model and all relevant fluorescent emission models) with the 1σ uncertainty envelope overplotted in bronze. (A–D) shows the detections of OCS in comet T7, ER61, and G-Z respectively. The zoomed subplot highlights the location and intensity of OCS emission lines with respect to 1σ uncertainty envelope plotted in bronze, each subplot has the same units as the larger plot.

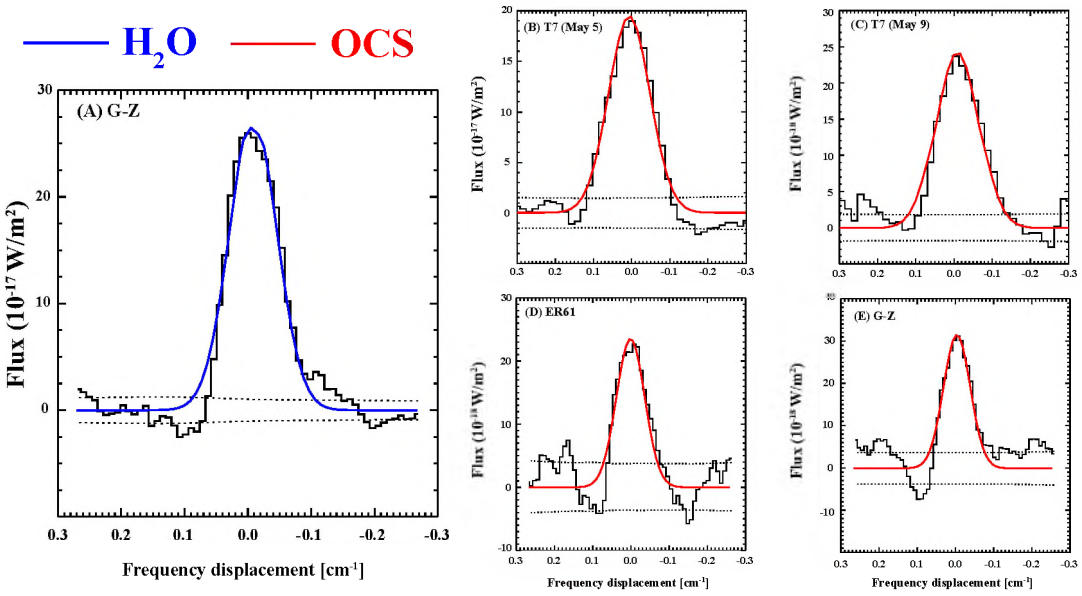

Figure 4. OCS composite emission line in comets T7, G-Z, and ER61. Panel A shows H_2O composite emission line in comet G-Z. (B–E) shows the composite OCS emission line by combining unblended individual OCS lines for each comet. The 1σ noise envelope is shown in dotted lines. The H_2O and OCS models are plotted in blue and red respectively.

OCS is one of the under-represented molecules in comet studies due largely to limitations in sensitivity and lack of spectral coverage in earlier instruments (see Section 1 & 2, and discussion in Dello Russo et al., 2016a). However, other sulfur species (e.g., H_2S, H_2CS, SO_2, SO, CS, CS_2, S_2, and NS) have been detected in many comets (see Table 5 in Le Roy et al., 2015, Table 1 in Bockelée-Morvan et al., 2004, and Table A2 in Calmonte et al., 2016 for the list of detected sulfur-bearing species and their abundances in comets).

In contrast, detections of OCS have been reported in only six comets to date (mostly OCCs). It was first detected through its radio lines at 145.947 GHz by Woodney

et al., (1997) in comet Hyakutake, and confirmed by several other radio lines in comet Hale-Bopp (e.g., Bockelée-Morvan et al., 2000). Strong IR OCS lines close to 4.9 μm were reported by Dello Russo et al., (1998) in both Hyakutake and Hale-Bopp. The Rosetta spacecraft detected OCS in comet 67P (Le Roy et al., 2015; Bockelée-Morvan et al., 2016). Additional ground-based detections have been reported for comets ISON (Dello Russo et al., 2016a), Lovejoy (Biver et al., 2015), and 2P/Encke (at 4σ) (Roth et al., 2018). In this paper, we add two OCCs (comet T7 and ER61) and one JFC (G-Z) to this list (see Figure 5 and Table 2). Our OCS measurement in comet G-Z represents its first secure ground-based detection in a JFC. Abundances are given in Table 3.

Ecliptic (short period) comets and specifically JFCs are typically depleted in certain trace volatiles relative to OCCs, perhaps due to thermal processing (Dello Russo et al., 2016b; DiSanti et al., 2017; Roth et al., 2018, 2020). The first OCS measurement for a short period comet did not occur until 2015 via the Rosetta mission to comet 67P, for which the large orbital obliquity (~ 52°) of its rotation axis leads to strong seasonal effects on its nucleus. Le Roy et al., (2015) searched for multiple sulfur species, including OCS, in the coma of 67P and found an OCS abundance of 0.017% relative to H_2O (similar to our 3σ upper limit in Wirtanen; Table 2) for summer and 0.098% (similar to our measured OCS abundance in G-Z, for T_{rot} = 64 K) for the winter hemisphere (see Table 3 and Le Roy et al., 2015 for further details).

Bockelée-Morvan et al., (2016) found an average OCS abundance of 0.12% relative to H_2O for pre-perihelion observations (8 July – 10 Aug 2015) and a higher average of 0.18% relative to H_2O (due to outburst and high depth of ablation) for post-perihelion observations (16 Aug – 27 Sep 2015). The average OCS abundance in comet

67P is similar to our measured abundance in comet G-Z. Recently, Calmonte et al., (2016) reported the detection of new sulfur-bearing species (e.g., CH_3SH, C_2H_6S) in the coma of comet 67P.

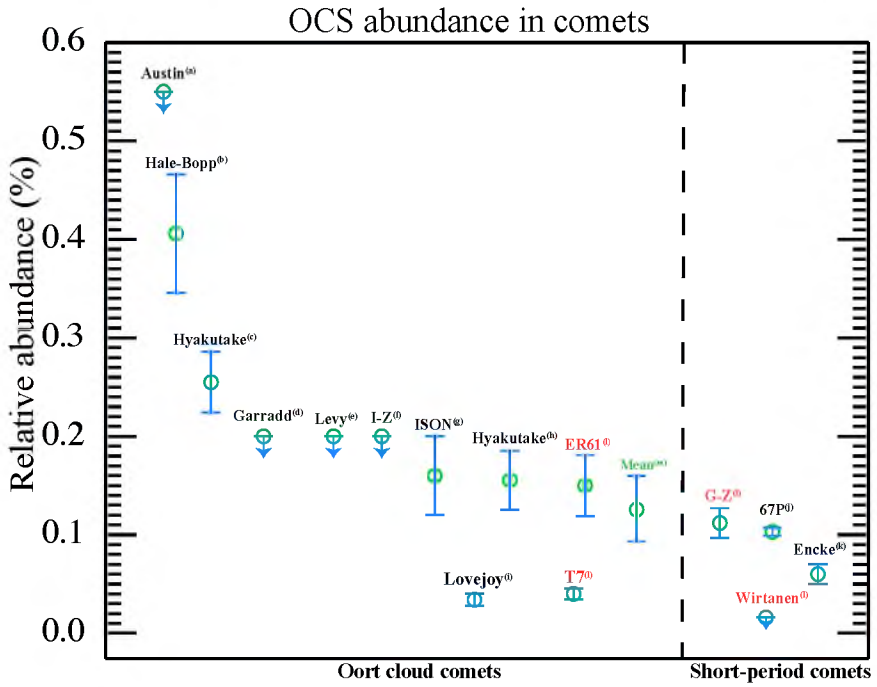

Figure 5. Measured OCS abundances (relative to H_2O) in comets. [a] DiSanti et al., 1992. [b] Dello Russo et al., 1998 (IR), Bockelée-Morvan et al., 2000 (Radio). [c] Dello Russo et al., 1998 (NIR). [d] Paganini et al., 2012. [e] Bockelée-Morvan et al., 1990. [f] Bockelée-Morvan et al., 2004. [g] Dello Russo et al., 2016. [h] Woodney et al., 1997, Biver et al., 1999. [i] Biver et al., 2015. [j] Le Roy et al., 2015, Bockelée-Morvan et al., 2016. [k] Roth et al., 2018. [l] This work. [m] OCS unweighted mean abundance among comets (0.126 ± 0.034 %). Note: owing to the significance of Wirtanen's upper limit we have included half of its value when calculating the unweighted mean.

Bockelée-Morvan et al., (2016) found an average OCS abundance of 0.12% relative to H_2O for pre-perihelion observations (8 July – 10 Aug 2015) and a higher average of 0.18% relative to H_2O (due to outburst and high depth of ablation) for post-

perihelion observations (16 Aug – 27 Sep 2015). The average OCS abundance in comet 67P is similar to our measured abundance in comet G-Z. Recently, Calmonte et al., (2016) reported the detection of new sulfur-bearing species (e.g., CH_3SH, C_2H_6S) in the coma of comet 67P.

Table 3. OCS abundance (relative to H_2O) in other comets.

Comet	OCS Abundance in (%)
C/1999 H1 (Lee)[a]	< 3.6
1P/Halley[b]	< 0.8
C/1989 C1 (Austin)[c]	< 0.55
Hale–Bopp[d]	0.413 ± 0.077
Hale–Bopp[e]	0.4
Hyakutake[f]	< 0.53
Hyakutake[g]	0.21
Hyakutake[h]	0.3
Hyakutake[i]	0.1
Hyakutake[j]	0.2
Lovejoy[k]	0.034 ± 0.006
ISON[l]	0.16 ± 0.04
67P[m]	0.12
67P[m]	0.18
67P[n]	0.017
67P[n]	0.098
2P/Encke[o]	0.06 ± 0.01
C/1993 F2 Shoemaker-Levy[p]	< 0.2
C/2009 P1(Garradd)[q]	< 0.2
153P/Ikeya-Zhang[r]	< 0.2

Note. [a] Biver et al., (2000). [b] Combes et al., (1988) (at 2.5σ). [c] DiSanti et al., (1992). [d] Dello Russo et al., (1998) (near-IR). [e] Bockelée-Morvan et al., (2000) (radio). [f] Dello Russo et al., (1998) (3σ upper limit on March 24.5). [g] Dello Russo et al., (1998) (March 19). [h] Dello Russo et al., (1998) (using OH* production rate derived by Schleicher et al., 1996; March 19). [i] Woodney et al., (1997) (radio). [j] Biver et al., (1999) (radio). [k] Biver et al., (2015). [l] Dello Russo et al., (2016a). [m] Bockelée-Morvan et al., (2016). [n] Le Roy et al., (2015). [o] Roth et al., (2018). [p] Bockelée-Morvan et al., (1990). [q] Paganini et al., (2012). [r] Bockelée-Morvan et al., (2004). The values reported for comets C/1999 H1 Lee and 1P/Halley are not stringent as they are much higher compared to the highest abundances measured in other comets and therefore we have excluded them from Figure 5.

5.2. FORMATION OF OCS

Carbonyl sulfide (OCS) has been identified in a variety of astronomical environments. OCS can catalyze the coupling of amino acids and so is of particular interest for astrobiology (Leman et al., 2004). It has been observed in the atmospheres of Venus, Jupiter, and Io as well as in interstellar ice and comets (e.g., Kamp & Taylor 1990; Woodney et al., 1997, Dello Russo et al., 1998; Sakai et al., 2014; Le Roy et al., 2015). Only $< 0.1\%$ of the sulfur cosmic abundance can be accounted for in gas-phase molecules (Tieftrunk et al., 1994; also see Le Gal et al., 2019 for further details), suggesting that most sulfur-bearing species are locked into icy mantles coating interstellar dust grains (Millar & Herbst 1990; Ruffle et al., 1999; Vidal et al., 2017; Laas & Caselli 2019).

Recent spectral line surveys have increased the number of known interstellar sulfur molecules (see Vastel et al., 2018 and references therein), and recent astrochemical models have improved our understanding of sulfur-bearing species in interstellar environments (e.g., Woods et al., 2015; Vidal et al., 2017; Vidal & Wakelam 2018). Laas and Caselli (2019) used a new sulfur depletion model that accurately reproduced most of the known gas-phase sulfur-bearing molecular abundances observed in interstellar clouds. Their model also predicts that most of the sulfur-bearing species are trapped on icy grains, consistent with observations. Processing of interstellar ice mixtures containing simple sulfur-bearing species yields a highly heterogeneous mixture of products similar to the chemistry that has been detected in both cometary ices and meteoritic material (see Ehrenfreund et al., 2002; Jiménez-Escobar et al., 2014; Calmonte et al., 2016 and references therein).

OCS is also one of the sulfur-bearing molecules detected in icy grain mantles toward protostars and disks (e.g., Geballe et al., 1985; Palumbo et al., 1997; Zasowski et al., 2009; Fuente et al., 2010; Guilloteau et al., 2013, 2016; Teague et al., 2018; Pacheco-Vázquez et al., 2016; Sakai et al., 2016; Phuong et al., 2018). Palumbo et al., (1997) found that OCS is embedded in CH_3OH rich ices in protostar W33A. Understanding the path that could contribute to OCS formation in these environments requires both modeling and laboratory experiments.

Extensive experimental studies have been performed analyzing the formation of OCS both in H_2O-free and H_2O-dominated ices using CO or CO_2 as the C-bearing species and H_2S or SO_2 as the sulfur-bearing sources (see Moore et al., 2007; Ferrante et al., 2008 and references therein). The CO abundance is relatively high in interstellar ices, and Hawkins et al., (1985) demonstrated that CO is capable of capturing S atoms to produce OCS. Experiments have also shown that H_2S can dissociate into 2H and S (Isoniemi et al., 1999). Therefore, one possible reaction sequence to produce OCS is: $H_2S \rightarrow 2H + S$ and $S + CO \rightarrow OCS$ (see Ferrante et al., 2008).

OCS can also be produced, though at a lower abundance, from irradiation of a mixture of CO_2, which dissociates the CO_2 into CO, and H_2S. We compared OCS with CO abundances for comets when both values were reported in the literature. Since the OCS vacuum sublimation temperature is ~ 85 K (Palumbo et al., 1995; Ferrante et al., 2008), the high volatility and lower thermal threshold of CO makes evolutionary processing effects more important for CO than for OCS. Figure 6 suggests a higher CO abundance may be correlated with a higher OCS abundance, however the very small

number of OCS measurements to date in comets precludes establishing a clear correlation between CO and OCS at this time.

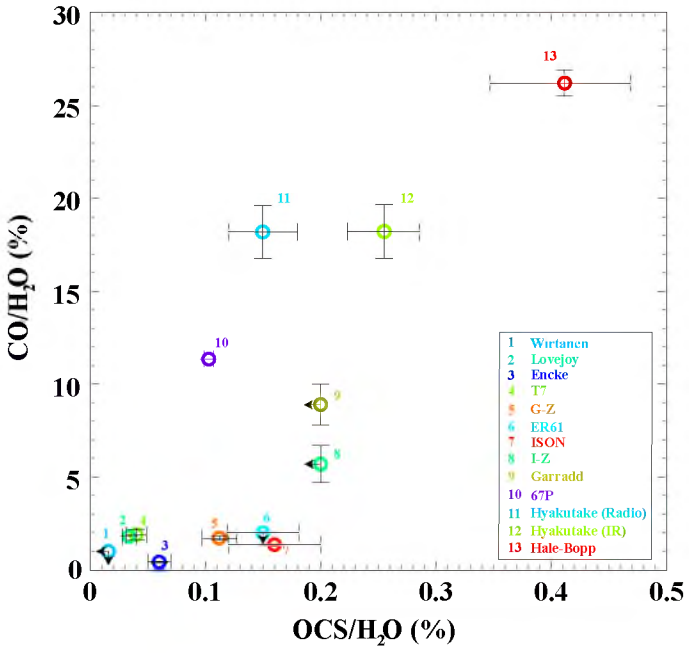

Figure 6. Average OCS abundances plotted against the average CO abundances (both relative to H_2O in %). Number and color assigned to each comet are given in the plot legend. The references for OCS abundances are presented in Figure 5 caption. CO abundances are from: [(1)] McKay et al., 2021. [(2)] Biver et al., 2015. [(3)] Roth et al., 2018. [(5)] Roth et al., 2020. [(6)] Saki et al., 2021. [(10)] Le Roy et al., 2015. [(4,7,8,9,10,11,13)] Dello Russo et al., 2016b.

The free sulfur required to produce OCS can also come from the dissociation of sulfur dioxide (SO_2) (Okabe 1978, p. 247; Ferrante et al., 2008). Sulfur atoms can also be oxidized by H_2O molecules, yielding SO_2 (Moore et al., 2007); sufficient oxidation might completely block OCS formation (see Figure 6 of Ferrante et al., 2008). Thus, the formation of OCS in H_2O-dominated ices might be expected to be smaller, which could

be the case in parts of the mid-plane of the proto-planetary disk where comets formed. It is not clear how much of the interstellar sulfur molecules survive during star formation to be incorporated into disks, or whether the sulfur chemistry in such environments is mostly reset.

6. CONCLUSION

OCS is an extremely under-represented species in the current taxonomy of cometary volatiles. In this work, **(1)** we found clear detections of OCS and H_2O in comets T7, ER61, and G-Z, and presented a stringent 3σ upper limit in comet Wirtanen, consistent with the lowest reported value in comets to date (see Figure 5, and Table 2 & 3). **(2)** Our work significantly expands the range of OCS abundances, increases the number of OCS measurements in comets, and contributes extensively to establishing a more meaningful statistic for this prebiotically important sulfur-bearing species.

Compared to the mean abundances among comets observed to date (see Figure 4), OCS mixing ratios in comets T7 and Wirtanen are consistent with depleted, while values for G-Z and ER61 are close to the unweighted mean value. The availability of future space-based platforms, such as James Webb Space Telescope (scheduled to launch in 2021), along with the powerful, recently commissioned facility spectrometer iSHELL at the NASA-IRTF enables for the first time simultaneously measuring OCS together with H_2O and CO in comets, further improving our understanding of their chemical diversity.

REFERENCES

A'Hearn, M. F., 'Comets: looking ahead,' Philosophical Transactions of the Royal Society A, 2017, 375(2097), p. 20160261.

Anderson, W. M. 2010, PhD thesis, The Catholic Univ. America

Biver, N., Bockelée-Morvan, D., Crovisier, J., Davies, J. K., Matthews, H. E., Wink, J. E., Rauer, H., Colom, P., Dent, W. R. F., Despois, D., Moreno, R., Paubert, G., Jewitt, D., and Senay, M., 'Spectroscopic monitoring of comet C/1996 B2 (Hyakutake) with the JCMT and IRAM radio telescopes,' The Astronomical Journal, 1999, 118, pp. 1850–1872.

Biver, N., Bockelée-Morvan, D., Crovisier, J., Henry, F., Davies, J. K., Matthews, H. E.,Colom, P., Gérard, E., Lis, D. C., Phillips, T. G., Rantakyrö, F., Haikala, L., andWeaver, H. A., 'Spectroscopic observations of comet c/1999 h1 (lee) with the sest, jcmt, cso, iram, and nançay radio telescopes,' The Astronomical Journal, 2000, 120, pp. 1554–1570.

Biver, N., Bockelée-Morvan, D., Moreno, R., Crovisier, J., Colom, P., Lis, D. C., Sandqvist, A., Boissier, J., Despois, D., and Milam, S. N., 'Ethyl alcohol and sugar in comet C/2014 Q2 (Lovejoy,' Science Advances, 2015, 1, p. e1500863.

Biver, N., Bockelée-Morvan, D., Crovisier, J., Lis, D. C., Moreno, R., Colom, P., Henry, F., Herpin, F., Paubert, G., andWomack, M., 'Radiowavelength molecular observations of comets C/1999 T1 (McNaught-Hartley), C/2001 A2 (LINEAR), C/2000 WM1 (LINEAR) and 153P/Ikeya-Zhang,' Astronomy and Astrophysics, 2006, 449(3), p.1255.

Bockelée-Morvan, D., Crovisier, J., and Colom, P., 'in proc. of the 24th eslab symp., formation of stars and planets and the evolution of the solar system,' ed. B. Battrick (Paris: ESA), 1990, 143.

Bockelée-Morvan, D., Lis, D. C., Wink, J. E., Despois, D., Crovisier, J., Bachiller, R., Benford, D. J., Biver, N., Colom, P., Davies, J. K., Gérard, E., Germain, B., Houde, M., Mehringer, D., Moreno, R., Paubert, G., Phillips, T. G., and Rauer, H., 'New molecules found in comet c/1995 o1 (hale-bopp). investigating the link between cometary and interstellar material,' AAP, 2000, 353.

Bockelée-Morvan, D., Crovisier, J., Erard, S., Capaccioni, F., Leyrat, C., Filacchione, G., Drossart, P., Encrenaz, T., Biver, N., de Sanctis M.-C., Schmitt, B., Kührt, E., M.-T., C., Combes, M., Combi, M., Fougere, N., Arnold, G., Fink, U., Ip, W., Migliorini, A., Piccioni, G., and Tozzi, G., 'Evolution of CO2, CH4, and OCS abundances relative to H2O in the coma of comet 67P around perihelion from Rosetta/VIRTISH observations,' Monthly Notices of the Royal Astronomical Society, 2016, 462(1), pp. S1270–S183.

Bockelée-Morvan, D., Crovisier, J., Mumma, M. J., and Weaver, H. A., 'The composition of cometary volatiles, in comets ii, ed. m. c. festou, h. u. keller, h. a. weaver,' Univ. Arizona Press, 2004, p. 391.

Bonev, B. P., Towards a Chemical Taxonomy of Comets: Infrared Spectroscopic Methods for Quantitative Measurements of Cometary Water (With an Independent Chapter on Mars Polar Science), phdthesis, The University of Toledo, 2005.

Bonev, B. P., Mumma, M. J., Radeva, Y. L., DiSanti, M. A., Gibb, E. L., and Villanueva, G. L., 'The peculiar volatile composition of comet 8P/Tuttle: A contact binary of chemically distinct cometesimals?' The Astrophysical Journal Letters, 2008b, 680(1), p. L61.

Brooke, T. Y., Weaver, H. A., Chin, G., Bockelée-Morvan, D., Kim, S. J., and Xu, L. H., 'Spectroscopy of comet Hale-Bopp in the infrared,' Icarus, 2003, 166(1), pp. 167–187.

Calmonte,U., Altwegg, K., Balsiger, H., Berthelier, J. J., Bieler, A., Cessateur, G., Dhooghe, F., van Dishoeck, E. F., Fiethe, B., Fuselier, S. A., Gasc, S., Gombosi, T. I., Hässig, M., Le Roy, L., Rubin, M., Sémon, T., Tzou, C. Y., and Wampfler, S. F., 'Sulphurbearing species in the coma of comet 67p/churyumov-gerasimenko,' MNRAS, 2016, 462, pp. S253–S273.

Cochran, A. L., Levasseur-Regourd, A.-C., Cordiner, M., Hadamcik, E., Lasue, J., Gicquel, A., Schleicher, D., Charnley, S. B., Mumma, M. J., Paganini, L., Bockelée-Morvan, D., Biver, N., and Kuan, Y.-J., 'The composition of comets,' Space Science Reviews, 2015, 197(1-4), pp. 9–46.

Combes, M., Moroz, V. I., Crovisier, J., Encrenaz, T., Bibring, J. P., Grigoriev, A. V., Sanko, N. F., Coron, N., Crifo, J. F., Gispert, R., Bockelée-Morvan, D., Nikolsky, Y. V., Krasnopolsky, V. A., Owen, T., Emerich, C., Lamarre, J. M., and Rocard, F., 'The 2.5-12 `m spectrum of comet halley from the iks-vega experiment,' ICARUS, 1988, 76, pp. 404–436.

Cordiner, M. A., Rem.an, A. J., Boissier, J., Milam, S. N., Mumma, M. J., Charnley, S. B., Paganini, L., Villanueva, G., Bockelée-Morvan, D., Kuan, Y. J., Chuang, Y. L., Lis, D. C., Biver, N., Crovisier, J., Minniti, D., and Coulson, I. M., 'Mapping the release of volatiles in the inner comae of comets C/2012 F6 (Lemmon) and C/2012 S1 (ISON) using the Atacama Large Millimeter/Submillimeter Array,' The Astrophysical Journal Letters, 2014, 792, p. L2.

Dello Russo, N., DiSanti, M. A., Mumma, M. J., Magee-Sauer, K., and Rettig, T. W., 'Carbonyl sulfide in comets C/1996 B2 (Hyakutake) and C/1995 O1 (Hale-Bopp): Evidence for an extended source in Hale-Bopp,' Icarus, 1998, 135(2), pp. 377–388.

Dello Russo, N., Kawakita, H., Jr., V. R. J., and Weaver H., A., 'Emerging trends and a comet taxonomy based on the volatile chemistry measured in thirty comets with high-resolution infrared spectroscopy between 1997 and 2013,' Icarus, 2016a, 278, pp. 301–332.

Dello Russo, N., Vervack, R. J. J., Kawakita, H., Cochran, A., McKay, A. J., Harris,W. M., Weaver, H. A., Lisse, C. M., DiSanti, M. A., Kobayashi, H., Biver, N., Bockelée-Morvan, D., Crovisier, J., Opitom, C., and Jehin, E., 'The compositional evolution of C/2012 S1 (ISON) from ground-based high-resolution infrared spectroscopy as part of a worldwide observing campaign,' Icarus, 2016b, 266, pp. 152–175.

DiSanti, M. A., Bonev, B. P., Dello Russo, N., Vervack, R. J. J., Gibb, E. L., Roth, N. X., McKay, A. J., and Kawakita, H., 'Hypervolatiles in a Jupiter-family comet: Observations of 45P/Honda-Mrkos-Pajdušáková using iSHELL at theNASA-IRTF,' The Astronomical Journal, 2017, 154(6), p. 246.

DiSanti, M. A., Bonev, B. P., Gibb, E. L., Paganini, L., Villanueva, G. L., Mumma, M. J., Keane, J. V., Blake, G. A., Dello Russo, N., Meech, K., Vervack, R. J. J., and McKay, A. J., 'En route to destruction: The evolution in composition of ices in comet D/2012 S1 (ISON) between 1.2 and 0.34 au from the Sun as revealed at infrared wavelengths,' The Astrophysical Journal, 2016, 820(1), p. 20.

DiSanti, M. A., Bonev, B. P., Magee-Sauer, K., Dello Russo, N., Mumma, M. J., Reuter, D. C., and Villanueva, G. L., 'Detection of formaldehyde emission in comet C/2002 T7 (LINEAR) at infrared wavelengths: Line-by-line validation of modeled fluorescent intensities,' The Astrophysical Journal, 2006, 650(1), pp. 470–483.

DiSanti, M. A., Mumma, M. J., Dello Russo, N., and Magee-Sauer, K., 'Carbon monoxide production and excitation in comet C/1995 O1 (Hale-Bopp): Isolation of native and distributed CO sources,' Icarus, 2001, 153(2), pp. 361–390.

Disanti, M. A., Mumma, M. J., and Lacy, J. H., 'A sensitive upper limit to ocs in comet Austin (1989 C1) from a search for ν_3 emission at 4.85 `m,' ICARUS, 1992, 97, pp. 155–158.

DiSanti, M. A., Villanueva, G. L., Paganini, L., Bonev, B. P., Keane, J. V., Meech, K. J., and Mumma, M. J., 'Pre- and post-perihelion observations of C/2009 P1 (Garradd): Evidence for an oxygen-rich heritage?' Icarus, 2014, 228, pp. 167–180.

Ehrenfreund, P., Irvine, W., Becker, L., Blank, J., Brucato, J. R., Colangeli, L., Derenne, S., Despois, D., Dutrey, A., Fraa.e, H., Lazcano, A., Owen, T., Robert, F., and ISSI-Team, I. S. S. I., 'Astrophysical and astrochemical insights into the origin of life,' Reports on Progress in Physics, 2002, 65, p. 10.

Ferrante, R. F., Moore, M. H., Spiliotis, M. M., and Hudson, R. L., 'Formation of interstellar OCS: Radiation chemistry and ir spectra of precursor ices,' APJ, 2008, 684, pp. 1210–1220.

Fuente, A., Cernicharo, J., Agúndez, M., Berné, O., Goicoechea, J. R., Alonso-Albi, T., and Marcelino, N., 'Molecular content of the circumstellar disk in ab aurigae. First detection of so in a circumstellar disk,' AAP, 2010, 524, p. A19.

Geballe, T. R., Baas, F., Greenberg, J. M., and Schutte, W., 'New infrared absorption features due to solid phase molecules containing sulfur in w 33a.' AAP, 1985, 146, pp. L6–L8.

Gibb, E. L., Bonev, B. P., Villanueva, G., DiSanti, M. A., Mumma, M. J., Sudholt, E., and Radeva, Y., 'Chemical composition of comet C/2007 N3 (Lulin): Another "atypical" comet,' The Astrophysical Journal, 2012, 750(2), p. 102.

Gomes, R., Levison, H. F., Tsiganis, K., and Morbidelli, A., 'Origin of the cataclysmic late heavy bombardment period of the terrestrial planets,' Nature, 2005, 435(7041), pp. 466–469.

Greene, T. P., Tokunaga, A. T., Toomey, D. W., and Carr, J. B., 'CSHELL: a high spectral resolution 1-5 um cryogenic echelle spectrograph for the IRTF,' Proceedings of the SPIE, 1993, 1946, pp. 313–324.

Guilloteau, S., Di Folco, E., Dutrey, A., Simon, M., Grosso, N., and Piétu, V., 'A sensitive survey for 13co, cn, h2co, and so in the disks of t tauri and herbig ae stars,' AAP, 2013, 549, p. A92.

Guilloteau, S., Reboussin, L., Dutrey, A., Chapillon, E., Wakelam, V., Piétu, V., Di Folco, E., Semenov, D., and Henning, T., 'Chemistry in disks. x. the molecular content of protoplanetary disks in taurus,' AAP, 2016, 592, p. A124.

Isoniemi, E., Pettersson, M., Khriachtchev, L., Lundell, J., and Räsänen, M., 'Infrared spectroscopy of h2s and sh in rare-gas matrixes,' Journal of Physical Chemistry A, 1999, 103, pp. 679–685.

Jiménez-Escobar, A., Muñoz Caro, G. M., and Chen, Y. J., 'Sulphur depletion in denseclouds and circumstellar regions. organic products made from uv photoprocessing of realistic ice analogs containing h2s,' MNRAS, 2014, 443, pp. 343–354.

Kamp, L. W. and Taylor, F. W., 'Radiative-transfer models of the night side of venus,' ICARUS, 1990, 86, pp. 510–529.

Laas, J. C. and Caselli, P., 'Modeling sulfur depletion in interstellar clouds,' AAP, 2019, 624, p. A108.

Le Gal, R., Öberg, K. I., Loomis, R. A., Pegues, J., and Bergner, J. B., 'Sulfur chemistry in protoplanetary disks: Cs and H_2CS,' APJ, 2019, 1, p. 72.

Le Roy, L., Altwegg, K., Balsiger, H., Berthelier, J.-J., Bieler, A., Briois, C., Calmonte, U., Combi, M. R., De Keyser, J., Dhooghe, F., Fiethe, B., Fuselier, S. A., Gasc, S., Gombosi, T. I., Hässig, M., Jäckel, A., Rubin, M., and Tzou, C.-Y., 'Inventory of the volatiles on comet 67P/Churyumov-Gerasimenko from Rosetta/ROSINA,' Astronomy & Astrophysics, 2015, 583, p. A1.

Leman, L., Orgel, L., and Ghadiri., M. R., 'Carbonyl sulfide-mediated prebiotic formation of peptides,' Science, 2004, 306, pp. 283–286.

Levison, H. F., Morbidelli, A., Tsiganis, K., Nesvorny, D., and Gomes, R., 'Late orbital instabilities in the outer planets induced by interaction with a self-gravitating planetesimal disk,' The Astronomical Journal, 2011, 142(5), p. 152.

McKay, A. J., DiSant, M. A., Cochran, A. L., Bonev, B. P., Dello Russo, N., Vervack, R. J., Jr. Gibb, E., Roth, N. X., Saki, M., Khan, Y., Kawakita, H., 'Quantifying the Hypervolatile Abundances in Jupiter-family Comet 46P/Wirtanen,' The Planetary Science Journal, 2021, 2, P. 21.

Millar, T. J. and Herbst, E., 'Organo-sulphur chemistry in dense interstellar clouds.' AAP, 1990, 231, pp. 466–472.

Moore, M. H., Hudson, R. L., and Carlson, R. W., 'The radiolysis of so 2 and h 2s in water ice: Implications for the icy jovian satellites,' ICARUS, 2007, 189, pp. 409–423.

Mumma, M. J. and Charnley, S. B., 'The chemical composition of comets – emerging taxonomies and natal heritage,' Annual Review of Astronomy and Astrophysics, 2011, 49(1), pp. 471–524.

Okabe, H., 'Photochemistry of small molecules,' https://ui.adsabs.harvard.edu/abs/1978psm..book.....O, 1978, Provided by the SAO/NASA Astrophysics Data System.

Pacheco-Vázquez, S., Fuente, A., Baruteau, C., Berné, O., Agúndez, M., Neri, R., Goicoechea, J. R., Cernicharo, J., and Bachiller, R., 'High spatial resolution imaging of so and h2co in ab auriga: The first so image in a transitional disk,' AAP, 2016, 589, p. A60.

Paganini, L. and Mumma, M. J., 'A solar-pumped fluorescence model for line-by-line emission intensities in the b–x, a–x, and x–x band systems of cn,' 2016, 226, p. 3.

Paganini, L., Mumma, M. J., Gibb, E. L., and Villanueva, G. L., 'Ground-based detection of deuterated water in comet C/2014 Q2 (Lovejoy) at IR wavelengths,' 2017, 836, p. L25.

Paganini, L., Mumma, M. J., Villanueva, G. L., DiSanti, M. A., Bonev, B. P., Lippi, M., and Boehnhardt, H., 'The chemical composition of CO-rich comet C/2009 P1 (Garradd) at Rh = 2.4 and 2.0 AU before perihelion,' The Astrophysical Journal Letters, 2012, 758(1), p. L13.

Palumbo, M. E., Geballe, T. R., and Tielens, A. G. G. M., 'Solid carbonyl sulfide (ocs) indense molecular clouds,' APJ, 1997, 479, pp. 839–844.

Palumbo, M. E., Tielens, A. G. G. M., and Tokunaga, A. T., 'Solid Carbonyl Sulphide (OCS) in w33a,' APJ, 1995, 449, p. 674.

Phuong, N. T., Chapillon, E., Majumdar, L., Dutrey, A., Guilloteau, S., Piétu, V., Wakelam, V., Diep, P. N., Tang, Y. W., Beck, T., and Bary, J., 'First detection of H_2S in a protoplanetary disk. the dense gg tauri a ring,' AAP, 2018, 616, p. L5.

Radeva, Y. L., Mumma, M. J., Bonev, B. P., DiSanti, M. A., Villanueva, G. L., Magee-Sauer, K., Gibb, E. L., and Weaver, H. A., 'The organic composition of comet C/2000 WM1 (LINEAR) revealed through infrared spectroscopy,' Icarus, 2010, 206(2), pp. 764–777.

Rayner, J., Bond, T., Bonnet, M., Jaffe, D., Muller, G., and Tokunaga, A., 'iSHELL: a1-5 micron cross-dispered R=70,000 immersion grating spectrograph for IRTF,' Proceedings of the SPIE, 2012, 8446, p. 84462C. 142

Rayner, J., Tokunaga, A., Jaffe, D., Bonnet, M., Ching, G., Connelley, M., Kokubun, D., Lockhart, C., and Warmbier, E., 'iSHELL: a construction, assembly and testing,' Proceedings of the SPIE, 2016, 9908, p. 990884.

Rickman, H., Marchi, S., A'Hearn, M. F., Barbieri, C., El-Maarry, M. R., Güttler, C., Ip, W.-H., Keller, H. U., Lamy, P., Marzari, F., Massironi, M., Naletto, G., Pajola, M., Sierks, H., Koschny, D., Rodrigo, R., Barucci, M. A., Bertaux, J.-L., Bertini, I., Cermonese, G., Da Deppo, V., Debei, S., De Cecco, M., Fornasier, S., Fulle, M., Groussin, O., Gutiérrez, P. J., Hviid, S. F., Jorda, L., Knollenberg, J., Kramm, J.-R., Kührt, E., Küppers, M., Lara, L. M., Lazzarin, M., Lopez-Moreno, J. J., Michalik, H., Sabau, L., Thomas, N., Vincent, J.-B., and Wenzel, K.-P., 'Comet 67P/Churyumov-Gerasimenko: Constraints on its origins from OSIRIS observations,' Astronomy & Astrophysics, 2015, 583, p. A44.

Roth, N. X., Gibb, E. L., Bonev, B. P., DiSanti, M. A., Dello Russo, N., McKay, A. J., Vervack, J., Ronald J., Kawakita, H., Saki, M., Biver, N., Bockelée-Morvan, D., Feaga, L. M., Fougere, N., Cochran, A. L., Combi, M., and Shou, Y., 'Probing the evolutionary history of comets: An investigation of the hypervolatiles CO, CH4, and C2H6 in the Jupiter-family comet 21P/Giacobini-Zinner,' The Astronomical Journal, 2020, 159, p. 42.

Roth, N. X., Gibb, E. L., Bonev, B. P., DiSanti, M. A., Dello Russo, N., Vervack, R. J. J., McKay, A. J., and Kawakita, H., 'A tale of "two" comets: The primary volatile composition of comet 2P/Encke across apparitions and implications for cometary science,' The Astronomical Journal, 2018, 156, p. 251.

Ruffle, D. P., Hartquist, T. W., Caselli, P., and Williams, D. A., 'The sulphur depletion problem,' MNRAS, 1999, 306, pp. 691–695.

Sakai, N., Oya, Y., López-Sepulcre, A., Watanabe, Y., Sakai, T., Hirota, T., Aikawa, Y., Ceccarelli, C., Lefloch, B., Caux, E., Vastel, C., Kahane, C., and Yamamoto, S., 'Subarcsecond analysis of the infalling-rotating envelope around the class i protostar iras 04365+2535,' APJL, 2016, 820, p. L34.

Sakai, N., Sakai, T., Hirota, T., Watanabe, Y., Ceccarelli, C., Kahane, C., Bottinelli, S., Caux, E., Demyk, K., Vastel, C., Coutens, A., Taquet, V., Ohashi, N., Takakuwa, S., Yen, H., Aikawa, Y., and Yamamoto, S., 'Change in the chemical composition of infalling gas forming a disk around a protostar,' NAT, 2014, 507, pp. 78–80.

Saki, M., Gibb, E., Bonev, B., Roth, N., DiSanti, M., Khan, Y., Dello Russo, N., Vervack, R., McKay, Kawakita, H., 'An Investigation of the Abundances of Hypervolatiles CO, CH_4, and C_2H_6 in Jupiter-family Comet 46P/Wirtanen,' Astronomical Journal, 2021, in pres.

Schleicher, D., Millis, R., Jorda, L., Lecacheux, J., Colas, F., Woodney, L. M., McMullin, J., and A'Hearn, M. F., 'Comet c/1996 b2 (hyakutake),' IAUCIRC, 1996, 6344, p. 1.

Stern, S. A., 'The evolution of comets in the Oort cloud and Kuiper belt,' Nature, 2003, 424(6949), pp. 639–642.

Teague, R., Henning, T., Guilloteau, S., Bergin, E. A., Semenov, D., Dutrey, A., Flock, M., Gorti, U., and Birnstiel, T., 'Temperature, mass, and turbulence: A spatially resolved multiband non-lte analysis of cs in tw hya,' APJ, 2018, 864, p. 133.

Tieftrunk, A., Pineau des Forets, G., Schilke, P., and Walmsley, C. M., 'SO and H_2S in low density molecular clouds.' AAP, 1994, 289, pp. 579–596.

Tokunaga, A. T., Toomey, D. W., Carr, J., Hall, D. N. B., and Epps, H. W., 'Design for a 1-5 micron cryogenic echelle spectrograph for the NASA IRTF,' Proceedings of the SPIE, 1990, 1235, p. 131.

Vidal, T. H. G., Loison, J., Jaziri, A. Y., Ruaud, M., Gratier, P., and Wakelam, V., 'On the reservoir of sulphur in dark clouds: chemistry and elemental abundance reconciled,' MNRAS, 2017, 469, pp. 435–447.

Vidal, T. H. G. andWakelam, V., 'A new look at sulphur chemistry in hot cores and corinos,' MNRAS, 2018, 474, pp. 5575–5587.

Villanueva, G. L., Mumma, M. J., Bonev, B. P., DiSanti, M. A., Gibb, E. L., Boehnhardt, H., and Lippi, M., 'A sensitive search for deuterated water in comet 8P/Tuttle,' The Astrophysical Journal Letters, 2009, 690(1), pp. L5–L9.

Villanueva, G. L., Mumma, M. J., Bonev, B. P., Novak, R. E., Barber, R. J., and DiSanti, M. A., 'Water in planetary and cometary atmospheres: H2O/HDO transmittance and fluorescence models,' Journal of Quantitative Spectroscopy and Radiative Transfer, 2012, 113(3), pp. 202–220.

Villanueva, G. L., Mumma, M. J., DiSanti, M. A., Bonev, B. P., Gibb, E. L., Magee-Sauer, K., Blake, G. A., and Salyk, C., 'The molecular composition of comet C/2007 W1 (Boattini): Evidence of a peculiar outgassing and a rich history,' Icarus, 2011, 216(1), pp. 227–240.

Villanueva, G. L., Mumma, M. J., Novak, R. E., and Hewagama, T., 'Identification of a new band system of isotopic CO2 near 3.3 um: Implications for remote sensing of biomarker gases on Mars,' Icarus, 2008, 195(1), pp. 34–44.

Villanueva, G. L., Smith, M. D., Protopapa, S., Faggi, S., and Mandell, A. M., 'Planetary spectrum generator: An accurate online radiative transfer suite for atmospheres, comets, small bodies and exoplanets,' 2018, 217, pp. 86–104.

Vokrouhlicky, D., Nesvorny, D., Dones, L., 'Origin and Evolution of Long-period Comets,' AJ, 2019, 157, P. 181

Woodney, L. M., McMullin, J., and A'Hearn, M. F., 'Nitrogen sulfide in comets hyakutake (C/1996 B2) and hale–bopp (C/1995 O1),' PSS, 1997, 45, p. 717.

Woods, P. M., Occhiogrosso, A., Viti, S., Kanuchová, Z., Palumbo, M. E., and Price, S. D., 'A new study of an old sink of sulphur in hot molecular cores: the Sulphur residue,' MNRAS, 2015, 450, pp. 1256–1267.

Zasowski, G., Kemper, F., Watson, D. M., Furlan, E., Bohac, C. J., Hull, C., and Green, J. D., 'Spitzer infrared spectrograph observations of class i/ii objects in taurus: Composition and thermal history of the circumstellar ices,' APJ, 2009, 694, pp. 459–478.

Zolensky, M. E., Zega, T. J., Yano, H., Wirick, S., Westphal, A. J., Weisberg, M. K., Weber, I., Warren, J. L., Velbel, M. A., Tsuchiyama, A., Tsou, P., Toppani, A., Tomioka, N., Tomeoka, K., Teslich, N., Taheri, M., Susini, J., Stroud, R., Stephan, T., Stadermann, F. J., Snead, C. J., Simon, S. B., Simionovici, A., See, T. H., Robert, F., Rietme.er, F. J. M., Rao,W., Perronnet, M. C., Papanastassiou, D. A., Okudaira, K., Ohsumi, K., Ohnishi, I., Nakamura-Messenger, K., Nakamura, T., Mostefaoui, S., mikouchi, T., Meibom, A., Matrajt, G., Marcus, M. A., Leroux, H., Lemelle, L., Le, L., Lanzirotti, A., Langenhort, F., Krot, A. N., Keller, L. P., Kearsey, A. T., Joswiak, D., Jacob, D., Ishii, H., Harvey, R., Hagiya, K., Grossman, L., Grossman, J. N., Graham, g. A., Gounelle, M., Gillet, P., Genge, M. J., Flynn, G., Ferroir, T., Fallon, F., Ebel, D. S., Dai, Z. R., Cordier, P., Clark, B., Chi, M., Butterworth, A. L., Brownlee, D. E., Bridges, J. C., Brennan, S., Brearley, A., Bradley, J. P., Bleuet, P., Bland, P. A., and Bastien, R., 'Mineralogy and petrology of comet 81P/Wild 2 nucleus samples,' Science, 2006, 314(5806), p. 1735.

II. CHEMICAL COMPOSITION OF OUTBURSTING COMET C/2015 ER61 (PANSTARRS)

ABSTRACT

Comet C/2015 ER61 (PanSTARRS) is a long period Oort cloud comet whose favorable approach to the inner parts of solar system in April-May 2017 enabled us to characterize its primary volatile composition using the iSHELL spectrograph mounted on the 3-m NASA Infrared Telescope Facility (IRTF) on Mauna Kea, Hawaii. We used three iSHELL settings (covering ~ 2.8 – 5.2 μm) to sample fluorescent emissions from H_2O, OH, CH_3OH, HCN, C_2H_2, NH_3, CO, CH_4, C_2H_6, H_2CO, and OCS on multiple dates ranging from UT 2017 April 15 (shortly after its April 4 outburst) to May 13, nearly 30 days before the detection of its double nucleus. Our observations also offered the opportunity to obtain sensitive 3σ upper limits for cyanoacetylene (HC_3N). We report rotational temperatures (T_{rot}), production rates (Qs), abundance (mixing) ratios (relative to H_2O and C_2H_6), and spatial distributions in the coma. ER61 exhibits variability in production rates of many species on short (day-to-day) and long (pre- vs. post-perihelion) timescales. The relative abundances of these volatile species remained consistent within uncertainties during our pre-perihelion observations but tended to decrease during our post-perihelion observations (with the exception of CH_3OH and HCN). The short-timescale variability in the production rates of these volatiles could be due to diurnal effects (over the course of the rotation of the nucleus) and/or the effect of its outburst. The decrease in the production rates and hence the mixing ratios in some volatiles in post-perihelion dates could be due to the presence of seasonal effects in ER61.

1. INTRODUCTION

Comets are small, volatile-rich, relatively unprocessed remnants of the early solar system. They formed in the protosolar nebula in the giant planet region between 5 – 30 au (or more) from the Sun. They were ejected into their current stable dynamical reservoir of either the Oort cloud (Vokrouhlický et al., 2019) or the Kuiper belt (Nesvorný et al., 2017) by the migration of giant planets. Owing to their small size, comets lack a known mechanism for internal self-heating; thus, it is likely that the interior compositions of comets have not been significantly modified and should reflect the composition and the conditions where (and when) they formed (Mumma and Charnley 2011; Bockelée-Morvan et al., 2004). Owing to increasing solar radiation as comets enter the inner solar system (heliocentric distance < 3 au), a freely expanding atmosphere (i.e., coma) along with dust tail and ion tail will form. We can study these features using spectroscopy. The primary volatile composition of the coma can be used as a proxy for the chemical composition of its nucleus, and therefore provide insights into the initial conditions and subsequent evolution of the early solar system.

Long period Oort cloud comets represent excellent targets for study as their nuclei have likely been less modified since their formation than those of short-period comets (Vokrouhlický et al., 2019). Most processes that can change the properties of comet nuclei only affect a thin layer (a few meters deep) from the surface, which is thought to be excavated over the course of a perihelion passage into the inner solar system (Stern et al., 2003; Le Roy et al., 2015; Gronoff et al., 2020; Saki et al., 2020a). This emphasizes the importance of obtaining both pre- and post-perihelion observations of comets whenever

possible. Some comets exhibit a sudden eruption of materials, referred to as an outburst, close to their perihelion passage. Outbursts are known to start with the sudden appearance and steep brightening of an unresolved plume of material and are often described by a nuclear magnitude (Sekanina 2010, 2017). Comets that outburst represent additional opportunities to probe the likely more pristine material below a comet's topmost surface layers.

High-resolution infrared (IR) spectroscopy is a valuable way to characterize the primary volatile composition of the nucleus through analysis of fluorescent emissions in the coma. Coupled with protoplanetary disk models, the nucleus composition inferred from these studies may place observational constraints on the physics and chemistry operating in the nascent protoplanetary disk mid-plane where comets formed. With about 40 comets characterized in the IR and radio and more than 200 comets cataloged in photo-dissociation products at optical wavelengths, a large number of species have been identified in cometary atmospheres, both from ground- and space-based observations (e.g., Cochran et al., 2015; Le Roy et al., 2015; Biver et al., 2015a; Dello Russo et al., 2016b; Roth et al., 2018; Saki et al., 2020a, 2020b).

Certain primary volatiles — C_2H_2, CO, CH_4, and OCS — are under-represented in studies of comets as a whole (Saki et al., 2020a; Dello Russo et al., 2016a). IR coma studies indicate that Jupiter-family comets (JFCs; originate from the Kuiper belt and have short orbital periods) are in general depleted relative to Oort cloud comets (OCCs; originate from the Oort cloud and have long orbital periods) in the hypervolatiles CO and CH_4, which may reflect the effects of repeated close perihelion passages on their volatile content (Roth et al., 2020; Saki et al., 2020b; Dello Russo et al., 2016a). On the other hand, large optical

surveys of product species found no correlation in depleted chemistry and dynamical age in JFCs, suggesting that compositional differences may instead be primordial and indicative of differences in formation histories for Jupiter-family comets compared to Oort cloud comets (A'Hearn et al., 1995). The detection of crystalline silicates in some comets, coupled with updates in dynamical models (e.g., Levison et al., 2011), suggests that scattering processes and large-scale mixing of materials in the early solar nebula have complicated the distinction between comet-forming regions (Bockelée-Morvan et al., 2000, 2016; Gomes et al., 2005; Zolensky et al., 2006; Dello Russo et al., 2016b). Therefore, both the Oort cloud and Kuiper belt could contain comets that represent varying (or, at the other extreme, largely overlapping) formation regions in the solar nebula. The Rosetta mission to comet 67P/Churyumov–Gerasimenko (hereafter 67P) revealed a heterogeneous nucleus, adding more complexity to these scenarios (Rickman et al., 2015; Le Roy et al., 2015; A'Hearn 2017).

In this work we characterize the chemical composition of comet C/2015 ER61 (PanSTARRS) (hereafter ER61) shortly after its 2017 April 4 outburst. We report the detection of H_2O, OCS, C_2H_6, CH_3OH, H_2CO, NH_3, C_2H_2, and HCN, as well as stringent 3σ upper-limits for CO, CH_4, and HC_3N. In Section 2, we discuss the outburst of ER61. In Section 3, we discuss our observations and our data reduction methodology. In Section 4, we present our results. In Section 5, we discuss our results and place them in the context of comets characterized to date.

2. OUTBURST IN ER61

Outbursts appear to be activated by gases released from a reservoir of a highly volatile material stored in the nucleus that heats up and/or becomes pressurized as the comet gets closer to the Sun (Sekanina 2017). An in-situ example is provided by cliff collapses in comet 67P's northern and southern hemispheres and outbursts near the sharp boundary in the small lobe observed in 2015, during the Rosetta mission (Vincent et al., 2016; El-Maarry et al., 2017, Pajola et al., 2017). The products observed during an outburst are the escaping gases and ice/dust grains that are dragged from the nucleus by the released gases, and outbursts are characterized as gas-dominated or dust dominated depending on which component prevails (see Sekanina 2017 for details).

These two types of outburst (dust- or gas-dominated) have both similarities and differences (see Figure 6 in Sekanina 2017). An important similarity is an active phase: the activity of the outburst source on the nucleus begins at the time of onset and terminates at the time of peak magnitude. The duration of the active phase is thus defined as the interval between the onset and the peak. The light curves can be used to distinguish between the two types of outbursts. Dust-dominated outbursts are exemplified by a plateau during which the comet's brightness subsides gradually. Gas-dominated outbursts are characterized by a steep decline in brightness after the peak that nearly mirrors the initial brightening (see Section 2.4 of Sekanina 2017 for details). This occurs because the brightness variations in the gas-dominated outbursts are determined by the fairly short dissociation and ionization lifetimes of the radiating molecules in the coma, coupled with relatively high gas velocities ($\sim$1 km s^{-1}). Because of the lower velocities of solid particles,

however, the residence times of dust in the coma are substantially longer than those of radiating molecules, so a post-peak plateau in the dust-dominated outbursts is observed.

If the outburst is preceded by one or more precursor eruptions, the event becomes a composite explosion. Dust particles might also fragment in the coma, expanding their total cross-sectional area and increasing the comet's brightness over a longer period of time; such a scenario is referred to as an extended dust-dominated outburst (Sekanina 2010, 2017). The sources of outbursts typically have a fairly limited extent on the scale of nuclear dimensions, so most outbursts can be classified as either local or regional episodes. Under exceptional conditions, a major part of the nucleus may be involved. Such events are global in extent, with potentially severe implications for the comet's future evolution; they are referred to as giant explosions (Sekanina 2010, 2017). However, most cometary outbursts appear to be fairly short-lived, at least in terms of the total brightness, with the light curve exhibiting a sharp peak rather than a plateau, and thus no signature of dust dominance (see Figures 1– 4 in Sekanina 2017; Clements & Fernandez 2021).

Outbursts have been observed in many comets such as 29P/Schwassmann-Wachmann 1 (Wierzchos & Womack 2020), 73P/Schwassmann-Wachmann (Kobayashi et al., 2007), 168P/Hergenrother (Sekanina 2014), 17P/Holmes (Shinnaka et al., 2018), and 1P/Halley (Gronkowski 2002), and in the extreme signifying disruption of the nucleus in comets such as C/2001 A2 (Sekanina et al., 2002) and C/1999 S4 (Chubko et al., 2005; Dello Russo et al., 2005). Examination of the visual light curve for ER61 indicates that its magnitude was 8.3 on UT April 3.8 (equal in brightness to two days earlier), whereas 9 hours later, on UT April 4.17, it was estimated to be 7.4, 0.7 magnitude brighter, implying a brightening rate of 1.9 mag per day. This suggests that the outburst likely started on UT

April 3.9 ± 0.1 and peaked on UT April 6.5 (±1 day). The overall variation in amplitude amounted to 2.1± 0.1 mag (see Section 4 of Sekanina (2017) for a detailed discussion).

Two months after its outburst, on UT 2017 June 13, a double nucleus was observed, with a faint companion, of apparent magnitude ~16, located in the primary's coma but displaced ~ 0.2' in the anti-sunward direction (Masi & Schwartz 2017; Sekanina 2017). An in-depth investigation of the companion's motion and its variable magnitude over a course of three weeks in June-July 2017 was conducted by Sekanina (2017). Given the temporal correlations between outbursts and nucleus fragmentation of many comets, Sekanina (2017) concluded that the observed outburst and nuclear fragmentation of ER61 might be the products of the same event (Sekanina, 2017). Our ER61 April observations were conducted approximately 11 days after its major outburst and our May observations were conducted about 30 days before the first detection of its double nucleus.

3. OBSERVATIONS AND DATA REDUCTION

ER61 is a long period Oort Cloud comet which was first spotted in several images taken under the auspices of the Pan-STARRS project with the 180-cm f/2.7 Ritchey-Chretien reflector on Haleakala, Maui, on March 14–15, 2015 (Tubbiolo et al., 2015, Sekanina 2017). It was originally classified as an asteroid (2015 ER61) by the Minor Planet Center (2015), even though it was almost 9 AU from the Sun and following a nearly parabolic orbit (Sekanina 2017). The object was subsequently detected in several earlier Pan-STARRS images from January and February 2015 (Tubbiolo et al., 2015). When signs

of cometary activity were first noticed in late December 2015 and confirmed in January 2016, the object was re-classified as a long-period comet (Sekanina 2017).

ER61 reached perihelion (1.042 AU) on UT 2017 May 9.77, approximately 35 days after its major outburst on April 4, and was closest to Earth (1.18 AU) on UT 2017 April 18. We observed ER61 on UT 2017 April 15–17 (near closest approach to Earth) and May 11–13 (near perihelion) using the high-resolution ($\lambda/\Delta\lambda \sim 40{,}000$) IR immersion grating echelle spectrograph iSHELL (Rayner et al., 2012, 2016) at the 3-m NASA Infrared Telescope Facility (IRTF) on Maunakea, HI. We characterized ER61 using three iSHELL settings: (1) our custom L-band setting ("Lcustom", ~ 2.8 – 3.2 μm) that contains emissions from C_2H_2, HCN, NH_3, and H_2O; (2) the M2 setting (~ 4.5 – 5.2 μm) that samples emissions of OCS, CO, and H_2O; and (3) the Lp1 setting (~ 3.2 – 3.6 μm) that samples emission lines of CH_4, C_2H_6, CH_3OH, H_2CO, and OH* (OH* represents OH from prompt emission, which is a direct proxy for the production and spatial distribution of H_2O; see Bonev et al., 2006). The fluorescence emissions of H_2O in the Lcustom setting sample a range of excitation energies and enable a robust determination of rotational temperature (see Figure 1, and Section 4.3). We also determined rotational temperatures for C_2H_6, HCN, and CH_3OH, which were all found to be consistent with that for H_2O, although less well constrained.

Table 1 shows our observing log for comet ER61. Observations were performed with a 0.75" (6-pixel) wide slit, oriented along the projected Sun-comet line with position angle (PA) ~ 252° on all dates. All observations were performed using a standard ABBA nod pattern (sequence of four scans) where the A and B beams were placed symmetrically about the midpoint along the 15" long slit and separated by half its length. Thus, the comet

was present in both beams, thereby providing increased signal-to-noise (by a factor of up to $\sqrt{2}$ compared with nodding to blank sky).

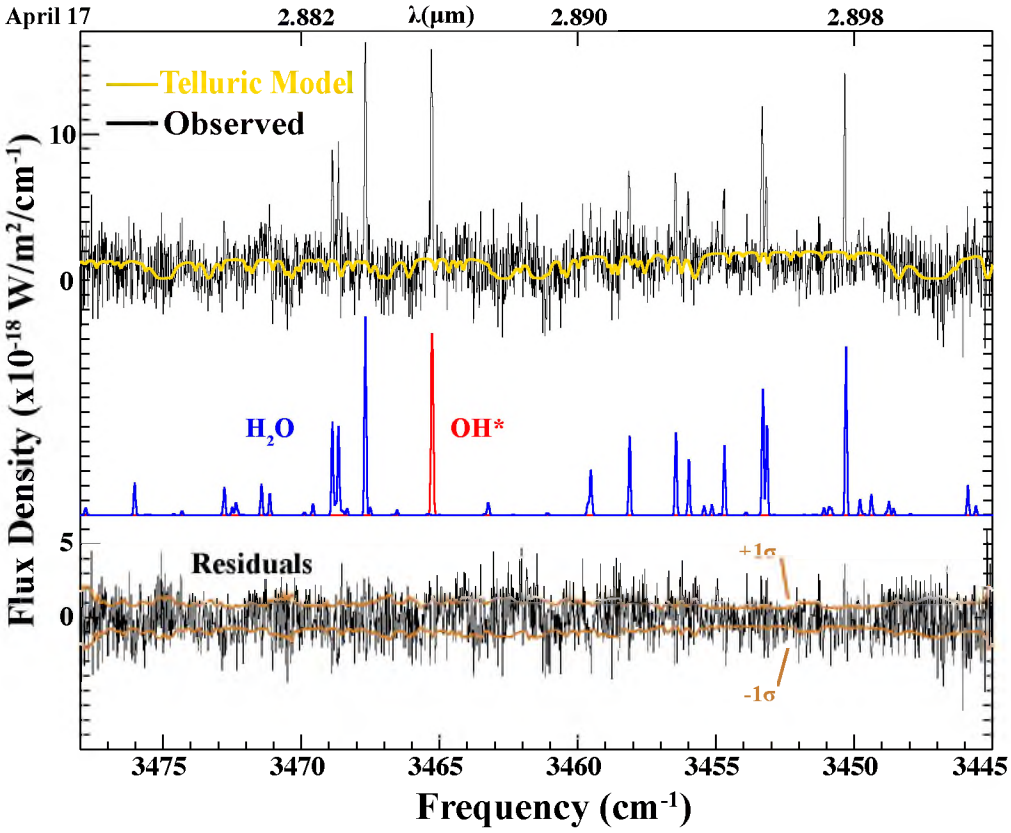

Figure 1. Extracted spectra showing fluorescence emission of H_2O and OH* in ER61. The yellow trace overplotted on the uppermost cometary spectrum is the best-fit telluric transmittance model (convolved to the instrumental resolution). The fluorescence emission models of H_2O and OH* (color-coded for clarity) are plotted below. At the bottom of the panel is the residual spectrum (after subtracting the telluric absorption model and the fluorescence models), with the 1σ uncertainty envelope overplotted in bronze.

Combining the frames as A-B-B+A (comet-sky-sky+comet) canceled out background thermal continuum, sky emission (lines and continuum), and instrumental biases to second order in airmass (see Figure 2 of DiSanti et al., 2001). The data were

cleaned of cosmic ray hits and hot pixels and rectified to produce two-dimensional (spatial-spectral) frames, where each row corresponds to a constant (and unique) spatial position along the slit, and each column to a unique wavelength.

Table 1. Observing Log for ER61.

UT Date (2017)-Setting	UT time	R_h (AU)	Δ (AU)	$d\Delta/dt$ (km s^{-1})	T_{int} (minutes)	Slit PA
April 15- Lp1	15:29-15:48	1.11	1.18	-2.29	20	253°
April 16-Lp1	15:24-17:44	1.11	1.17	-1.62	76	252°
April 16-Lcustom	18:37-20:12	1.11	1.17	-1.25	44	252°
April 17-Lcustom	15:01-15:40	1.10	1.17	-1.19	36	252°
May 11-Lp1	14:29-15:44	1.04	1.24	8.94	96	250°
May 12-M2	14:16-17:16	1.04	1.25	9.21	94	250°
May 12-Lp1	17:36-19:25	1.04	1.25	9.56	60	250°
May 13-Lcustom	14:34-20:55	1.04	1.25	9.68	80	250°

Notes. R_h, Δ, and $d\Delta/dt$ are heliocentric distance, geocentric distance, and geocentric velocity, respectively, of ER61, and T_{int} is total integration time on source. The slit position angle (PA) was oriented along the projected Sun-comet line on all dates.

The Planetary Spectrum Generator (Villanueva et al., 2018), optimized for Maunakea's atmospheric conditions, was used to generate atmospheric models, to assign wavelength scales to the spectra, and to establish absolute column burdens of the component absorbing species in the terrestrial atmosphere. The atmospheric models were binned to the resolution of the comet spectrum and scaled to the comet's continuum intensity. They were then subtracted from each row of the cometary spectra; co-addition of multiple rows (15 rows, approximately 2.5") resulted in the comet emission spectra. Figure 1 shows this procedure. The fully-resolved best-fit model provided a precise value for the transmittance at each Doppler-shifted line position. Our observational procedures and data

reduction algorithms have been rigorously tested and well documented in peer-reviewed literature (Bonev 2005; Dello Russo et al., 1998; DiSanti et al., 2001, 2006, 2014, 2017; Villanueva et al., 2009; Radeva et al., 2010). We note that spatially resampling using a third-order polynomial more completely removed the curvature in the spatial dimension from iSHELL frames, so we employed this in place of the previously used second-order polynomials (DiSanti et al., 2017; Roth et al., 2018).

For flux calibration, a suitably bright IR flux standard star was observed using a 4" wide slit on each date and for each setting (using a wider slit for the star than was used for the comet helps minimize loss of signal and thereby achieve a truer measure of the stellar continuum; see Bonev 2005; Radeva et al., 2010; Villanueva et al., 2011a, 2011b for further details regarding flux calibrations). Seeing was consistently ~0.7″ in our April dates. It was ~0.6″ on UT May 11, and ~ 0.8″ and 0.7″ on UT May 12 and May 13 respectively.

4. RESULTS

We determined rotational temperatures (T_{rot}), volatile production rates (Q, molecules s^{-1}), and the abundance (or "mixing") ratios Q_X/Q_{H2O} (expressed in %) for volatile species in ER61. We found consistent results and excellent fits to the comet spectra, both for telluric absorptions and for cometary emission features.

4.1. SPATIAL PROFILE

Long-slit high-resolution infrared observations of comets permit investigations of processes in the inner coma, where both nucleus and extended sources (i.e., release from

one or more sources in the coma) may contribute to the production and spatial distribution of a particular volatile. Analysis of spatial profiles of emissions for coma molecules can indicate whether their distributions differ from that expected for direct sublimation from the nucleus, as opposed to release from extended sources in the coma (Dello Russo et al., 1998, 2016a; DiSanti et al., 2001; Brooke et al., 2003). The spatial profiles for molecules produced by direct sublimation peak in intensity at (or at least near) the position of the nucleus before falling off with increasing nucleocentric distance (ρ) as ρ^{-1}, whereas molecules having an extended source display a flatter distribution, falling off more slowly with ρ (e.g., see Figure 3 in Dello Russo et al., 1998, and Figure 5 in Dello Russo et al., 2016). By summing the spatial profiles of all individual lines for each species within a grating setting, we were able to extract spatial profiles for emission from H_2O, CH_3OH, HCN, OH* and C_2H_6 in ER61 (see Figure 2 A-H).

There is a slight asymmetry in dust profile on April 16 and on May 12-13. Our measurements may suggest a consistent enhancement in the sunward direction of H_2O and C_2H_6 compared to the dust profile on May 11. The signal-to-noise ratio is not sufficient to say with certainty whether CH_3OH also follows this trend. The profiles for dust and all molecules track one another, suggesting that molecules are co-released.

4.2. MOLECULAR FLUORESCENCE ANALYSIS

Synthetic models of fluorescence emission for each targeted species were compared to observed line intensities, after correcting each modeled line intensity (g-factor) for the monochromatic atmospheric transmittance at its Doppler-shifted wavelength (according to the geocentric velocity of the comet at the time of the observations).

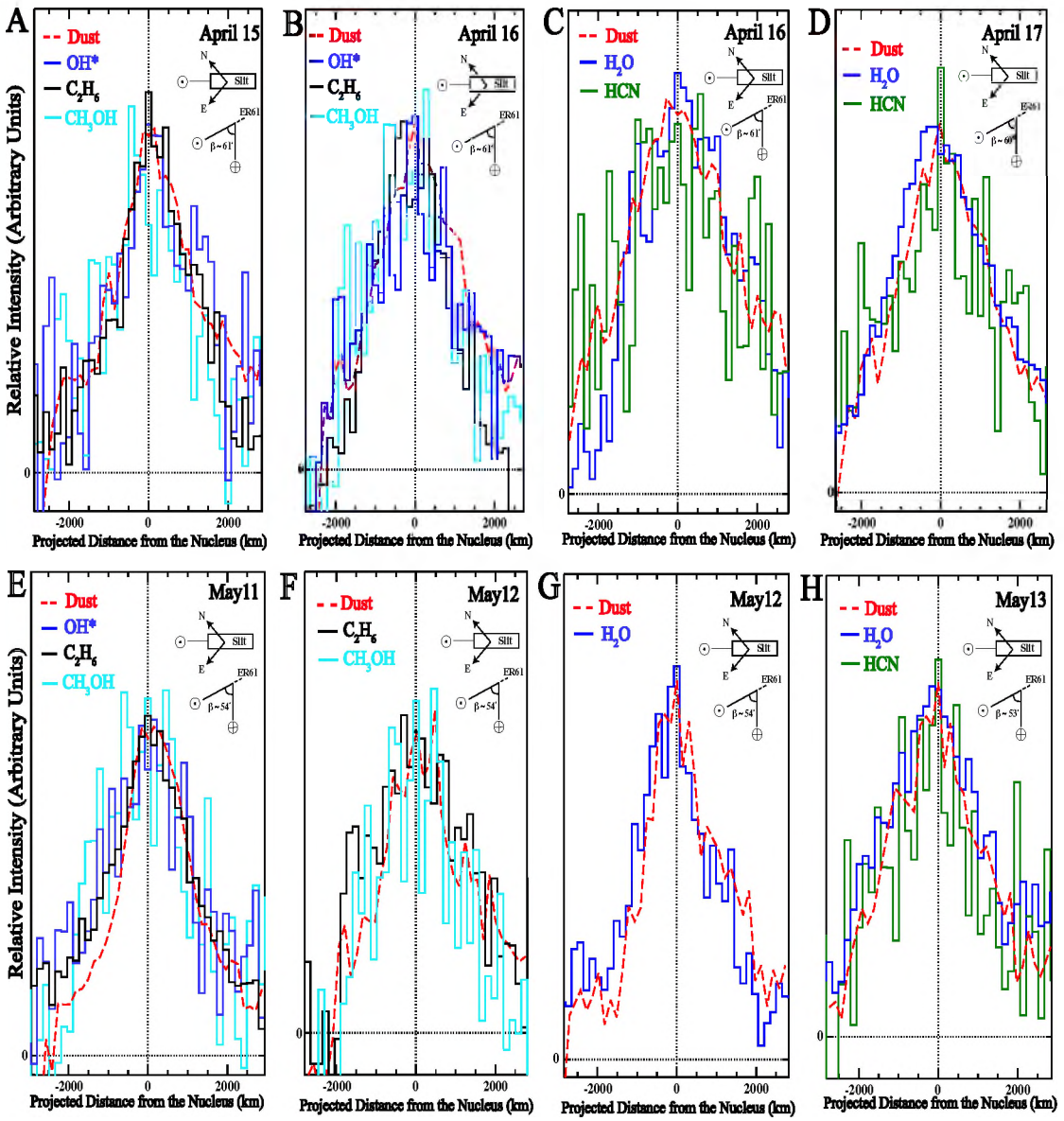

Figure 2. Spatial profile of multiple species measured in comet ER61. Panels A-H show spatial profiles of multiple volatiles simultaneously measured with dust (red dash line) in comet ER61 spanning UT 2017 April 15 to May 13. The slit was oriented along the projected Sun-comet line (position angle ~ 252°), with the Sun-facing direction to the left as indicated. The Sun-comet-Earth angle (phase angle, β) is also shown on each panel for each date.

The g-factors used in synthetic emission models in this study were generated with quantum mechanical models developed for H_2O (Villanueva et al., 2012a), OH* (Bonev et al., 2006), C_2H_6 (Villanueva et al., 2011b), CO, C_2H_2, and CH_4 (Paganini et al., 2013; Villanueva et al., 2011a; Gibb et al., 2003), NH_3, HCN (Villanueva et al., 2013; Lippi et al., 2013), H_2CO (DiSanti et al., 2006), and CH_3OH (Villanueva et al., 2012b; DiSanti et al., 2013). Production rates for each sampled species were determined from the appropriate fluorescence model at the best-fit rotational temperature of each molecule (see Section 4.3).

A line by line analysis and a Levenberg-Marquardt nonlinear minimization technique (Villanueva et al., 2008) was used to fit fluorescence emission from all species simultaneously within each echelle order, allowing for high-precision results, even in spectrally crowded regions containing many spectral lines within a single instrumental resolution element.

4.3. DETERMINATION OF ROTATIONAL TEMPERATURE

Rotational temperatures (T_{rot}) were determined using correlation and excitation analyses that have been extensively described in the literature (e.g., Bonev 2005; Bonev et al., 2008; DiSanti et al., 2006; Villanueva et al., 2008). In general, well-constrained rotational temperatures can be determined for individual species with intrinsically bright lines and for which a sufficiently broad range of excitation energies is sampled. These conditions are met for several molecules in multiple iSHELL orders, including strong H_2O lines in Lcustom order 179 with iSHELL spanning ~ 3437.8 – 3465.8 cm^{-1}; these are augmented by including H_2O lines in additional iSHELL orders (see Figure 1 and Table 2).

We found consistent rotational temperatures for several molecules on all of our dates. The T_{rot} for CH_3OH was well constrained on April 15 (78 ± 8 K) and was consistent (within uncertainty) with those for C_2H_6 and H_2CO on the same date, and with those of HCN, CH_3OH, and H_2O on April 16 and 17 (see Table 2). Rotational temperatures for our May dates were also in agreement, being 61 ± 8 K and 63^{+13}_{-11} K for CH_3OH on May 11 and May 12, 60^{+6}_{-5} K and 61^{+11}_{-8} K for H_2O on May 12 (Saki et al., 2020a) and May 13, respectively. The T_{rot} derived for other molecules were in formal agreement with those of H_2O in ER61 (see Table 2); however, we adopted the rotational temperature of simultaneously measured H_2O (or CH_3OH and C_2H_6 in Lp1 setting with no H_2O emission lines) within the same setting for species without a well-constrained T_{rot} (C_2H_2, NH_3, OCS, CO, CH_4, HC_3N).

Although ER61 was slightly closer to the Sun in May (1.04 AU) compared with April (1.11 AU), our measurements are consistent with a higher T_{rot} in April compared with May, perhaps owing to the higher production rates (Qs) of volatiles in the coma in April resulting from the recent outburst (Wesołowski et al., 2020). Higher production rates and T_{rot} have also been observed in other outbursting comets (see Sekanina 2010, 2017 and references therein).

Rotational temperatures for different molecules for the same comet and within the same instrumental setting are generally found to be consistent, even for molecules with differing photo-dissociation lifetimes (e.g., see Bonev 2005, DiSanti et al., 2006; Gibb et al., 2012; and DiSanti et al., 2016 supporting this approach).

Table 2. Molecular species measured in comet ER61.

Molecule	T_{rot}[a] (K)	GF[b]	Q[c] (molecules s^{-1})	Q_x/Q_{H2O}[d] (%)	Q_x/Q_{C2H6}[e]
2017 April 15, R_h = 1.11 au, Δ = 1.18 au, $d\Delta/dt$ = -2.39 km s^{-1}, Lp1 setting					
OH*[f]	(78)	2.37±0.20	$(1.22 \pm 0.17) \times 10^{29}$	100	156 ± 27
CH_3OH	78±8	2.33±0.32	$(3.22 \pm 0.15) \times 10^{27}$	2.63 ± 0.45	4.13 ± 0.47
H_2CO	(78)	(2.37)	$(4.50 \pm 0.88) \times 10^{26}$	0.36 ± 0.11	0.57 ± 0.13
	74^{+25}_{-19}	(2.37)	$(4.39 \pm 0.85) \times 10^{26}$	0.35 ± 0.10	0.56 ± 0.12
C_2H_6	78^{+12}_{-10}	2.37± 0.15	$(7.89 \pm 0.24) \times 10^{26}$	0.64 ± 0.11	1
2017 April 16, R_h = 1.11 au, Δ = 1.17 au, $d\Delta/dt$ = -1.25 km s^{-1}, Lcustom and Lp1 setting					
H_2O	75±4	2.27± 0.16	$(6.50 \pm 0.31) \times 10^{28}$	100	152 ± 17
C_2H_2	(75)	(2.27)	$< 7.28 \times 10^{25}$	< 0.11[g]	<0.17
HCN	68^{+27}_{-20}	(2.27)	$(8.76 \pm 0.8) \times 10^{25}$	0.14 ± 0.02	0.20 ± 0.03
	(75)	(2.27)	$(9.05 \pm 0.91) \times 10^{25}$	0.13 ± 0.02	0.21 ± 0.03
HC_3N	(75)	(2.27)	$< 1.32 \times 10^{25}$	< 0.02[g]	<0.03
NH_3	(75)	(2.27)	$< 4.99 \times 10^{26}$	< 0.76[g]	<1.17
CH_3OH	(75)	(2.27)	$(2.24 \pm 0.07) \times 10^{27}$	3.44 ± 0.40	5.25 ± 0.58
	68±8	(2.27)	$(2.06 \pm 0.06) \times 10^{27}$	3.17 ± 0.36	4.83 ± 0.53
H_2CO	(75)	(2.27)	$(2.08 \pm 0.15) \times 10^{26}$	0.32 ± 0.11	0.48 ± 0.06
C_2H_6	(75)	(2.27)	$(4.26 \pm 0.15) \times 10^{26}$	0.65 ± 0.07	1.00
2017 April 17, R_h = 1.10 au, Δ = 1.17 au, $d\Delta/dt$ = -1.19 km s^{-1}, Lcustom setting					
H_2O	74^{+6}_{-5}	2.34 ± 0.12	$(1.07 \pm 0.03) \times 10^{29}$	100	N/A
C_2H_2	(74)	(2.34)	$(1.39 \pm 0.37) \times 10^{26}$	0.13 ± 0.04[i]	N/A
HCN	87^{+15}_{-17}	(2.34)	$(1.22 \pm 0.16) \times 10^{26}$	0.11 ± 0.02	N/A
	(74)	(2.34)	$(1.18 \pm 0.15) \times 10^{26}$	0.11 ± 0.02	N/A
HC_3N	(74)	(2.34)	$< 1.45 \times 10^{25}$	< 0.01[g]	N/A
NH_3	(74)	(2.34)	$(7.47 \pm 1.40) \times 10^{26}$	0.70 ± 0.14	N/A

Notes. [a] Rotational temperature. Values in parentheses are assumed. [b] Growth factor. Values in parentheses are assumed. [c] Global production rate. Errors in production rate include line-by-line deviation between modeled and observed intensities and photon noise (see Dello Russo et al., 2004; Bonev 2005; Bonev et al., 2007). [d] Molecular abundance with respect to H_2O. [e] Abundance ratios with respect to C_2H_6 (for dates on which C_2H_6 was measured). [f] OH^* (OH prompt emission) used as a proxy for H_2O. [g] 3σ upper limit. [h] The GF of CH_3OH (2.50 ± 0.38) on April 16 was in agreement with that of H_2O. For CH_3OH and C_2H_6, the GF was 2.19 ± 0.36 and 2.38 ± 0.20 on May12 respectively; thus, we assumed the GF of H_2O when calculating Qs and mixing ratios for those molecules. [i] 4σ detection. [j] Values for H_2O and OCS are from Saki et al., (2020a).

Table 2. Molecular species measured in comet ER61. (Cont.)

2017 May 11, R_h = 1.04 au, Δ = 1.24 au, dΔ/dt = 9.00 km s^{-1}, Lp1 setting					
$OH^{*(f)}$	(61)	2.21± 0.20	$(7.22 \pm 0.95) \times 10^{28}$	100	174 ± 32
CH_3OH	61± 8	(2.21)	$(2.12 \pm 0.15) \times 10^{27}$	2.94 ± 0.79	5.10 ± 0.75
H_2CO	(61)	(2.21)	$(2.03 \pm 0.63) \times 10^{26}$	0.28 ± 0.09	0.48 ± 0.16
	67^{+28}_{-19}	(2.21)	$(2.18 \pm 0.66) \times 10^{26}$	0.30 ± 0.11	0.52 ± 0.17
CH_4	(61)	(2.21)	$< 4.81 \times 10^{27}$	$< 0.89^{(g)}$	< 11.6
C_2H_6	55^{+18}_{-13}	(2.25±0.20)	$(4.07 \pm 0.33) \times 10^{26}$	0.56 ± 0.15	N/A
	(61)	(2.21)	$(4.15 \pm 0.34) \times 10^{26}$	0.57 ± 0.15	1.00
2017 May 12, R_h = 1.04 au, Δ = 1.25 au, dΔ/dt = 9.25 km s^{-1}, M2 and Lp1 setting					
H_2O	60^{+6}_{-5}	2.34 ± 0.36	$(7.04 \pm 0.25) \times 10^{28}$	100	283 ± 34
OCS	(60)	(2.34)	$(1.06 \pm 0.19) \times 10^{26}$	0.15 ± 0.03	0.42 ± 0.09
CO	(60)	(2.34)	$< 4.44 \times 10^{26}$	$< 0.63^{(g)}$	< 1.79
CH_3OH	(60)	(2.34)	$(1.42 \pm 0.10) \times 10^{27}$	2.02 ± 0.26	5.72 ± 0.77
	63^{+13}_{-11}	(2.34)	$(1.38 \pm 0.13) \times 10^{27}$	1.96 ± 0.28	5.56 ± 0.82
H_2CO	(60)	(2.34)	$(8.40 \pm 1.77) \times 10^{25}$	0.12 ± 0.03	0.34 ± 0.08
CH_4	(60)	(2.34)	$< 4.01 \times 10^{26}$	$< 0.57^{(g)}$	<1.61
C_2H_6	(60)	(2.34)	$(2.48 \pm 0.14) \times 10^{26}$	0.35 ± 0.04	1.00
2017 May 13, R_h = 1.04 au, Δ = 1.25 au, dΔ/dt = 9.70 km s^{-1}, Lcustom setting					
H_2O	61^{+11}_{-8}	2.19 ± 0.15	$(3.98 \pm 0.45) \times 10^{28}$	100	N/A
C_2H_2	(61)	(2.19)	$(2.87 \pm 0.19) \times 10^{25}$	0.07 ± 0.01	N/A
HCN	57 ± 9	(2.19)	$(4.30 \pm 0.33) \times 10^{25}$	0.10 ± 0.02	N/A
	(61)	(2.19)	$(4.62 \pm 0.83) \times 10^{25}$	0.11 ± 0.02	N/A
HC_3N	(61)	(2.19)	$< 5.20 \times 10^{24}$	$< 0.04^{(g)}$	N/A
NH_3	(61)	(2.19)	$(1.51 \pm 0.29) \times 10^{26}$	0.37 ± 0.09	N/A

Notes. [a] Rotational temperature. Values in parentheses are assumed. [b] Growth factor. Values in parentheses are assumed. [c] Global production rate. Errors in production rate include line-by-line deviation between modeled and observed intensities and photon noise (see Dello Russo et al., 2004; Bonev 2005; Bonev et al., 2007). [d] Molecular abundance with respect to H_2O. [e] Abundance ratios with respect to C_2H_6 (for dates on which C_2H_6 was measured). [f] OH^* (OH prompt emission) used as a proxy for H_2O. [g] 3σ upper limit. [h] The GF of CH_3OH (2.50 ± 0.38) on April 16 was in agreement with that of H_2O. For CH_3OH and C_2H_6, the GF was 2.19 ± 0.36 and 2.38 ± 0.20 on May12 respectively; thus, we assumed the GF of H_2O when calculating Qs and mixing ratios for those molecules. [i] 4σ detection. [j] Values for H_2O and OCS are from Saki et al., (2020a).

4.4. PRODUCTION RATES AND MIXING RATIOS

Production rates for sampled species were determined using the appropriate fluorescence model at the measured (or assumed) rotational temperature. Nucleus-centered production rates (Q_{NC}, molecules s^{-1}) were calculated using the well-established formalism relating line flux, fluorescence g-factor, and physical (gas outflow speed, photo-dissociation lifetime) and geometric parameters (R_h, Δ; see Dello Russo et al., 1998; DiSanti et al., 2001, 2006, 2014; Bonev 2005). Q_{NC} is then scaled by a growth factor (GF), which relates molecular production rates in regions of the coma along the column included in the beam (of size 0.75" × 2.5") to the global production rate (Q_{global}). This method analyzes spatial profiles of emission using the "Q-curve" formalism, dating back to the analysis of OCS in comet Hale-Bopp (Dello Russo et al., 1998). A canonical spherically symmetric outflow velocity, v_{gas} = 800 $R_h^{-0.5}$ m s^{-1}, was assumed in determining our production rates. This velocity is based on velocity-resolved observations of several moderately bright comets at radio wavelengths (Biver et al., 2006; Cordiner et al., 2014; also see Bonev 2005 supporting this assumption). When calculating production rates, we assumed the GF of simultaneously measured OH* (proxy for H_2O, when water is not sampled) on April 15 and May 11 (consistent with the GF measured for C_2H_6 and CH_3OH on April 15 and with C_2H_6 on May 11) and of H_2O on April 16-17 and on May 12-13. This is supported by their similar profiles (Figure 2). Global production rates for all the targeted species and their mixing ratios relative to water are presented in Table 2. Figures 3A-B show sampled extracted spectra with clear emissions from many volatiles in comet ER61 (with traces and labels as described in Figure 1. Using alternative compositional baselines other than H_2O (Q_X/Q_{H2O} %) can provide richer insights in comparing comets. For instance,

Biver & Bockelée-Morvan (2019) used CH_3OH as their measurement baseline in comparing complex organic molecules in comets.

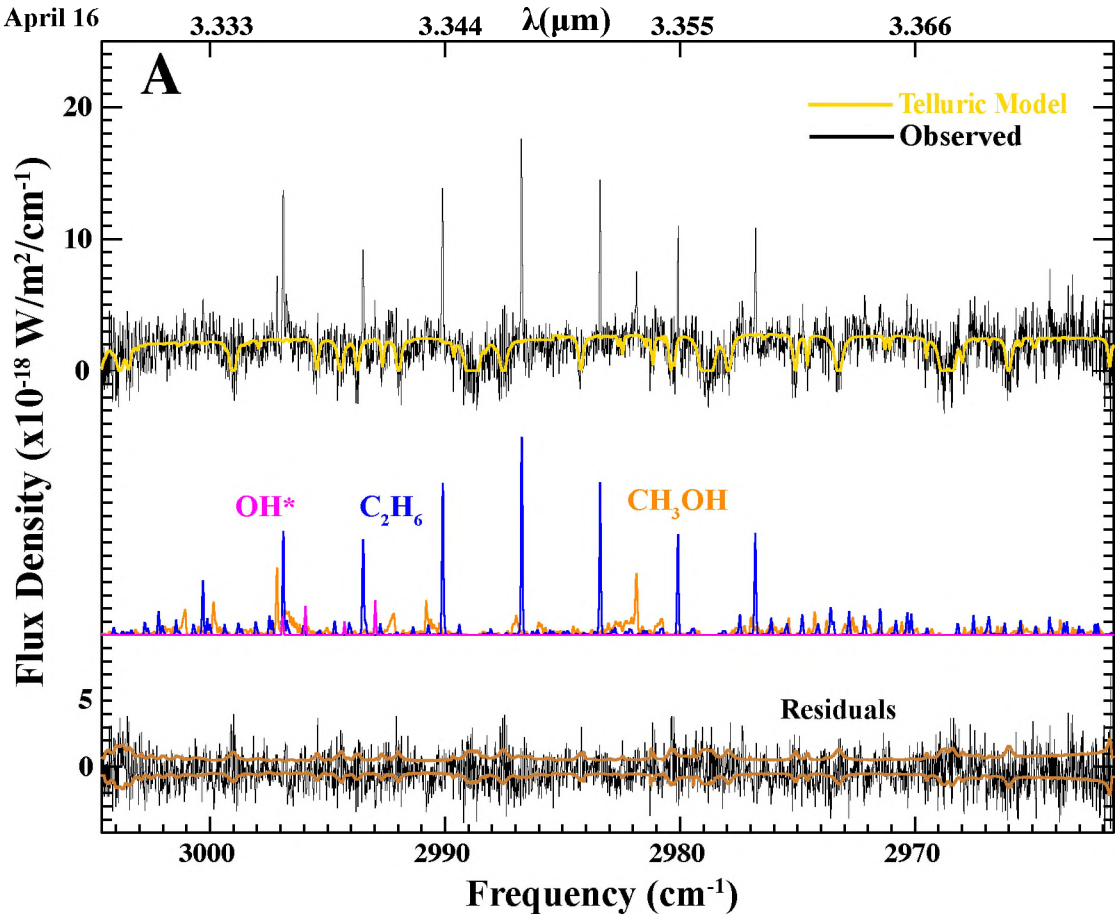

Figure 3. Fluorescence emission of multiple species in comet ER61. Panels A-B show cometary spectra on UT 2017 April 16 and 17, respectively. The yellow traces overplotted on the uppermost cometary spectra are the telluric absorption models (convolved to the instrumental resolution). Individual fluorescence emission models (color-coded by species for clarity) are plotted below. At the bottom of each panel is the residual spectrum (after subtracting the telluric absorption model and all relevant fluorescent emission models) with the 1σ uncertainty envelope overplotted in bronze. The zoomed subplot in Figure B highlights the location and intensity of emission lines of many volatiles with respect to the 1σ uncertainty envelope plotted in bronze; each subplot has the same units as the larger plot.

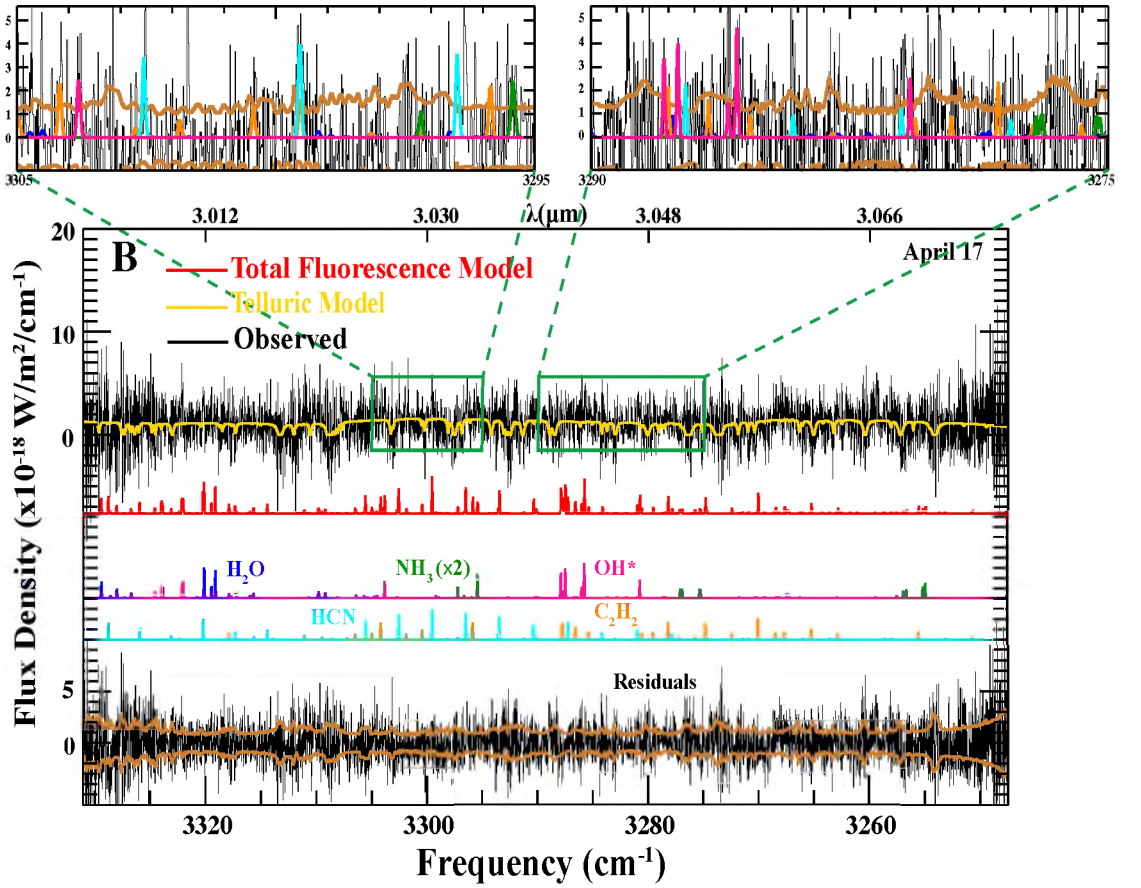

Figure 3. Fluorescence emission of multiple species in comet ER61. Panels A-B show cometary spectra on UT 2017 April 16 and 17, respectively. The yellow traces overplotted on the uppermost cometary spectra are the telluric absorption models (convolved to the instrumental resolution). Individual fluorescence emission models (color-coded by species for clarity) are plotted below. At the bottom of each panel is the residual spectrum (after subtracting the telluric absorption model and all relevant fluorescent emission models) with the 1σ uncertainty envelope overplotted in bronze. The zoomed subplot in Figure B highlights the location and intensity of emission lines of many volatiles with respect to the 1σ uncertainty envelope plotted in bronze; each subplot has the same units as the larger plot. (Cont.)

Owing to the low vacuum sublimation temperature of C_2H_6, distinct outgassing morphologies in many comets compared with H_2O, and the easy detectability of this molecule at near-infrared wavelengths, C_2H_6 can serve as a possible alternative

compositional baseline (see Section 5.4.2 in Bonev et al., 2021 for details). Therefore, we present abundances with respect to both H_2O and C_2H_6 (when we have C_2H_6 detection available; see Table 2).

5. DISCUSSION

5.1. VARIABILITY OF PRODUCTION RATES AND MIXING RATIOS

The nucleus of ER61 was estimated to be ~10 km in radius (Meech et al., 2017). Its geocentric distance and obscuration by the bright coma make it impossible to directly measure individual surface sublimation regions. However, as a comet rotates, different sublimation regions of the nucleus are activated and may give rise to short-term variability in production rates or (in the case of a heterogeneous nucleus) mixing ratios (e.g., Roth et al., 2018; Hässig et al., 2015).

We saw clear variability in production rates of most species over the course of our ER61 observations (UT 2017 April 15 – May 13). The production rates of H_2O, CH_3OH, C_2H_6, H_2CO decreased from April 15 to April 16, followed by an increase in the production rates of H_2O, NH_3, C_2H_2, HCN from April 16 to 17, whereas the 3σ upper-limits for HC_3N were consistent. CH_3OH, C_2H_6, and H_2CO were not targeted on April 17, making it difficult to compare their production rates with those on April 16. We observed a clear decrease in the production rates of some volatile species from April 17 to May 11 (near perihelion) through May 13 (post-perihelion) (see Figure 4). Our measured abundances indicate that (within uncertainties) the mixing ratios of CH_3OH, C_2H_6, H_2CO, HCN, NH_3 and C_2H_2 remained consistent from 3-plus weeks pre-perihelion to near perihelion (May

11), whereas abundances of all volatile species except CH_3OH, HCN, and the 3σ upper-limit for HC_3N decreased post-perihelion (May 12-13). ER61 was more volatile poor (with respect to H_2O) post- vs. pre-perihelion. This could be because of its recent outburst on April 4 (close to our April observations). Outbursts release more material from subsurface areas of the nucleus that may be more volatile rich, causing a possible variability in the production rates and mixing ratios of volatiles similar to those seen in ER61.

Chemically heterogeneous sources on the nucleus, dominating volatile release at different times owing to seasonal effects, may be the most plausible cause for the observed pre- vs. post-perihelion variability in ER61. Such asymmetries with respect to perihelion are observed in some previous comets, including 2P/Encke (A'Hearn et al., 1985; Roth et al., 2018), 67P (e.g., Hässig et al., 2015; Le Roy et al., 2015), and C/2009 P1 (Garradd; Bodewits et al., 2014; McKay et al., 2015).

The Rosetta mission to comet 67P found that mixing ratios of some species (e.g., CO, CO_2, OCS) varied owing to seasonal effects on the nucleus (Hässig et al., 2015). In comet C/2009 P1 (Garradd) the production rate of CO increased even after the comet passed perihelion, perhaps owing to the existence of seasonal effects, whereas the production rate of H_2O followed the predicted heliocentric dependence (decreasing as the comet passed perihelion, Bodewits et al., 2014; McKay et al., 2015). The depleted CH_3OH reported during Encke's 2017 apparition (Roth et al., 2018) compared with its enriched abundance in 2003 (Radeva et al., 2013), plus other compositional differences observed in 2017 compared to 2003, may also have resulted from seasonal effects (see Roth et al., 2018 for a detailed discussion of seasonal effects on the volatile content of comets).

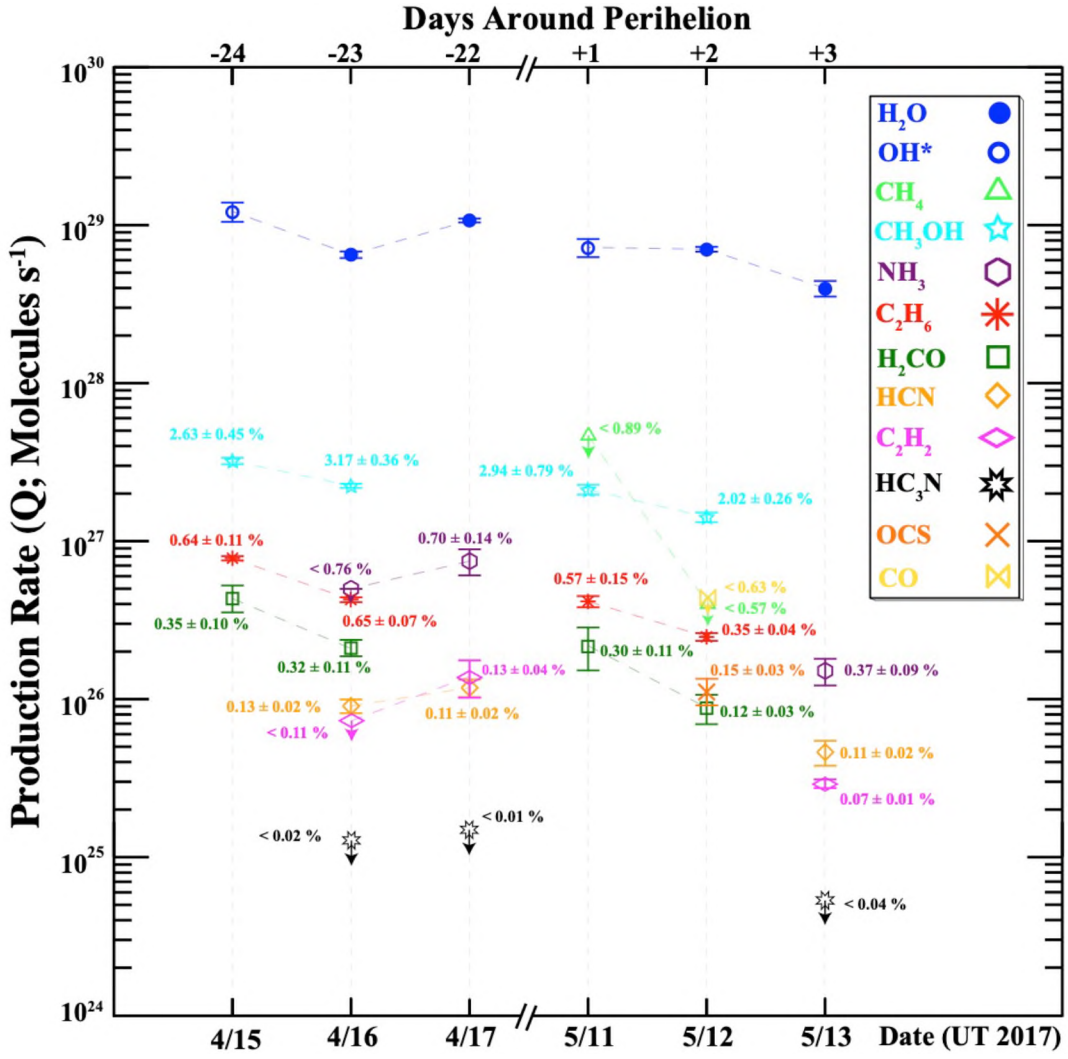

Figure 4. Production rates and mixing ratios (in % relative to H_2O) of trace species sampled on multiple dates in ER61. Variability of production rates and mixing ratios of some volatile species on short and long-time scales are shown.

5.2. THE 3σ UPPER-LIMIT OF HC_3N

The improved sensitivity and spectral coverage of iSHELL allowed us to measure or constrain molecules that we previously could not, such as HC_3N, which has been suggested as a possible parent for CN (e.g., Fray et al., 2005; Bockelée-Morvan and

Crovisier, 1985). HC_3N has been observed via radio wavelengths in many comets (with mixing ratios ranging from 0.002 – 0.07 % with respect to H_2O). Upper limits for HC_3N have also been reported in many comets, including comet 46P/Wirtanen during its 2018 apparition with an abundance of <0.007% (the most stringent upper limit to date at near-infrared wavelengths; Khan et al., 2021), similar to its abundance in comet 1P/Halley (see Khan et al., 2021; Bockelée-Morvan et al., 1987). Crovisier et al., (1993) reported a 3σ upper limit of < 0.00019% in radio observations of comet Levy 1990 XX (the lowest abundance yet reported in any comet). In ER61, combining the unblended HC_3N lines (see Figure 5) enabled us to achieve a sensitive 3σ upper limit (< 0.02 %, averaged over three days), similar to those reported for comets C/2009 P1 (Garradd) (< 0.03%; Villanueva et al., 2012a) and 103P/Hartley 2 (< 0.024%; Dello Russo et al., 2011).

5.3. COMPARISON WITH OTHER OCCS

Compared to mean abundances among OCCs characterized to date at near-infrared wavelengths (Dello Russo et al., 2016a), our measurements in ER61 indicate that CH_3OH was enriched pre-perihelion and 'typical' post-perihelion. HCN was slightly depleted both pre- and post-perihelion. NH_3, H_2CO, C_2H_2, and C_2H_6 were typical pre-perihelion and slightly depleted post-perihelion, whereas OCS was typical (see Table 3 and Figure 6; also see Figure 5 in Saki et al., 2020 and Table 8 in Dello Russo et al., 2016a).

With the large spectral grasp of iSHELL, many of the trace molecules reported here were observed simultaneously (and with H_2O and/or OH*) within a single iSHELL setting. This is not necessarily the case for comets observed with other near-infrared spectrographs that represent the current database of IR observations used to delineate abundance

categories, and the effects of non-simultaneous measurements of H_2O and other trace species must be considered when interpreting mixing ratios (Dello Russo et al., 2016a).

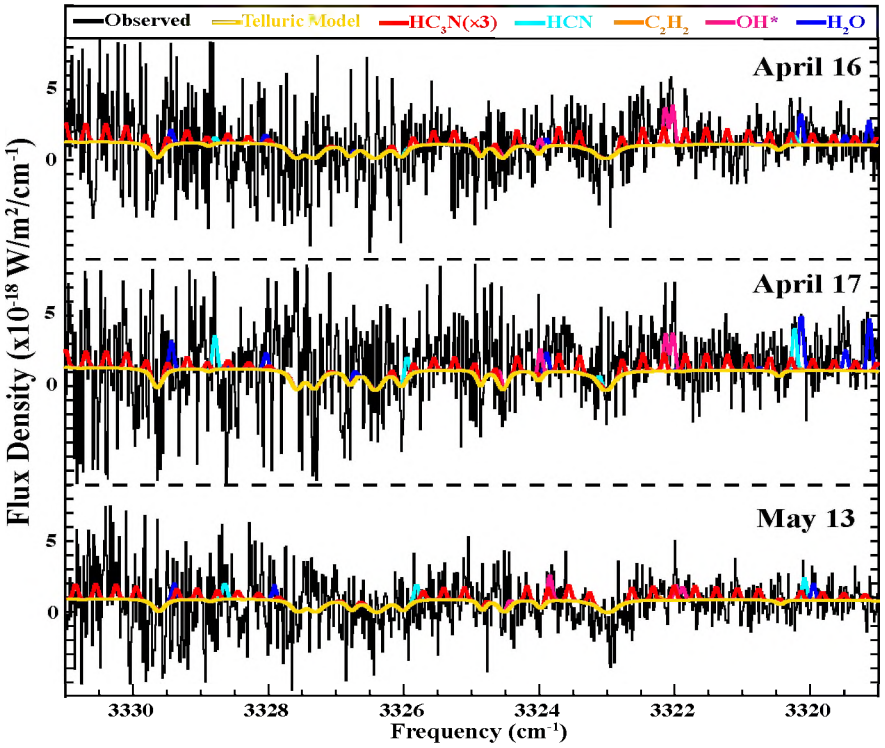

Figure 5. Fluorescence emissions of cyanoacetylene (HC_3N) centered around 3325 cm^{-1} on UT 2017 April 16, 17 and May 13. The yellow traces overplotted on the uppermost cometary spectra are the telluric absorption models (convolved to the instrumental resolution). Individual fluorescence emission models (color-coded by species for clarity) are overplotted.

Early results obtained at near-infrared wavelengths suggested three taxonomic classes: (1) organics-depleted, (2) organics-normal, and (3) organics- enriched (Mumma & Charnley 2011), but additional observations have revealed comets that do not fit neatly into these taxonomic classes (i.e., comets can be depleted in certain volatiles while enriched in

others; e.g., Gibb et al., 2012, Radeva et al., 2013, Dello Russo et al., 2016, Roth et al., 2017). Recently, new (and still evolving) taxonomic classes and volatile relationships in comets have been suggested (see Dello Russo et al., 2016a for details). The overall weighted averages in ER61 indicate that it is enriched in CH_3OH, consistent with average in OCS (Saki et al., 2020a) and depleted in the remaining volatiles (see Figure 6). The pre- to post-perihelion variation in relative abundances makes it difficult to classify ER61, though it has the most compositional similarities on its pre-perihelion dates to comet 2P/Encke and on post- perihelion dates to comet C/2012 S1 ISON when it was at $R_h \geq 0.83$ AU (Dello Russo et al., 2016a and references therein). Table 3 shows mean primary volatile abundance ratios (for species with more than a single measurement) in ER61 on pre-perihelion, near-perihelion and post-perihelion dates and the mean abundances among OCCs.

Table 3. ER61 mean abundances for molecules with more than a single measurement.

Molecule	Pre-perihelion abundance [(a)] (%)	Near-Perihelion abundance [(b)] (%)	Post-perihelion abundance [(c)] (%)	OCC Average [(d)] (%)
C_2H_2	0.13 ± 0.04		0.07 ± 0.01	0.16 ± 0.03
HCN	0.12 ± 0.01		0.11 ± 0.02	0.22 ± 0.03
NH_3	0.70 ± 0.15		0.37 ± 0.09	0.91 ± 0.30
H_2CO	0.34 ± 0.06	0.30 ± 0.09	0.12 ± 0.03	0.33 ± 0.08
CH_3OH	3.11 ± 0.23	2.94 ± 0.79	2.02 ± 0.26	2.21 ± 0.24
C_2H_6	0.64 ± 0.06	0.57 ± 0.15	0.35 ± 0.04	0.63 ± 0.10

Notes. In calculating the mean abundances, we have excluded the 3σ upper limits for species with both detections and upper limits as reported in this work (see Table 2.). [(a)] Weighted mean of all the pre-perihelion measurements. [(b)] Near-perihelion measurements on May 11. [(c)] OCS (Saki et al., 2020a), CO, and CH_4 (upper-limits) were only measured on May dates (see Table 2), so these species have been excluded from this table. [(d)] Averages among all OCCs from Dello Russo et al., (2016a).

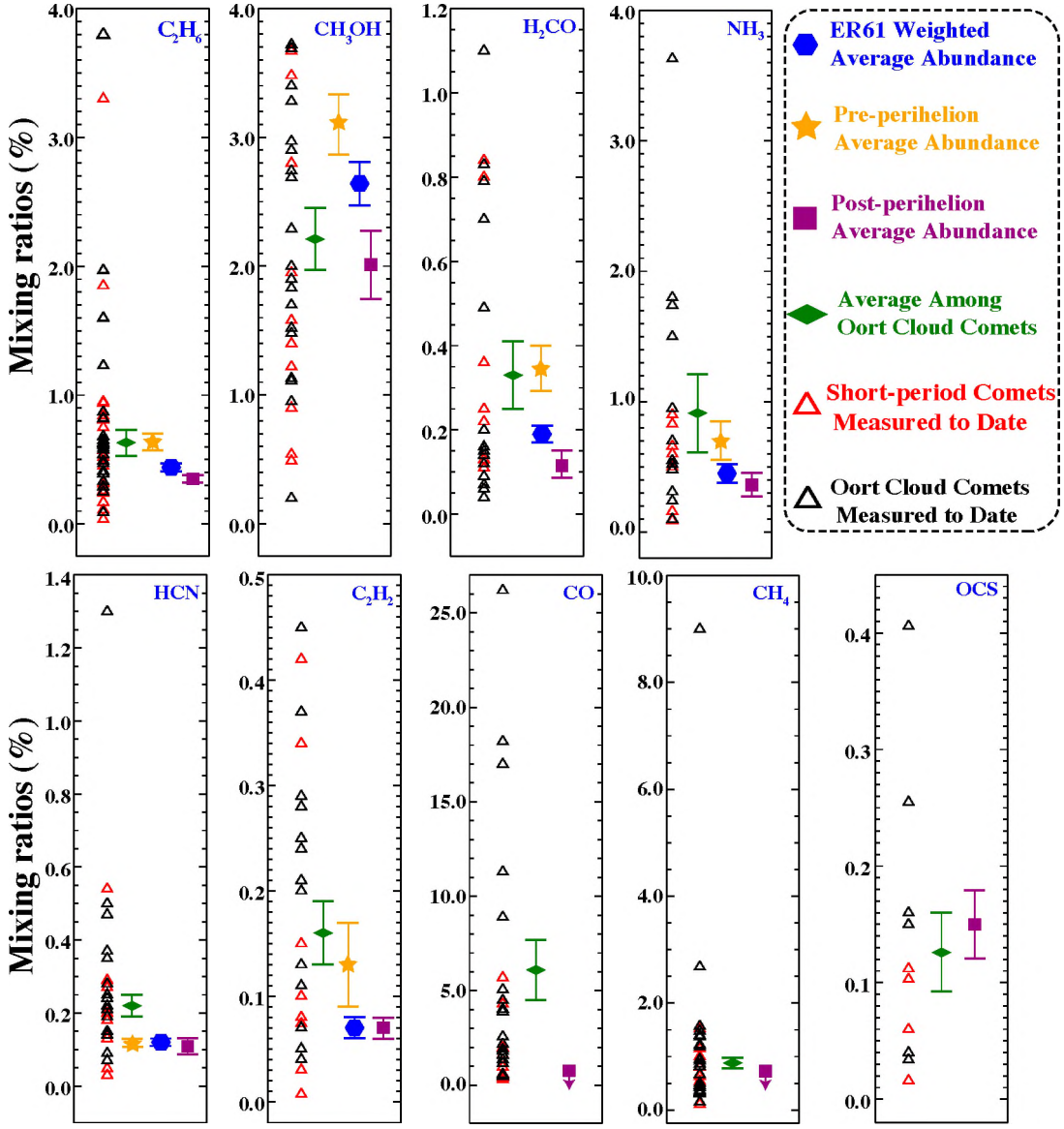

Figure 6. Comparison of ER61's mixing ratios with other comets measured to date. Near-infrared measurements of each volatile in OCCs and JFCs are shown in black and red respectively, while the respective mean values for each volatile among OCCs is plotted in green (Dello Russo et al., 2016, 2020; DiSanti et al., 2017; Roth et al., 2017, 2018, 2020; Faggi et al., 2018; Saki et al., 2020a). Error bars indicate 1σ uncertainties on detections, whereas downward arrows indicate 3σ upper limits (for hypervolatiles CO, and CH_4). Note that for plotting purposes we have excluded the highly enriched CO comets such as C/2016 R2 (PanSTARRS) (Biver et al., 2018; McKay et al., 2019), and C/2010 G2 Hill (Kawakita et al., 2014) with >100% CO content relative to H_2O.

6. SUMMARY

We characterize ER61 primary volatile composition and spatial associations using iSHELL at NASA-IRTF on UT 2017 April 15-17 (shortly after its April 4 outburst) and on May 11-13. Our measurements indicate the following results:

(1) We obtained production rates and mixing ratios with respect to H_2O (and C_2H_6 when a C_2H_6 measurement was available) of the primary volatiles CH_3OH, HCN, C_2H_2, NH_3, H_2CO, OCS, and obtained a stringent 3σ upper-limit for CO, CH_4, and HC_3N.

(2) We were able to extract spatial profiles for H_2O, C_2H_6, CH_3OH, OH*, HCN, and co-measured dust on pre-perihelion, near-perihelion, and post-perihelion dates. These profiles might suggest a slight asymmetric outgassing of dust on April 16 and May 13. Our measurements on May 11 suggest a consistent enhancement in the sunward direction of H_2O and C_2H_6 compared to the dust profile. Owing to a low signal-to-noise ratio, it is not clear if CH_3OH follows this trend.

(3) We found that ER61 exhibits short-term (day-to-day) and long-term (pre- vs. post-perihelion) variability, perhaps owing to its outburst on April 4 (shortly before our April measurements) or seasonal effects along its orbit similar to variability seen in comets 2P/Encke and 67P/C-G.

(4) We placed the chemical composition of ER61 in the context of other OCCs measured to date at near-infrared wavelengths and found that ER61 is overall enriched in CH_3OH, consistent with the average in OCS, and depleted in the remaining volatiles. The pre- to post-perihelion variation in relative abundances

makes it difficult to classify ER61, though it has the most compositional similarities on its pre-perihelion dates to comet 2P/Encke and on post- perihelion dates to comet C/2012 S1 ISON when it was at $R_h \geq 0.83$ AU. Differences in observational circumstances, techniques, and instruments need to be considered in order to better compare properties between comets within the population.

(5) Our ER61 measurements indicate the necessity of comet volatile measurements in both short (day-to-day) and long (pre- vs. post-perihelion) timescales to address the "snapshot" bias associated with cometary observations taken over a limited range of dates and/or heliocentric distances.

REFERENCES

A'Hearn, M. F., 'Comets: looking ahead,' Philosophical Transactions of the Royal Society A, 2017, 375(2097), p. 20160261.

A'Hearn, M. F., Birch, P. V., Feldman, P. D., and Millis, R. L., 'Comet Encke – gas production and lightcurve,' Icarus, 1985, 64(1), pp. 1–10.

A'Hearn, M. F., Millis, R. C., Schleicher, D. O., Osip, D. J., and Birch, P. V., 'The ensemble properties of comets: Results from narrowband photometry of 85 comets, 1976-1992,' Icarus, 1995, 118(2), pp. 223–270.

Biver, N., Bockelée-Morvan, D., Moreno, R., Crovisier, J., Colom, P., Lis, D. C., Sandqvist, A., Boissier, J., Despois, D., and Milam, S. N., 'Ethyl alcohol and sugar in comet C/2014 Q2 (Lovejoy,' Science Advances, 2015, 1, p. e1500863.

Biver, N., Bockelée-Morvan, D., Crovisier, J., Lis, D. C., Moreno, R., Colom, P., Henry, F., Herpin, F., Paubert, G., andWomack, M., 'Radiowavelength molecular observations of comets C/1999 T1 (McNaught-Hartley), C/2001 A2 (LINEAR), C/2000 WM1 (LINEAR) and 153P/Ikeya-Zhang,' Astronomy and Astrophysics, 2006, 449(3), p. 1255.

Biver, N., Bockelée-Morvan, D., Hofstadter, M., Lellouch, E., Choukroun, M., Gulkis, S., Crovisier, J., Schloerb, F. P., Rezac, L., von Allmen, P., Lee, S., Leyrat, C., Ip, W. H., Hartogh, P., Encrenaz, P., Beaudin, G., and the MIRO team, 'Long-term monitoring of the outgassing and composition of comet 67P/Churyumov-Gerasimenko with the Rosetta/MIRO instrument,' Astronomy & Astrophysics, 2019, 3, pp. 1550–1555.

Bockelée-Morvan, D., Lis, D. C., Wink, J. E., Despois, D., Crovisier, J., Bachiller, R., Benford, D. J., Biver, N., Colom, P., Davies, J. K., Gérard, E., Germain, B., Houde, M., Mehringer, D., Moreno, R., Paubert, G., Phillips, T. G., and Rauer, H., 'New molecules found in comet C/1995 O1 (hale-bopp). investigating the link between cometary and interstellar material,' AAP, 2000, 353.

Bockelée-Morvan, D., Crovisier, J., Erard, S., Capaccioni, F., Leyrat, C., Filacchione, G., Drossart, P., Encrenaz, T., Biver, N., de Sanctis M.-C., Schmitt, B., Kührt, E., M.-T., C., Combes, M., Combi, M., Fougere, N., Arnold, G., Fink, U., Ip, W., Migliorini, A., Piccioni, G., and Tozzi, G., 'Evolution of CO2, CH4, and OCS abundances relative to H_2O in the coma of comet 67P around perihelion from Rosetta/VIRTISH observations,' Monthly Notices of the Royal Astronomical Society, 2016, 462(1), pp. S1270–S183.

Bockelée-Morvan, D., Crovisier, J., Mumma, M. J., and Weaver, H. A., 'The composition of cometary volatiles, in comets ii, ed. m. c. festou, h. u. keller, h. a. weaver,' Univ. Arizona Press, 2004, p. 391.

Bockelée-Morvan, D. and Crovisier, J., 'Possible parents for the cometary CN radical - Photochemistry and excitation conditions,' AAP, 1985, 151, pp. 90-100.

Bockelée-Morvan, D., Crovisier, J., Despois, D., Forveille, T., Gerard, E., Schraml, J., Thum, C., 'Molecular obserations of comets P/Giacobini-Zinner 1984e and P/Halley 1982i at millimetre wavelengths,' AAP, 1987, 180, pp. 253–262.

Bodewits, D., Farnham, T. L., A'Hearn, M. F., Feaga, L. M., McKay, A., Schleicher, D. G., and Sunshine, J. M., 'The evolving activity of the dynamically young comet C/2009 P1 (Garradd),' The Astrophysical Journal, 2014, 786, p. 48.

Bonev, B. P., Towards a Chemical Taxonomy of Comets: Infrared Spectroscopic Methods for Quantitative Measurements of Cometary Water (With an Independent Chapter on Mars Polar Science), phdthesis, The University of Toledo, 2005.

Bonev, B. P., Mumma, M. J., DiSanti, M. A., Dello Russo, N., Magee-Sauer, K., Ellis, R. S., and Stark, D. P., 'A comprehensive study of infrared OH prompt emission in two comets. i. observations and effective g-factors,' The Astrophysical Journal, 2006, 653(1), pp. 774–787.

Bonev, B. P., Mumma, M. J., Kawakita, H., Kobayashi, H., and Villanueva, G. L., 'Ircs/subaru observations of water in the inner coma of comet 73P-B/Schwassmann Wachmann 3: Spatially resolved rotational temperatures and ortho para ratios,' Icarus, 2008a, 196(1), pp. 241–248.

Bonev, B. P., Dello Russo, N., DiSanti, M. A., Martin, E. C., Doppmann, G., Vervack, J., R. J., Villanueva, G. L., Kawakita, H., Gibb, E. L., Combi, M. R., Roth, N. X., Saki, M., McKay, A. J., Cordiner, M. A., Bodewits, D., Crovisier, J., Biver, N., Cochran, A. L., Shou, Y., Khan, Y., and Venkataramani, K., 'First comet observations with NIRSPEC-2 at Keck: Outgassing sources of parent volatiles and abundances based on alternative taxonomic compositional baselines in 46p/wirtanen,' The Planetary Science Journal, 2021, 2, p. 45.

Brooke, T. Y., Weaver, H. A., Chin, G., Bockelée-Morvan, D., Kim, S. J., and Xu, L. H., 'Spectroscopy of comet Hale-Bopp in the infrared,' Icarus, 2003, 166(1), pp. 167–187.

Chubko, L. S., Churyumov, K. I., Lukýanyk, I. V., and Guliev, A. S., 'Changes in the spectra of comet C/1999 S4 in July 2000,' Highlights of Astronomy, 2005, 13, p. 768.

Clements, T. D. and Fernandez, Y., 'Dust production from mini outbursts of comet 29p/Schwassmann-Wachmann 1,' Astronomical Journal, 2021, 161, p. 73.

Cochran, A. L., Levasseur-Regourd, A.-C., Cordiner, M., Hadamcik, E., Lasue, J., Gicquel, A., Schleicher, D., Charnley, S. B., Mumma, M. J., Paganini, L., Bockelée-Morvan, D., Biver, N., and Kuan, Y.-J., 'The composition of comets,' Space Science Reviews, 2015, 197(1-4), pp. 9–46.

Cordiner, M. A., Rem.an, A. J., Boissier, J., Milam, S. N., Mumma, M. J., Charnley, S. B., Paganini, L., Villanueva, G., Bockelée-Morvan, D., Kuan, Y. J., Chuang, Y. L., Lis, D. C., Biver, N., Crovisier, J., Minniti, D., and Coulson, I. M., 'Mapping the release of volatiles in the inner comae of comets C/2012 F6 (Lemmon) and C/2012 S1 (ISON) using the Atacama Large Millimeter/Submillimeter Array,' The Astrophysical Journal Letters, 2014, 792, p. L2.

Crovisier, J., Bockelee-Morvan, D., Colom, P., Despois, D., and Paubert, G., 'A search for parent molecules at millimetre wavelengths in comets austin 1990 v and levy 1990 XX- upper limits for undetected species,' AAP, 1993, 269, pp. 527 540.

Dello Russo, N., Bonev, B. P., DiSanti, M. A., Mumma, M. J., Gibb, E. L., Magee-Sauer, K., Barber, R. J., and Tennyson, J., 'Water production rates, rotational temperatures, and spin temperatures in comets C/1999 H1 (Lee), C/1999 S4, and C/2001 A2,' APJ, 2005, 621, pp. 537–544.

Dello Russo, N., DiSanti, M. A., Mumma, M. J., Magee-Sauer, K., and Rettig, T. W., 'Carbonyl sulfide in comets C/1996 B2 (Hyakutake) and C/1995 O1 (Hale-Bopp): Evidence for an extended source in Hale-Bopp,' Icarus, 1998, 135(2), pp. 377–388.

Dello Russo, N., Kawakita, H., Jr., V. R. J., and Weaver H., A., 'Emerging trends and a comet taxonomy based on the volatile chemistry measured in thirty comets with high-resolution infrared spectroscopy between 1997 and 2013,' Icarus, 2016a, 278, pp. 301–332.

Dello Russo, N., Vervack, R. J. J., Kawakita, H., Cochran, A., McKay, A. J., Harris, W. M., Weaver, H. A., Lisse, C. M., DiSanti, M. A., Kobayashi, H., Biver, N., Bockelée- Morvan, D., Crovisier, J., Opitom, C., and Jehin, E., 'The compositional evolution of C/2012 S1 (ISON) from ground-based high-resolution infrared spectroscopy as part of a worldwide observing campaign,' Icarus, 2016b, 266, pp. 152–175.

Dello Russo, N., Vervack, R. J. J., Lisse, C. M., Weaver, H. A., Kawakita, H., Kobayashi, H., Cochran, A. L., Harris, W. M., McKay, A. J., Biver, N., Bockelée-Morvan, D., and Crovisier, J., 'The volatile composition and activity of comet 103P/Hartley 2 during the EPOXI closest approach,' The Astrophysical Journal Letters, 2011, 734(1), p. L8.

DiSanti, M. A., Bonev, B. P., Dello Russo, N., Vervack, R. J. J., Gibb, E. L., Roth, N. X., McKay, A. J., and Kawakita, H., 'Hypervolatiles in a Jupiter-family comet: Observations of 45P/Honda-Mrkos-Pajdušáková using iSHELL at the NASA-IRTF,' The Astronomical Journal, 2017, 154(6), p. 246.

DiSanti, M. A., Bonev, B. P., Magee-Sauer, K., Dello Russo, N., Mumma, M. J., Reuter, D. C., and Villanueva, G. L., 'Detection of formaldehyde emission in comet C/2002 T7 (LINEAR) at infrared wavelengths: Line-by-line validation of modeled fluorescent intensities,' The Astrophysical Journal, 2006, 650(1), pp. 470–483.

DiSanti, M. A., Bonev, B. P., Villanueva, G. L., and Mumma, M. J., 'Highly depleted ethane and mildly depleted methanol in comet 21P/Giacobini-Zinner: Application of a new emprical ν_2-band model for CH_3OH near 50 K,' The Astrophysical Journal, 2013, 763(1), p. 19.

DiSanti, M. A., Mumma, M. J., Dello Russo, N., and Magee-Sauer, K., 'Carbon monoxide production and excitation in comet C/1995 O1 (Hale-Bopp): Isolation of native and distributed CO sources,' Icarus, 2001, 153(2), pp. 361–390.

DiSanti, M. A., Villanueva, G. L., Paganini, L., Bonev, B. P., Keane, J. V., Meech, K. J., and Mumma, M. J., 'Pre- and post-perihelion observations of C/2009 P1 (Garradd): Evidence for an oxygen-rich heritage?' Icarus, 2014, 228, pp. 167–180.

El-Maarry, M. R., Groussin, O., Thomas, N., Pajola, M., Auger, A. T., Davidsson, B., Hu, X., Hviid, S. F., Knollenberg, J., Güttler, C., Tubiana, C., Bodewits, D., Fornasier, S., and Sierks, H., 'Remarkable surface changes of comet 67p/churyumovgerasimenko's nucleus around perihelion,' Lunar and Planetary Science Conference, 2017, p. 2791.

Fray, N., Bénilan, Y., Cottin, H., Gazeau, M. C., and Crovisier, J., 'The origin of the CN radical in comets: A review from observations and models,' PLANSS, 2005, 53, pp. 1243–1262.

Gibb, E. L., Bonev, B. P., Villanueva, G., DiSanti, M. A., Mumma, M. J., Sudholt, E., and Radeva, Y., 'Chemical composition of comet C/2007 N3 (Lulin): Another "atypical" comet,' The Astrophysical Journal, 2012, 750(2), p. 102.

Gibb, E. L., Mumma, M. J., Dello Russo, N., DiSanti, M. A., and Magee-Sauer, K., 'Methane in Oort cloud comets,' Icarus, 2003, 165(2), pp. 391–406.

Gomes, R., Levison, H. F., Tsiganis, K., and Morbidelli, A., 'Origin of the cataclysmic late heavy bombardment period of the terrestrial planets,' Nature, 2005, 435(7041), pp. 466–469.

Gronoff, G., Maggiolo, R., Cessateur, G., Moore, W. B., Airapetian, V., De Keyser, J., Dhooghe, F., Gibbons, A., Gunell, H., Mertens, C. J., Rubin, M., Hosseini, S., 'The Effect of Cosmic Rays on Cometary Nuclei. I. Dose Deposition,' ApJ, 2020, 890, 1, P. 89.

Hässig, M., Altwegg, K., Balsiger, H., Bar-Nun, A., Berthelier, J. J., Bochsler, P., Briois, C., Calmonte, U., Combi, M., De Keyser, J., Eberhardt, P., Fiethe, B., Fuselier, S. A., Galand, M., Gasc, S., Gombosi, T. I., Hansen, K. C., Jäckel, A., Keller, H. U., Kopp, E., Korth, A., Kührt, E., Le Roy, L., Mall, U., Marty, B., Mousis, O., Neefs, E., Owen, T., Rème, H., Rubin, M., Sémon, T., Tornow, C., Tzou, C.- Y., Waite, J. H., and Wurz, P., 'Tie variability and heterogeneity in the coma of 67P/Churyumov-Gerasimenko,' Science, 2015, 347(6220), p. aaa0276.

Khan, Y., Gibb, E. L., Bonev, B. P., Roth, N. X., Saki, M., DiSanti, M. A., Dello Russo, N., Vervack, J., R. J., McKay, A. J., Combi, M. R., Shou, Y., Cordiner, M. A., Kawakita, H., Fougere, N., and Protopapa, S., 'Testing short-term variability and sampling of primary volatiles in comet 46p/wirtanen,' The Planetary Science Journal, 2021, 2, p. 20.

Kobayashi, H., Kawakita, H., Mumma, M. J., Bonev, B. P., Watanabe, J., and Fuse, T., 'Organic volatiles in comet 73p-b/schwassmann-wachmann 3 observed during its outburst: A clue to the formation region of the jupiter-family comets,' APJL, 2007, 668, pp. L75–L78.

Le Roy, L., Altwegg, K., Balsiger, H., Berthelier, J.-J., Bieler, A., Briois, C., Calmonte, U., Combi, M. R., De Keyser, J., Dhooghe, F., Fiethe, B., Fuselier, S. A., Gasc, S., Gombosi, T. I., Hässig, M., Jäckel, A., Rubin, M., and Tzou, C.-Y., 'Inventory of the volatiles on comet 67P/Churyumov-Gerasimenko from Rosetta/ROSINA,' Astronomy & Astrophysics, 2015, 583, p. A1.

Levison, H. F., Morbidelli, A., Tsiganis, K., Nesvorny, D., and Gomes, R., 'Late orbital instabilities in the outer planets induced by interaction with a self-gravitating planetesimal disk,' The Astronomical Journal, 2011, 142(5), p. 152.

Lippi, M., Villanueva, G. L., DiSanti, M. A., Böhnhardt, H., Mumma, M. J., Bonev, B. P., and Prialnik, D., 'A new model for the ν_1 vibrational band of HCN in cometary comae, with application to three comets,' Astronomy & Astrophysics, 2013, 551, p. A51.

Masi, G., Schwartz, M., Holvorcem, P., Hambsch, F. J., Bryssinck, E., and Williams, G. V., 'Comet c/2015 er61-b (panstarrs),' Minor Planet Electronic Circulars, 2017, M09.

McKay, A. J., Cochran, A. L., DiSanti, M. A., Villanueva, G., Dello Russo, N., Vervack, R. J. J., Morgenthaler, J. P., Harris, W. M., and Chanover, N. J., 'Evolution of H_2O, CO, and CO_2 production in comet C/2009 P1 Garradd during the 2011-2012 apparition,' Icarus, 2015, 250, pp. 504–515.

McKay, A. J., DiSanti, M. A., Kelley, M. S. P., Knight, M. M., Womack, M., Wierzchos, K., Harrington Pinto, O., Bonev, B. P., Villanueva, G. L., Dello Russo, N., Cochran, A. L., Biver, N., Bauer, J., Vervack, J., R. J., Gibb, E., Roth, N., and Kawakita, H., 'The peculiar volatile composition of co-dominated comet C/2016 R2 (PanSTARRS),' Astronomical Journal, 2019, 158, p. 128.

Meech, K. J., Schambeau, C. A., Sorli, J. T., K.and Kleyna, Micheli, M., Bauer, J., Denneau, L., Keane, J. V., Toller, E., Wainscoat, R., Hainaut, O., Bhatt, B., Sah, D., Yang, B., Kramer, E., and Magnier, G., 'Beginning of activity in long-period comet C/2015 ER61 (PanSTARRS),' Astronomical Journal, 2017, 153, p. 206.

Mumma, M. J. and Charnley, S. B., 'The chemical composition of comets –emerging taxonomies and natal heritage,' Annual Review of Astronomy and Astrophysics, 2011, 49(1), pp. 471–524.

Nesvorny, D., Vokrouhlicky, D., Dones, L., Levison, H. F., Kaib, N., Morbidelli, A., 'Origin and Evolution of Short-period Comets,' APJ, 2017, 845, 1, PP. 27

Opitom, C., Yang, B., Selman, F., Reyes, C., 'First observations of an outbursting comet with the MUSE integral-field spectrograph,' AAP, 2019, 628, PP. A128

Paganini, L., Blake, G. A., Villanueva, G. L., DiSanti, M. A., Bonev, B. P., Gibb, E. L., and Mumma, M. J., 'Comet C/2012 S1 (Ison),' IAU Circular, 2013, (9263).

Pajola, M., Höfner, S., Vincent, J. B., Oklay, N., Scholten, F., Mottola, S., Naletto, G., Fornasier, S., Lowry, S., Feller, C., Hasselmann, P. H., Güttler, C., Tubiana, C., Sierks, H., and Keller, H. U., 'The aswan cliff collapse on comet 67P/Churyumov-Gerasimenko,' European Planetary Science Congress, 2017, pp. EPSC2017–70.

Radeva, Y. L., Mumma, M. J., Bonev, B. P., DiSanti, M. A., Villanueva, G. L., Magee-Sauer, K., Gibb, E. L., and Weaver, H. A., 'The organic composition of comet C/2000 WM1 (LINEAR) revealed through infrared spectroscopy,' Icarus, 2010, 206 (2), pp. 764–777.

Radeva, Y. L., Mumma, M. J., Villanueva, G. L., Bonev, B. P., DiSanti, M. A., A'Hearn, M. F., and Dello Russo, N., 'High-resolution infrared spectroscopic measurements of comet 2P/Encke: Unusual organic composition and low rotational temperatures,' Icarus, 2013, 223(1), pp. 298–307.

Rayner, J., Bond, T., Bonnet, M., Jaffe, D., Muller, G., and Tokunaga, A., 'iSHELL: a 1-5 micron cross-dispered R=70,000 immersion grating spectrograph for IRTF,' Proceedings of the SPIE, 2012, 8446, p. 84462C.

Rayner, J., Tokunaga, A., Jaffe, D., Bonnet, M., Ching, G., Connelley, M., Kokubun, D., Lockhart, C., and Warmbier, E., 'iSHELL: a construction, assembly and testing,' Proceedings of the SPIE, 2016, 9908, p. 990884.

Rickman, H., Marchi, S., A'Hearn, M. F., Barbieri, C., El-Maarry, M. R., Guttler, C., Ip, W. H., Keller, H. U., and Lamy, P., Marzari, F., Massironi, M., Naletto, G., Pajola, M., Sierks, H., Koschny, D., Rodrigo, R., Barucci, M. A., Bertaux, J. L., Bertini, I., Cremonese, G., Da Deppo, V., Debei, S., De Cecco, M., Fornasier, S., Fulle, M., Groussin, O., Gutierrez, P. J., Hviid, S. F., Jorda, L., Knollenberg, J., Kramm, J. R., Kuhrt, E., Kuppers, M., Lara, L. M., Lazzarin, M., Lopez Moreno, J. J., Michalik, H., Sabau, L., Thomas, N., Vincent, J. B., Wenzel, K. P., ' Comet 67P/Churyumov-Gerasimenko: Constraints on its origin from OSIRIS observations, AAP, 2015, 583, PP. A44.

Roth, N. X., Gibb, E. L., Bonev, B. P., DiSanti, M. A., Dello Russo, N., McKay, A. J., Vervack, J., Ronald J., Kawakita, H., Saki, M., Biver, N., Bockelée-Morvan, D., Feaga, L. M., Fougere, N., Cochran, A. L., Combi, M., and Shou, Y., 'Probing the evolutionary history of comets: An investigation of the hypervolatiles CO, CH_4, and C_2H_6 in the Jupiter-family comet 21P/Giacobini-Zinner,' The Astronomical Journal, 2020, 159, p. 42.

Roth, N. X., Gibb, E. L., Bonev, B. P., DiSanti, M. A., Dello Russo, N., Vervack, R. J. J., McKay, A. J., and Kawakita, H., 'A tale of "two" comets: The primary volatile composition of comet 2P/Encke across apparitions and implications for cometary science,' The Astronomical Journal, 2018, 156, p. 251.

Roth, N. X., Gibb, E. L., Bonev, B. P., DiSanti, M. A., Mumma, M. J., Villanueva, G. L., and Paganini, L., 'The composition of comet C/2012 K1 (PanSTARRS) and the distribution of primary volatile abundances among comets,' The Astronomical Journal, 2017, 153, p. 168.

Roth, N. X., Bonev, B. P., DiSanti, M. A., Dello Russo, N., McKay, A. J., Gibb, E. L., Saki, M., Khan, Y., Vervack, R. J. Jr., and Kawakita, H., Cochran, A. L., Biver, N., Cordiner, M. A., Crovisier, J., Jehin, E., Weaver H., ' The Volatile Composition of the Inner Coma of Comet 46P/Wirtanen: Coordinated Observations Using iSHELL at the NASA-IRTF and Keck/NIRSPEC-2, The Planetary Science Journal, 2021, 2, P. 54.

Saki, M., Gibb, E. L., Bonev, B. P., Roth, N. X., DiSanti, M. A., Dello Russo, N., Vervack, R. J. J., McKay, A. J., and Kawakita, H., 'Carbonyl Sulfide (OCS): Detections in Comets C/2002 T7 (LINEAR), C/2015 ER61 (PanSTARRS), and 21P/Giacobini-Zinner and Stringent Upper Limits in 46P/Wirtanen,' The Astronomical Journal, 2020a, 160(4), p. 184.

Saki, M., Gibb, E., Bonev, B., Roth, N., DiSanti, M., Dello Russo, N., Vervack, R., McKay, A., Khan, Y., Kawakita, H., 'An Investigation of the Abundances of Hypervolatiles CO, CH_4, and C_2H_6 in Jupiter-family Comet 46P/Wirtanen,' AAS/Division for Planetary Sciences Meeting Abstracts, 2020b, 52, P. 212.04.

Sekanina, Z., 'Recurrence of super-massive explosions and orbital evolution of comet 17P/Holmes: Ii. search for historical records, and outlook for future research,' International Comet Quarterly, 2010, 32, pp. 3–32.

Sekanina, Z., 'Temporal correlation between outbursts and fragmentation events of comet 168P/Hergenrother,' arXiv e-prints, 2014, p. 1409.7641.

Sekanina, Z., 'Major outburst and splitting of long-period comet C/2015 ER61 (panstarrs),' arXiv e-prints, 2017, 2017, p. 1712.03197.

Sekanina, Z., Jehin, E., Boehnhardt, H., Bonfils, X., Schuetz, O., and Thomas, D., 'Recurring outbursts and nuclear fragmentation of comet C/2001 A2 (Linear),' APJ, 2002, 572, pp. 679–684.

Stern, S. A., 'The evolution of comets in the Oort cloud and Kuiper belt,' Nature, 2003, 424(6949), pp. 639–642.

Tubbiolo, A. F., Gibson, B., Goggia, T., Primak, N., Schultz, A., Willman, M., Chambers, K., Chastel, S., Denneau, L., Flewelling, H., Huber, M., Magnier, E., Schunova, E., Wainscoat, R., Waters, C., Weryk, R., Buzzi, L., Vorobjov, T., Bolin, B., and Birtwhistle, P., '2015 er61,' Minor Planet Electronic Circulars, 2015, F124.

Villanueva, G. L., DiSanti, M. A., Mumma, M. J., and Xu, L. H., 'A quantum band model of the ν_1 fundamental of methanol (CH_3OH) and its application to fluorescence spectra of comets,' The Astrophysical Journal, 2012a, 747(1), p. 3.

Villanueva, G. L., Magee-Sauer, K., and Mumma, M. J., 'Modeling of nitrogen compounds in cometary atmospheres: Fluorescence models of ammonia (NH_3), hydrogen cyanide (HCN), hydrogen isocyanide (HNC) and cyanoacetylene (HC_3N),' Journal of Quantitative Spectroscopy and Radiative Transfer, 2013, 129, pp. 158–168.

Villanueva, G. L., Mumma, M. J., Bonev, B. P., DiSanti, M. A., Gibb, E. L., Boehnhardt, H., and Lippi, M., 'A sensitive search for deuterated water in comet 8P/Tuttle,' The Astrophysical Journal Letters, 2009, 690(1), pp. L5–L9.

Villanueva, G. L., Mumma, M. J., Bonev, B. P., Novak, R. E., Barber, R. J., and DiSanti, M. A., 'Water in planetary and cometary atmospheres: H_2O/HDO transmittance and fluorescence models,' Journal of Quantitative Spectroscopy and Radiative Transfer, 2012b, 113(3), pp. 202–220.

Villanueva, G. L., Mumma, M. J., DiSanti, M. A., Bonev, B. P., Gibb, E. L., Magee-Sauer, K., Blake, G. A., and Salyk, C., 'The molecular composition of comet C/2007 W1 (Boattini): Evidence of a peculiar outgassing and a rich history,' Icarus, 2011a, 216(1), pp. 227–240.

Villanueva, G. L., Mumma, M. J., and Magee-Sauer, K., 'Ethane in planetary and cometary atmospheres: Transmittance and fluorescence models of the ν_7 band at 3.3 um,' Journal of Geophysical Research, 2011b, 116(E8), p. E08012.

Villanueva, G. L., Mumma, M. J., Novak, R. E., and Hewagama, T., 'Identification of a new band system of isotopic CO_2 near 3.3 um: Implications for remote sensing of biomarker gases on Mars,' Icarus, 2008, 195(1), pp. 34–44.

Villanueva, G. L., Smith, M. D., Protopapa, S., Faggi, S., and Mandell, A. M., 'Planetary spectrum generator: An accurate online radiative transfer suite for atmospheres, comets, small bodies and exoplanets,', 2018, 217, pp. 86–104.

Vincent, J. B., A'Hearn, M. F., Lin, Z. Y., El-Maarry, M. R., Pajola, M., Sierks, H., Barbieri, C., Lamy, P. L., Rodrigo, R., Koschny, D., Rickman, H., Keller, H. U., Agarwal, J., Barucci, M. A., Bertaux, J. L., Bertini, I., Besse, S., Bodewits, D., Cremonese, G., Da Deppo, V., Davidsson, B., Debei, S., De Cecco, M., Deller, J., Fornasier, S., Fulle, M., Gicquel, A., Groussin, O., Gutiérrez, P. J., Gutiérrez-Marquez, P., Güttler, C., Höfner, S., Hofmann, M., Hviid, S. F., Ip, W. H., Jorda, L., Knollenberg, J., Kovacs, G., Kramm, J. R., Kührt, E., Küppers, M., Lara, L. M., Lazzarin, M., Lopez Moreno, J. J., Marzari, F., Massironi, M., Mottola, S., Naletto, G., Oklay, N., Preusker, F., Scholten, F., Shi, X., Thomas, N., Toth, I., and Tubiana, C., 'Summer fireworks on comet 67P,' mnras, 2016, 462, pp. S184–S194.

Vokrouhlicky, D., Nesvorny, D., Dones, L., 'Origin and Evolution of Long-period Comets,' AJ, 2019, 157, P. 181

Wesołowski, M., Gronkowski, P., and Tralle, I., 'Outbursts of comets at large heliocentric distances: Concise review and numerical simulations of brightness jumps,' planss, 2020, 184, p. 104867.

Wierzchos, K. andWomack, M., 'Co gas and dust outbursts from centaur 29P/Schwassmann-wachmann,' Astronomical Journal, 2020, 159, p. 136.

Yang, B., Hutsemékers, D., Shinnaka, Y., Opitom, C., Manfroid, J., Jehin, E., Meech, K. J., Hainaut, O. R., Keane, J. V., Gillon, M., 'Isotropic ratios in outbursting comet C/2015 ER61,' 2018, A&A 609, L4.

Zolensky, M. E., Zega, T. J., Yano, H., Wirick, S., Westphal, A. J., Weisberg, M. K., Weber, I., Warren, J. L., Velbel, M. A., Tsuchiyama, A., Tsou, P., Toppani, A., Tomioka, N., Tomeoka, K., Teslich, N., Taheri, M., Susini, J., Stroud, R., Stephan, T., Stadermann, F. J., Snead, C. J., Simon, S. B., Simionovici, A., See, T. H., Robert, F., Rietme.er, F. J. M., Rao, W., Perronnet, M. C., Papanastassiou, D. A., Okudaira, K., Ohsumi, K., Ohnishi, I., Nakamura-Messenger, K., Nakamura, T., Mostefaoui, S., mikouchi, T., Meibom, A., Matrajt, G., Marcus, M. A., Leroux, H., Lemelle, L., Le, L., Lanzirotti, A., Langenhort, F., Krot, A. N., Keller, L. P., Kearsey, A. T., Joswiak, D., Jacob, D., Ishii, H., Harvey, R., Hagiya, K., Grossman, L., Grossman, J. N., Graham, g. A., Gounelle, M., Gillet, P., Genge, M. J., Flynn, G., Ferroir, T., Fallon, F., Ebel, D. S., Dai, Z. R., Cordier, P., Clark, B., Chi, M., Butterworth, A. L., Brownlee, D. E., Bridges, J. C., Brennan, S., Brearley, A., Bradley, J. P., Bleuet, P., Bland, P. A., and Bastien, R., 'Mineralogy and petrology of comet 81P/Wild 2 nucleus samples,' Science, 2006, 314(5806), p. 1735.

SECTION

2. AN INVESTIGATION OF THE ABUNDANCES OF HYPERVOLATILES CO, CH_4, AND C_2H_6 IN JUPITER-FAMILY COMET 46P/WIRTANEN

About 40 comets have been characterized in the near-IR and radio and more than 200 comets have been cataloged at optical wavelengths. A large number of molecules have been identified in cometary atmospheres, both from ground- and space-based observations (Dello Russo et al., 2016a; Gibb et al., 2012; Bonev et al., 2017; Le Roy et al., 2015; Roth et al., 2018; Biver et al., 2015; Cochran et al., 2015). Roughly 15 Jupiter Family comets (JFCs) have been sampled in the near-IR, albeit at vastly different levels of detail (Roth et al., 2018, 2020; Bonev et al., 2021). Detections (or significant upper limits) are even sparser for the hypervolatiles CO and CH_4 due to observational challenges associated with this dynamical family. Although differences in abundances of parent species have been noted, such a small sample size has hampered development of a chemistry-based classification system.

2.1. DATA REDUCTION AND OBSERVATION OF 46P/WIRTANEN

46P/Wirtanen is a JFC whose favorable and close approach to Earth in Dec 2018 - Feb 2019 provided a great opportunity to improve our understanding of the distribution of volatiles in the early solar system and in this potential mission target. We observed 46P/Wirtanen using the high-resolution ($\lambda/\Delta\lambda \sim 40{,}000$) IR immersion grating echelle spectrograph iSHELL at the 3-m NASA Infrared Telescope Facility (IRTF) on UT February 4 and 5, 2019 (see Table 2.1). The superior IR active guiding capabilities of

iSHELL enabled us to achieve observing efficiency of up to 80%. Our observations were performed with a 0.75" wide (6-pixel wide) slit, oriented along the projected Sun-comet line on all dates. To achieve flux calibration, a suitably bright IR flux standard star was observed using a 4" wide slit on each date and for each setting (using a wider slit for the star than was used for the comet helps minimize loss of signal and thereby achieve a truer measure of the stellar continuum).

Table 2.1. Observing Log of 46P/Wirtanen.

UT Date (2019)	iSHELL Setting	UT time	R_h (AU)	Δ (AU)	$d\Delta/dt$ (km s^{-1})	T_{int} (minutes)	Slit PA
Feb 4	M2	09:37-11:30	1.27	0.33	13.20	78	187°
	Lp1	11:39-13:00	1.27	0.33	13.20	80	187°
Feb 5	Lp1	09:42-10:52	1.27	0.34	13.27	46	185°

Notes. R_h, Δ, and $d\Delta/dt$ are heliocentric distance, geocentric distance, and geocentric velocity, respectively, of 46P/Wirtanen, and T_{int} is total integration time on source. The slit position angle (PA) was oriented along the projected Sun-comet line on all dates.

We used two iSHELL settings: M2 (covering ~ 4.5 – 5.2 μm) which samples emissions of CO, CN, and H_2O simultaneously, and LP1 (covering ~ 3.2 – 3.6 μm) samples emission lines of CH_4, CH_3OH, C_2H_6, and H_2CO. All observations were performed using a standard ABBA nod pattern (sequence of four scans) where the A and B beams were placed symmetrically about the midpoint along the 15" long slit and separated by half its length. Thus, the comet was present in both beams. Combining the frames as A-B-B+A (comet-sky-sky+comet) canceled out background thermal continuum, sky emission (lines and continuum), and instrumental biases to second order in airmass. The data were then dark-subtracted (to account for high dark-current pixels), flat-fielded (using an internal

continuum lamp), cleaned of cosmic ray hits and hot pixels, and rectified to produce two-dimensional (spatial-spectral) frames, where each row corresponds to a constant (and unique) spatial position along the slit, and each column to a unique wavelength. We found that spatially resampling using a third-order polynomial more completely removed the curvature in the spatial dimension from iSHELL frames and so employed this in place of previously used second-order polynomials (DiSanti et al., 2017; Roth et al., 2017, 2018).

The spectral frames were spatially registered, and spectra were then extracted by summing signal over 15 rows (approximately 2.5"), seven rows to each side of the nucleus, defined as the peak of dust emission in a given spectral order. The Planetary Spectrum Generator (Villanueva et al., 2018) was used to generate atmospheric models, to assign a wavelength scale to the spectra, and to establish absolute column burdens of the component absorbing species in the terrestrial atmosphere. We convolved the fully resolved atmospheric transmittance function to the resolving power of the data and scaled it to the level of the comet continuum. We then subtracted the modeled continuum to isolate cometary emission lines as previously described. Synthetic models of fluorescent emission for our targeted species were compared to observed line intensities, after correcting each modeled line intensity for the monochromatic atmospheric transmittance at its Doppler-shifted wavelength (according to the geocentric velocity of the comet at the time of the observation).

2.2. RESULTS

We determined rotational temperatures (T_{rot}), volatile production rates (Q, molecules s^{-1}), and the abundance (or "mixing") ratios Q_X/Q_{H2O} (expressed in %) for

volatile species in 46P/Wirtanen. We found consistent results and excellent fits to the comet spectra, both for telluric absorptions and for cometary emission features.

2.2.1. Spatial Profile. Long-slit high-resolution infrared observations of comets permit investigations of processes in the inner coma, where both nucleus and extended sources (i.e., release from one or more sources in the coma) may contribute to the production and spatial distribution of a particular volatile. Analysis of spatial profiles of emissions for coma molecules can indicate whether their distributions differ from that expected for direct sublimation from the nucleus, as opposed to release from extended sources in the coma (Dello Russo et al., 1998, 2016a; DiSanti et al., 2001; Brooke et al., 2003). The spatial profiles for molecules produced by direct sublimation peak in intensity at (or at least near) the position of the nucleus before falling off with increasing nucleocentric distance (ρ) as ρ^{-1}, whereas molecules having an extended source display a flatter distribution, falling off more slowly with ρ (e.g., see Figure 3 in Dello Russo et al., 1998, and Figure 5 in Dello Russo et al., 2016). By summing the spatial profiles of all individual lines for each species within a grating setting, we were able to extract spatial profiles for emission from H_2O and C_2H_6 in 46P/Wirtanen (see Figure 2.1.).

The signal-to-noise ratio is not sufficient to see weaker species spatial profiles. The profiles for dust H_2O and C_2H_6 molecules track one another, suggesting that molecules are co-released.

2.2.2. Molecular Fluorescence Analysis. Synthetic models of fluorescence emission for each targeted species were compared to observed line intensities, after correcting each modeled line intensity (g-factor) for the monochromatic atmospheric transmittance at its Doppler-shifted wavelength (according to the geocentric velocity of the

comet at the time of the observations). The g-factors used in synthetic emission models in this study were generated with quantum mechanical models developed for H_2O (Villanueva et al., 2012a), C_2H_6 (Villanueva et al., 2011b), CO, and CH_4 (Paganini et al., 2013; Villanueva et al., 2011a; Gibb et al., 2003), H_2CO (DiSanti et al., 2006), and CH_3OH (Villanueva et al., 2012b; DiSanti et al., 2013). Production rates for each sampled species were determined from the appropriate fluorescence model at the best-fit rotational temperature of each molecule.

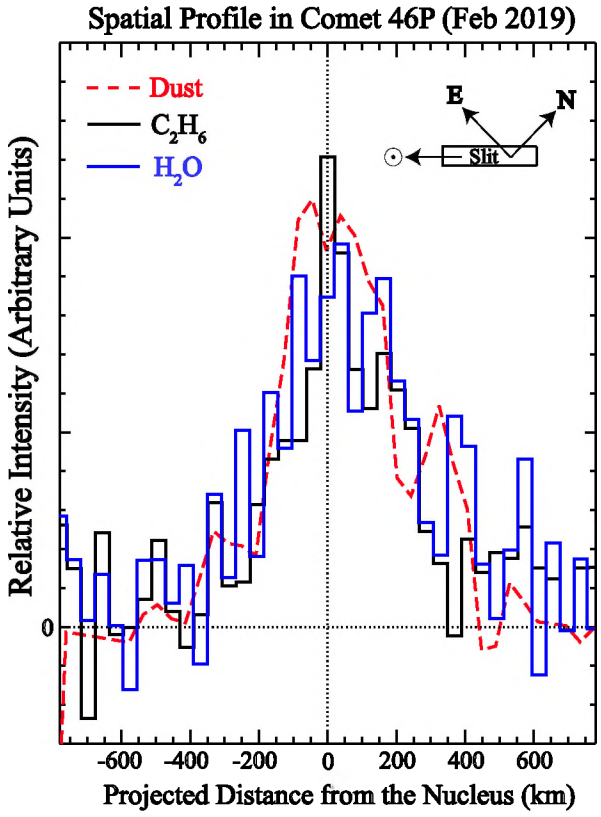

Figure 2.1. Spatial profile of H_2O, C_2H_6, and dust in comet 46P/Wirtanen on UT 2019 February 4. The slit was oriented along the Sun-comet line (~186°) for all of our 46P's February observations. The profiles suggest that the spatial distributions of C_2H_6 and H_2O tracked that of measured dust.

A line-by-line analysis and a Levenberg-Marquardt nonlinear minimization technique (Villanueva et al., 2008) was used to fit fluorescence emission from all species simultaneously within each echelle order, allowing for high-precision results, even in spectrally crowded regions containing many spectral lines within a single instrumental resolution element (see Figure 2.2).

2.2.3. Rotational Temperature, Production Rates, and Mixing Ratios. Maximum brightnesses of JFCs are often near their closest approach to Earth, when geocentric velocities (Δ_{dot}) are small. Measuring CO and CH_4 requires sufficiently high Δ_{dot} to shift cometary emissions from their highly opaque telluric counterparts to wavelengths with the adequate atmospheric transmission.

At the time of 46P/Wirtanen's closest approach (UT 2018 Dec-16), the geocentric velocity was insufficient for studies of CO and CH_4; however, by January (Δ_{dot}~10 km s^{-1}; McKay et al., 2021) to early February 2019 (Δ_{dot} ~ 13 km s^{-1}; this work) the geocentric velocity became large enough while the comet was still sufficiently bright to characterize 46P/Wirtanen hypervolatile content and place stringent upper limits on CO and CH_4.

Additionally, our February observations included fluorescent emission from other volatile species (most notably CH_3OH, and CN). We detected fluorescent emission from H_2O, C_2H_6, CH_3OH, and CN (at 4σ) and derived 3σ upper limits for CO, CH_4, and H_2CO (see Table 2.2). Mixing ratios of 46P/Wirtenen hypervolatiles in February were consistent with their mean values from our January observations (see McKay et al., 2021).

When calculating production rates, we assumed the GF of simultaneously measured H_2O, C_2H_6 on Feb 4 and Feb 5. Global production rates for all the targeted species and their mixing ratios relative to water are presented in Table 2.2.

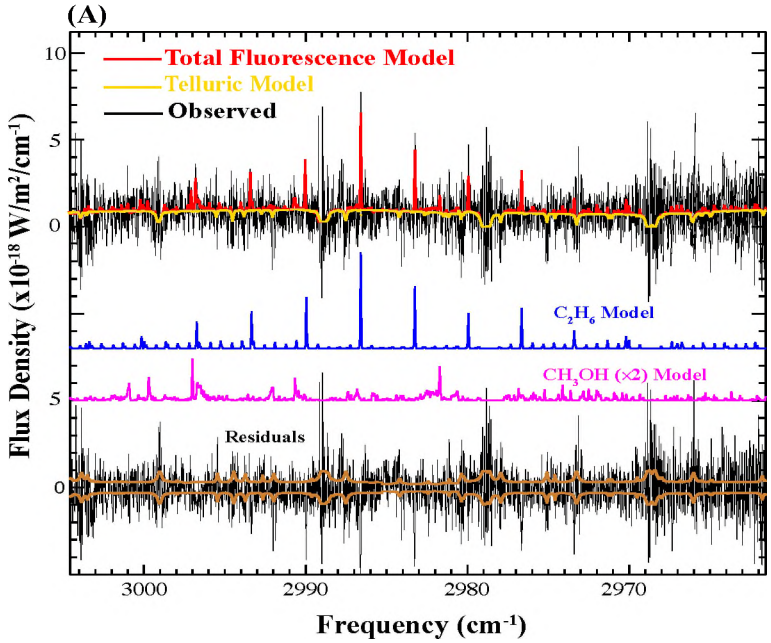

Figure 2.2 Fluorescence emissions of C_2H_6 and CH_3OH in comet 46P/Wirtanen on UT 2019 February 4. The gold trace overplotted on cometary spectrum is the telluric absorption model, while the sum of fluorescent emission models for all species is overplotted in red. Individual fluorescent emission models (color-coded by molecule) are plotted directly below, offset vertically for clarity. At the bottom of the panel is the residual spectrum (after subtracting the telluric absorption model and all fluorescent emission models) with the 1σ error envelope overplotted in bronze.

Rotational temperatures (T_{rot}) were determined using correlation and excitation analyses that have been extensively described in the literature (e.g., Bonev 2005; Bonev et al., 2008; DiSanti et al., 2006; Villanueva et al., 2008). In general, well-constrained rotational temperatures can be determined for individual species with intrinsically bright lines and for which a sufficiently broad range of excitation energies is sampled. These conditions were met for H_2O in M2 and C_2H_6 lines in Lp1 settings. The T_{rot} for H_2O was well constrained on Feb 4 (59 ± 10 K) and was consistent with that for C_2H_6 (59 ± 7 K) on the same date.

Table 2.2. Molecular species measured in comet 46P/Wirtanen.

Molecule	T_{rot}[a] (K)	GF[b]	Q[c] (molecules s^{-1})	Q_x/Q_{H2O}[d] (%)	Q_x/Q_{C2H6}[e]
2019 Feb 4, R_h = 1.27 au, Δ = 0.33 au, $d\Delta/dt$ = 13.20 km s^{-1}, M2 and Lp1 settings					
H_2O	59 ± 10	2.10 ± 0.20	(2.64 ± 0.34) × 10^{27}	100	118 ± 20
CO	(59)	(2.14)	< 1.49 × 10^{25}	< 1.69[f]	< 2.00
CN	(59)	(2.14)	(3.03 ± 0.55) × 10^{25}	1.14 ± 0.28	1.35 ± 0.29
C_2H_6	59 ± 7	1.95 ± 0.15	(2.23 ± 0.10) × 10^{25}	0.84 ± 0.14	1
CH_4	(59)	(1.95)	< 8.43 × 10^{24}	< 0.95[f]	< 1.13
CH_3OH	(59)	(1.95)	(3.01 ± 0.64) × 10^{25}	1.14 ± 0.30	1.34 ± 0.32
H_2CO	(59)	(1.95)	< 5.30 × 10^{24}	< 0.60[f]	< 0.71
2019 April 5, R_h = 1.27 au, Δ = 0.34 au, $d\Delta/dt$ = 13.27 km s^{-1}, Lp1 setting					
CH_4	(59)	(1.95)	< 2.75 × 10^{25}	< 3.12[f]	< 3.69
CH_3OH	(59)	(1.95)	< 1.55 × 10^{25}	< 1.76[f]	< 2.08
H_2CO	(59)	(1.95)	< 7.60 × 10^{24}	< 0.86[f]	< 1.02

Notes. [a] Rotational temperature. Values in parentheses are assumed. [b] Growth factor. Values in parentheses are assumed. [c] Global production rate. Errors in production rate include line-by-line deviation between modeled and observed intensities and photon noise (see Dello Russo et al., 2004; Bonev 2005; Bonev et al., 2007). [d] Molecular abundance with respect to H_2O. [e] Abundance ratios with respect to C_2H_6. [f] 3σ upper limit.

We adopted the rotational temperature of simultaneously measured H_2O (or C_2H_6 in Lp1 setting with no H_2O emission lines) within the same setting for species without a well-constrained T_{rot} (e.g., CO, CH_4). We also adopted the rotational temperature of H_2O and C_2H_6 from Feb 4 to analyse our data on Feb 5. Rotational temperatures for different molecules for the same comet and within the same instrumental setting are generally found to be consistent, even for molecules with differing photo-dissociation lifetimes (e.g., see Bonev 2005, DiSanti et al., 2006; Gibb et al., 2012; and DiSanti et al., 2016 supporting this approach).

Using alternative compositional baselines other than H_2O (Q_x/Q_{H2O} %) can provide richer insights in comparing comets. For instance, Biver & Bockelée-Morvan (2019) used

CH_3OH as their measurement baseline in comparing complex organic molecules in comets. Owing to the low vacuum sublimation temperature of C_2H_6, distinct outgassing morphologies in many comets compared with H_2O, and the easy detectability of this molecule at near-infrared wavelengths, C_2H_6 can serve as a possible alternative compositional baseline (see Section 5.4.2 in Bonev et al., 2021 for details). Therefore, we present abundances with respect to both H_2O and C_2H_6. C_2H_6 is one of the frequently observed molecules among comet populations (Dello Russo et al., 2016a). Its fluorescence emissions are located at regions of adequate atmospheric transmittance regardless of geocentric velocity (Δ_{dot}). Unlike water, C_2H_6 is a hypervolatile with one of the lowest vacuum sublimation temperatures and has shown distinct outgassing behavior in some comets, thus deriving mixing ratios with respect to C_2H_6 can be used as an alternative compositional baseline for future work (Bonev et al., 2021).

2.2.4. 46P/Wirtanen's Hypervolatiles Content in Context of Other Comets to Date. Hypervolatile abundances have been securely measured in only 22 comets to date in which only 4 of them are ecliptic comets (see Roth et al. 2020 for details). This highlights the statistics for these species in ecliptic comets (particularly CO and CH_4) are far from being firmly established (Roth et al. 2020). Figure 2.3 shows relative hypervolatile abundances and their wide range reported in all comets to date, including 46P and the measurements taken by Rosetta for comet 67P/Churyumov–Gerasimenko.

2.3. DISCUSSION

The water production rate (molecules s^{-1}) as measured in our February observation was approximately 50 – 75% smaller compared with January observations (McKay et al.,

2021). McKay et al., (2021) reported a clear variability in H_2O production rates on time scales of days and hours (The rotation period of the 46P's nucleus is ~ 9 hours; see Farnham et al., 2018), making it plausible that changes in water production rate could occur on time scales of a few hours (2-4 hours), owing to changes in insolation patterns that result from nucleus rotation.

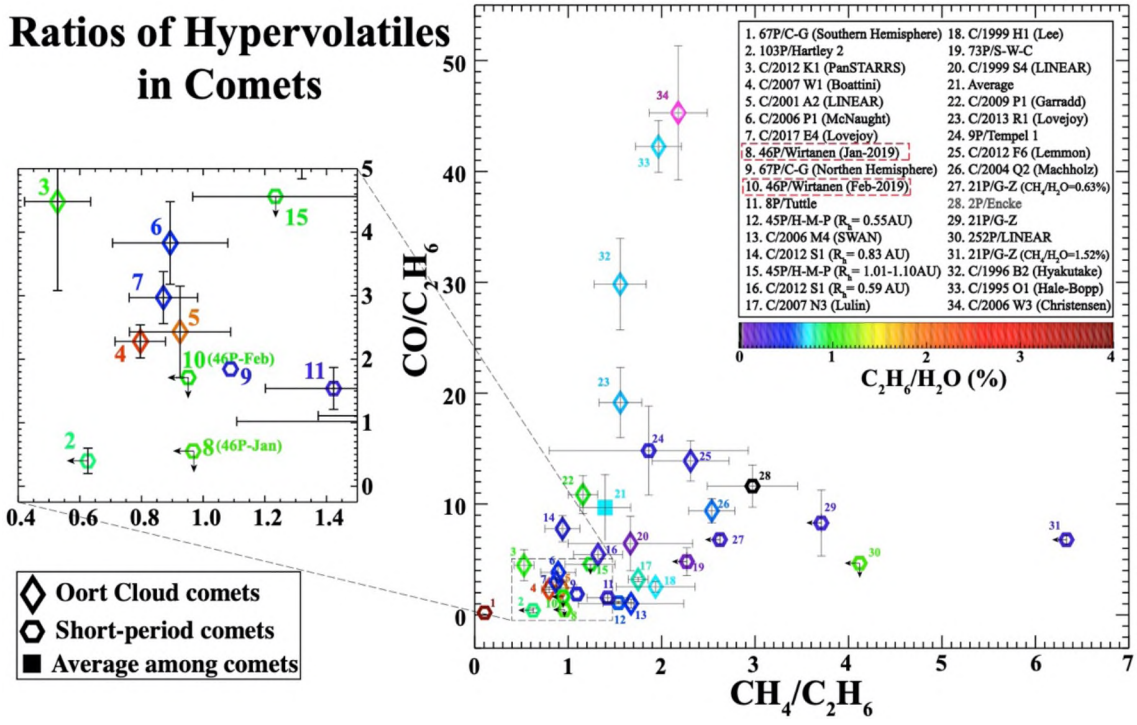

Figure 2.3. Ratios of hypervolatiles in comets measured to date. Comets are labeled with a bold number in the figure and in the figure's legend. The number of comets in which the complete hypervolatile inventories are available is small (22 comets so far, see Roth et al., 2020 for more details). The downward- and leftward-facing arrows indicate the (3σ) upper limits of CO/C_2H_6 and CH_4/C_2H_6. Comet are color coded by their mixing ratio of C_2H_6/H2O (%) with the exception of comet C/2006 W3 (Christensen), #34 and pink in the figure, for which H_2O was not detected.

Our derived mixing ratio for C_2H_6, and 3σ upper limits for CO and CH_4 are consistent with those in our January observations (see McKay et al., 2021). Additionally, our February observation also detected CN, and CH_3OH. McKay et al., (2021) reported a higher mixing ratio relative to H_2O (and closer to mean among comet population) for CH_3OH, whereas our February mixing ratios show a lower abundance for this molecule (~ 80 % smaller). This might indicate the existence of heliocentric related change in mixing ratios, however comparison of mixing ratios of C_2H_6 and CH_3OH from December – January do not show such asymmetry for these molecules (Bonev et al., 2021; McKay et al., 2021, Khan et al., 2021; Roth et al., 2021). Comparison with narrowband CN imaging from UT Feb 5 and 7 could help better our understanding of 46P/Wirtanen's CN content.

3. A SUMMARY OF THIS DISSERTATION AND FUTURE IN THE COMETARY SCIENCE

3.1. GOALS ADDRESSED BY THIS DISSERTATION

This dissertation is comprised of the results of eight observing programs with iSHELL; spread over three years as well as two observing proposals with CSHELL in 2004. These results have either been published (Saki et al., 2020a) or accepted for publication (Saki et al., 2021) in peer-reviewed academic journals. This section is dedicated to the major science goals addressed in each work and place these goals into the context of cometary science. An overview of future work and opportunities in the field of cometary science is also provided.

3.1.1. Carbonyl Sulfide (OCS): Detections in Comets C/2002 T7 (LINEAR), C/2015 ER61 (PanSTARRS), and 21P/Giacobini–Zinner and Stringent Upper-limits in 46P/Wirtanen. OCS is an extremely under-represented species in the current taxonomy of cometary volatiles. Saki et al., (2020) addressed this major paucity by reporting detections of this molecule in two Oort cloud comets (C/2015 ER61 and C/2002 T7) and for the "first" time in a Jupiter-family comet (21P/G-Z) from a ground-based facility. Saki et al., (2020) also reported a stringent 3σ upper-limit in 46P/Wirtanen (lowest reported in any comet). The first OCS measurement for a short-period comet did not occur until 2015 via the Rosetta mission to comet 67P. Saki et al., (2020) reported the detection of OCS in comet 21P/G-Z by combining the spectra of three dates. Jupiter-family comets are generally dim and not productive perhaps owing to repeated close perihelion passages into the inner solar system. The limitations in sensitivity in earlier instruments (see the discussion in Dello Russo et al., 2016a) and non-simiultanous measurements with other

volatiles along with the low productivity of these comets were the main reasons of this paucity.

Furthermore, Saki et al., (2020) searched for a possible correlation between OCS and CO when both measurements were available in literature. Owing to the OCS vacuum sublimation temperature of 85 K, the high volatility and lower thermal threshold of CO makes evolutionary processing effects potentially more important for CO than for OCS. Figure 6 in Saki et al., (2020) may suggest a higher OCS abundance is correlated with high CO abundance; However, the very small number of OCS measurements to date in comets precludes establishing a clear correlation between CO and OCS at this time. Saki et al., (2020) significantly expanded the range of OCS abundances, increased the number of OCS measurements in comets, and contributed extensively to establishing a more meaningful statistic for this prebiotically important sulfur-bearing species.

3.1.2. Chemical Composition of Outbursting Comet C/2015 ER61. Comet ER61 was a dynamically new young Oort cloud comet whose favorable approach in 2017 provided an excellent opportunity to examine its primary chemical composition. We observed comet ER61 in UT 2017 April 15-17 (shortly after its April 4 major outburst) as well as in May 11-13 when it just passed perihelion (May 10). Saki et al., (2021) found that ER61 exhibited variability in production rates of many species on short (day-to-day) and long (pre- vs. post-perihelion) timescales. The relative abundances of these volatile species remained consistent within uncertainties during pre-perihelion observations but tended to decrease during post-perihelion observations (with the exception of CH_3OH and HCN).

The short-timescale variability in the production rates of these volatiles could be due to diurnal effects (over the course of the rotation of the nucleus) and/or the effect of its

outburst. The decrease in the production rates and hence the mixing ratios in some volatiles in post-perihelion dates could be due to the presence of seasonal effects in ER61 (similar to the observed variations in comet 2P/Encke (Roth et al., 2018) and comet 67P/C-G (e.g., Le Roy et al., 2015)). Saki et al., (2021) also reported detection of weaker (difficult to detect) species such as C_2H_2, H_2CO, OCS and a sensitive 3σ upper limits for cyanoacetylene (HC_3N).

3.1.3. An Investigation of the Abundances of Hypervolatiles CO, CH_4, and C_2H_6 in Jupiter-family Comet 46P/Wirtanen. Comet 46P/Wirtanen is a Jupiter-family comet whose very close and favorable apporoch to Earth in December 2018 - February 2019 offered an excellent opportunity to measure the primary volatile composition in this potential mission target. At the time of 46P's closest approach (December 16), the geocentric velocity was insufficient for studies of CO and CH_4; however, by January ($\Delta \sim$ 10 km s^{-1}, McKay et al., 2021) to early February 2019 ($\Delta \sim$ 13 km s^{-1}, this work) the geocentric velocity became large enough while the comet was still sufficiently bright to characterize 46P hypervolatile content and place stringent upper limits on CO and CH_4.

Additionally, our 2019 February observations included fluorescent emission from other volatile species (most notably CH_3OH, and CN). We detected fluorescent emission from H_2O, C_2H_6, CH_3OH, and CN (at 4σ) and derived 3σ upper limits for CO, CH_4, and H_2CO (see Table 2.2). Mixing ratios of 46P/Wirtenen hypervolatiles in February were consistent with their mean values from our January observations (see McKay et al., 2021).

3.2. THE NEXT GENERATION OF COMETARY ASTRONOMY

The combination of new/upgraded and upcoming state-of-the-art instruments, such as the Atacama Large Millimeter/Submillimeter Array (ALMA), iSHELL at NASA-IRTF, NIRSPEC-2 (upgraded NIRSPEC) at W. M. Keck II, and the James Webb Space Telescope (JWST; schedule to lauch in late 2021) is enabling the next generation of cometary astronomy. These facilities are enabling searches for novel and less-understood behaviors in comets, such as compositional variability and small R_h studies (iSHELL), the detection and mapping of complex organics and tests of isotopic ratios in moderately bright comets (ALMA), and testing coma composition and spatial associations with unprecedented sensitivity and at large R_h (JWST).

JWST will provide highly complementary results to ground-based observations of comets. It will be particularly powerful for observing comets at $R_h > 3$ AU (where H_2O is not fully activated, and cometary activity is driven by CO and CO_2) and at excellent spatial resolution, enabling studies of coma volatile composition and spatial distributions at heliocentric distances that are often out of reach to ground-based IR and mm/sub-mm observatories. JWST will enable comprehensive studies of CO_2 in comets, a primary driver for cometary activity along with H_2O and CO, but which is unobservable from the ground and therefore not well understood (Kelley et al., 2016 and refs. therein). JWST will enable simultaneous or contemporaneous studies of the abundances and spatial distributions of all three species in comets over a range of R_h, providing highly complementary results to the ground-based spatial studies conducted at smaller R_h and dramatically improving the understanding of cometary behavior over all portions of an orbit.

The work in this dissertation will be continued and complemented by author's postdoctoral research addressing these topics as well as the archival near-infrared data of comets C/2002 T7 (LINEAR) and C/2017 T2 (PanSTARRS) (Saki et al., in prepration for Astronomical Journal).

3.3. FINAL REMARKS

The results of comet missions such as Deep Impact, EPOXI, and Rosetta have led to fundamental questions (posed by A'Hearn (2017)) regarding the nature of comets: How (or whether) the properties and behaviors of comets change with time? To what degree do comets retain cosmogonic signatures in their nuclei? How are comets ices put together? Are the behaviors seen by these missions exceptional or common? The results reported in this work seek to address these questions by characterizing the primary volatile composition of four comets and using these results to decode the history of volatile matter in the early solar system.

APPENDIX

COPYRIGHT AGREEMENTS FOR WORKS PUBLISHED

This dissertation includes materials from works published or accepted for publication in the American Astronomical Society's the Astronomical Journal. These include Section 2 (Saki et al., 2020), Section 3 (Saki et al., 2021). Included for reference are the copyright agreements signed by Saki and coauthors specifying the rights granted to them, including the right to reproduce all or part of their articles in their own future works, such as this dissertation (see figures below).

AMERICAN ASTRONOMICAL SOCIETY

This agreement must be electronically signed before the American Astronomical Society (AAS) can publish your paper. In the event the article is not judged acceptable for publication in the journal you will be notified in writing and the copyright and all rights conferred by this agreement shall revert to you.

PUBLICATION AND TRANSFER OF COPYRIGHT AGREEMENT Manuscript number: AAS23532

Article title: Carbonyl Sulfide (OCS): Detections in comets C/2002 T7 (LINEAR), C/2015 ER61 (PanSTARRS), and 21P/Giacobini-Zinner and stringent upper-limits in 46P/Wirtanen.

Names of authors: Mohammad Saki Erika Gibb Boncho Bonev Nathan Roth Michael DiSanti Neil Dello Russo Ronald Vervack Adam McKay Hideyo Kawakita

Author Rights: AAS grants to the author(s) (or their below-named employers, in the case of works made for hire) the following rights. All copies of the Article made under any of these rights shall include notice of the AAS copyright.

(1) All proprietary and statutory rights other than copyright, such as patent rights.

(2) The right after publication by the AAS to grant or refuse permission to third parties to republish all or part of the Article or a translation thereof. In the case of whole articles only, third parties must first obtain permission from the AAS before any right of further publication is granted. The AAS may choose to publish an abstract or portions of the Article before the AAS publishes it in a journal.

(3) The right to use all or part of the Article in future works and derivative works of their own of any type, and to make copies of all or part of the Article for the authors' use for educational or research purposes.

(4) In the case of a work made for hire, the right of the employer to make copies of the Article for the employer's internal use, but not for resale.

Copyright Assignment: Copyright in the Article is hereby transferred to the AAS for the full term of copyright throughout the world, effective as of date of acceptance of the Article for publication in a journal of the AAS. The copyright consists of all rights protected by copyright laws of the United States and of all foreign countries, in all languages and forms of communication, and includes all material to be published as part of the Article in any format or medium. The AAS shall have the right to register copyright to the Article in its name as claimant, whether separately or as part of the journal issue or other medium in which the Article is included and the right to sue, counterclaim, and recover for past, present and future infringement of the rights assigned under this agreement.

This Agreement shall be controlled, construed and enforced in accordance with the laws of the District of Columbia without reference to the conflict of laws provisions thereof. The Parties consent to jurisdiction of the state and federal courts located in the District of Columbia in connection with any proceeding related to this Agreement or its enforcement.

Authorized Signature: Mohammad Saki Date: 03/23/2020

Certification of Government Employment: An article prepared by a government officer or employee as part of his or her official duties may not be eligible for copyright, if the authors are all employed by one of the governments of Australia, Canada, New Zealand, the UK, or the US. If all the authors of the article are such government employees, one of the authors should sign here. If any of the authors is not such a government employee, do not sign in this box.

Authorized Signature:
Date:

local_p_id: 725755
time: 1584984677
ip address: 71.14.90.215

Figure A.1. Copyright agreement between Saki and coauthors and the American Astronomical Society for Saki et al., (2020).

AMERICAN ASTRONOMICAL SOCIETY

This agreement must be electronically signed before the American Astronomical Society (AAS) can publish your paper. In the event the article is not judged acceptable for publication in the journal you will be notified in writing and the copyright and all rights conferred by this agreement shall revert to you.

PUBLICATION AND TRANSFER OF COPYRIGHT AGREEMENT Manuscript number: AAS31091

Article title: Chemical Composition of Outbursting Comet C/2015 ER61(PanSTARRS).

Names of authors: Mohammad Saki Erika Gibb Boncho Bonev Nathan Roth Michael DiSanti Younas Khan Neil Dello Russo Ronald Vervack Adam McKay Hideyo Kawakita

Author Rights: AAS grants to the author(s) (or their below-named employers, in the case of works made for hire) the following rights. All copies of the Article made under any of these rights shall include notice of the AAS copyright.

(1) All proprietary and statutory rights other than copyright, such as patent rights.

(2) The right after publication by the AAS to grant or refuse permission to third parties to republish all or part of the Article or a translation thereof. In the case of whole articles only, third parties must first obtain permission from the AAS before any right of further publication is granted. The AAS may choose to publish an abstract or portions of the Article before the AAS publishes it in a journal.

(3) The right to use all or part of the Article in future works and derivative works of their own of any type, and to make copies of all or part of the Article for the authors' use for educational or research purposes.

(4) In the case of a work made for hire, the right of the employer to make copies of the Article for the employer's internal use, but not for resale.

Copyright Assignment: Copyright in the Article is hereby transferred to the AAS for the full term of copyright throughout the world, effective as of date of acceptance of the Article for publication in a journal of the AAS. The copyright consists of all rights protected by copyright laws of the United States and of all foreign countries, in all languages and forms of communication, and includes all material to be published as part of the Article in any format or medium. The AAS shall have the right to register copyright to the Article in its name as claimant, whether separately or as part of the journal issue or other medium in which the Article is included and the right to sue, counterclaim, and recover for past, present and future infringement of the rights assigned under this agreement.

This Agreement shall be controlled, construed and enforced in accordance with the laws of the District of Columbia without reference to the conflict of laws provisions thereof. The Parties consent to jurisdiction of the state and federal courts located in the District of Columbia in connection with any proceeding related to this Agreement or its enforcement.

Authorized Signature: Mohammad Saki Date: 03/19/2021

Certification of Government Employment: An article prepared by a government officer or employee as part of his or her official duties may not be eligible for copyright, if the authors are all employed by one of the governments of Australia, Canada, New Zealand, the UK, or the US. If all the authors of the article are such government employees, one of the authors should sign here. If any of the authors is not such a government employee, do not sign in this box.

Authorized Signature:
Date:

local_p_id: 725755
time: 1616182531
ip address: 71.14.90.215

Figure A.2. Copyright agreement between Saki and coauthors and the American Astronomical Society for Saki et al., (2021).

BIBLIOGRAPHY

A'Hearn, M. F., 'Comets: looking ahead,' Philosophical Transactions of the Royal Society A, 2017, 375(2097), p. 20160261.

A'Hearn, M. F., Millis, R. C., Schleicher, D. O., Osip, D. J., and Birch, P. V., 'The ensemble properties of comets: Results from narrowband photometry of 85 comets, 1976-1992,' Icarus, 1995, 118(2), pp. 223–270.

Bockelée-Morvan, D., Lis, D. C., Wink, J. E., Despois, D., Crovisier, J., Bachiller, R., Benford, D. J., Biver, N., Colom, P., Davies, J. K., Gérard, E., Germain, B., Houde, M., Mehringer, D., Moreno, R., Paubert, G., Phillips, T. G., and Rauer, H., 'New molecules found in comet C/1995 O1 (hale-bopp). investigating the link between cometary and interstellar material,' AAP, 2000, 353.

Bockelée-Morvan, D., Crovisier, J., Erard, S., Capaccioni, F., Leyrat, C., Filacchione, G., Drossart, P., Encrenaz, T., Biver, N., de Sanctis M.-C., Schmitt, B., Kührt, E., M.-T., C., Combes, M., Combi, M., Fougere, N., Arnold, G., Fink, U., Ip, W., Migliorini, A., Piccioni, G., and Tozzi, G., 'Evolution of CO2, CH4, and OCS abundances relative to H_2O in the coma of comet 67P around perihelion from Rosetta/VIRTISH observations,' Monthly Notices of the Royal Astronomical Society, 2016, 462(1), pp. S1270–S183.

Bonev, B. P., Towards a Chemical Taxonomy of Comets: Infrared Spectroscopic Methods for Quantitative Measurements of Cometary Water (With an Independent Chapter on Mars Polar Science), phdthesis, The University of Toledo, 2005.

Bonev, B. P., Mumma, M. J., DiSanti, M. A., Dello Russo, N., Magee-Sauer, K., Ellis, R. S., and Stark, D. P., 'A comprehensive study of infrared OH prompt emission in two comets. i. observations and effective g-factors,' The Astrophysical Journal, 2006, 653(1), pp. 774–787.

Bonev, B. P., Mumma, M. J., Kawakita, H., Kobayashi, H., and Villanueva, G. L., 'Ircs/subaru observations of water in the inner coma of comet 73P-B/Schwassmann Wachmann 3: Spatially resolved rotational temperatures and ortho para ratios,' Icarus, 2008a, 196(1), pp. 241–248.

Bonev, B. P., Dello Russo, N., DiSanti, M. A., Martin, E. C., Doppmann, G., Vervack, J., R. J., Villanueva, G. L., Kawakita, H., Gibb, E. L., Combi, M. R., Roth, N. X., Saki, M., McKay, A. J., Cordiner, M. A., Bodewits, D., Crovisier, J., Biver, N., Cochran, A. L., Shou, Y., Khan, Y., and Venkataramani, K., 'First comet observations with NIRSPEC-2 at Keck: Outgassing sources of parent volatiles and abundances based on alternative taxonomic compositional baselines in 46p/wirtanen,' The Planetary Science Journal, 2021, 2, p. 45.

Bonev, B. P., Mumma, M. J., Radeva, Y. L., DiSanti, M. A., Gibb, E. L., and Villanueva, G. L., 'The peculiar volatile composition of comet 8P/Tuttle: A contact binary of chemically distinct cometesimals?' The Astrophysical Journal Letters, 2008b, 680(1), p. L61.

Bregman, J. D., Witteborn, F. C., Allamandola, L. J., Campins, H., Wooden, D. H., Rank, D. M., Cohen, M., and Tielens, A. G. G. M., 'Airborn and groundbased spectrophotometry of comet P/Halley from 5-13 micrometers,' Astronomy and Astrophysics, 1987, 187(1-2), pp. 616–620.

Crovisier, J., Biver, N., Bockelée-Morvan, D., Bossier, J., Colom, P., and Lis, D. C., 'The chemical diversity of comets: Synergies between space exploration and groundbased radio observations,' Earth, Moon, and Planets, 2009, 105(2-4), pp. 267–272.

Cochran, A. L., Levasseur-Regourd, A.-C., Cordiner, M., Hadamcik, E., Lasue, J., Gicquel, A., Schleicher, D., Charnley, S. B., Mumma, M. J., Paganini, L., Bockelée-Morvan, D., Biver, N., and Kuan, Y.-J., 'The composition of comets,' Space Science Reviews, 2015, 197(1-4), pp. 9–46.

Cochran, A. L., Barker, E. S., and Gray, C. L., 'Thirty years of cometary spectroscopy from mcdonald observatory,' Icarus, 2012, 218(1), pp. 144–168.

Dello Russo, N., DiSanti, M. A., Mumma, M. J., Magee-Sauer, K., and Rettig, T. W., 'Carbonyl sulfide in comets C/1996 B2 (Hyakutake) and C/1995 O1 (Hale-Bopp): Evidence for an extended source in Hale-Bopp,' Icarus, 1998, 135(2), pp. 377–388.

Dello Russo, N., Kawakita, H., Jr., V. R. J., and Weaver H., A., 'Emerging trends and a comet taxonomy based on the volatile chemistry measured in thirty comets with high-resolution infrared spectroscopy between 1997 and 2013,' Icarus, 2016a, 278, pp. 301–332.

Dello Russo, N., Vervack, R. J. J., Kawakita, H., Cochran, A., McKay, A. J., Harris,W. M., Weaver, H. A., Lisse, C. M., DiSanti, M. A., Kobayashi, H., Biver, N., Bockelée-Morvan, D., Crovisier, J., Opitom, C., and Jehin, E., 'The compositional evolution of C/2012 S1 (ISON) from ground-based high-resolution infrared spectroscopy as part of a worldwide observing campaign,' Icarus, 2016b, 266, pp. 152–175.

Dello Russo, N., Mumma, M. J., DiSanti, M. A., and Magee-Sauer, K., 'Production of ethane and water in comet C/1996 B2 Hyakutake,' Journal of Geophysical Research (Planets), 2002b, 107(E11), p. 5095.

Dello Russo, N., Mumma, M. J., DiSanti, M. A., Magee-Sauer, K., and Novak, R., 'Ethane production and release in comet C/1995 O1 Hale-Bopp,' Icarus, 2001, 153(1), pp. 162–179.

Dello Russo, N., Mumma, M. J., DiSanti, M. A., Magee-Sauer, K., Novak, R., and Rettig, T.W., 'Water production and release in comet C/1995 O1 Hale-Bopp,' Icarus, 2000, 143(2), pp. 324–337.

Dello Russo, N., Vervack, R. J. J., Weaver, H. A., Biver, N., Bockelée-Morvan, D., Crovisier, J., and Lisse, C. M., 'Compositional homogeneity in the fragmented comet 73P/Schwassmann-Wachmann 3,' Nature, 2007, 448(7150), pp. 172–175.

DiSanti, M. A., Bonev, B. P., Magee-Sauer, K., Dello Russo, N., Mumma, M. J., Reuter, D. C., and Villanueva, G. L., 'Detection of formaldehyde emission in comet C/2002 T7 (LINEAR) at infrared wavelengths: Line-by-line validation of modeled fluorescent intensities,' The Astrophysical Journal, 2006, 650(1), pp. 470–483.

DiSanti, M. A., Bonev, B. P., Villanueva, G. L., and Mumma, M. J., 'Highly depleted ethane and mildly depleted methanol in comet 21P/Giacobini-Zinner: Application of a new emprical ν_2-band model for CH_3OH near 50 K,' The Astrophysical Journal, 2013, 763(1), p. 19.

DiSanti, M. A., Mumma, M. J., Dello Russo, N., and Magee-Sauer, K., 'Carbon monoxide production and excitation in comet C/1995 O1 (Hale-Bopp): Isolation of native and distributed CO sources,' Icarus, 2001, 153(2), pp. 361–390.

DiSanti, M. A., Villanueva, G. L., Paganini, L., Bonev, B. P., Keane, J. V., Meech, K. J., and Mumma, M. J., 'Pre- and post-perihelion observations of C/2009 P1 (Garradd): Evidence for an oxygen-rich heritage?' Icarus, 2014, 228, pp. 167–180.

DiSanti, M. A., Bonev, B. P., Gibb, E. L., Paganini, L., Villanueva, G. L., Mumma, M. J., Keane, J. V., Blake, G. A., Dello Russo, N., Meech, K., Vervack, R. J. J., and McKay, A. J., 'En route to destruction: The evolution in composition of ices in comet D/2012 S1 (ISON) between 1.2 and 0.34 au from the Sun as revealed at infrared wavelengths,' The Astrophysical Journal, 2016, 820(1), p. 20.

DiSanti, M. A., Mumma, M. J., Dello Russo, N., Magee-Sauer, K., and Griep, D. M., 'Evidence for a dominant native source of carbon monoxide in comet C/1996 B2 (Hyakutake),' Journal of Geophysical Research Planets, 2003, 108(E61), p. 5061.

Fink, U., Doose, L., Rinaldi, G., Bieler, A., Capaccioni, F., Bockelée-Morvan, D., Filacchione, G., Erard, S., Leyrat, C., Blecka, M., Capria, M. T., Combi, M., Crovisier, J., De Sanctis, M. C., Fougere, N., Taylor, F., Migliorini, A., and Piccioni, G., 'Investigation into the disparate origin of CO_2 and H_2O outgassing for comet 67/P,' Icarus, 2016, 277, pp. 78–97.

Feaga, L. M., A'Hearn, M. F., Farnham, T. L., Bodewits, D., Sunshine, J. M., Gersch, A. M., Protopapa, S., Yang, B., Drahus, M., and Schleicher, D. G., 'Uncorrelated volatile behavior during the 2011 apparition of Comet C/2009 P1 Garradd,' The Astronomical Journal, 2014, 147(1), p. 24.

Gibb, E. L., Bonev, B. P., Villanueva, G., DiSanti, M. A., Mumma, M. J., Sudholt, E., and Radeva, Y., 'Chemical composition of comet C/2007 N3 (Lulin): Another "atypical" comet,' The Astrophysical Journal, 2012, 750(2), p. 102.

Gibb, E. L., Mumma, M. J., Dello Russo, N., DiSanti, M. A., and Magee-Sauer, K., 'Methane in Oort cloud comets,' Icarus, 2003, 165(2), pp. 391–406.

Gomes, R., Levison, H. F., Tsiganis, K., and Morbidelli, A., 'Origin of the cataclysmic late heavy bombardment period of the terrestrial planets,' Nature, 2005, 435(7041), pp. 466–469.

Gronoff, G., Maggiolo, R., Cessateur, G., Moore, W. B., Airapetian, V., De Keyser, J., Dhooghe, F., Gibbons, A., Gunell, H., Mertens, C. J., Rubin, M., Hosseini, S., 'The Effect of Cosmic Rays on Cometary Nuclei. I. Dose Deposition,' ApJ, 2020, 890, 1, P. 89.

Harker, D. E., Woodward, C. E., and Wooden, D. H., 'The dust grains from 9P/Tempel 1 before and after the encounter with Deep Impact,' Science, 2005, 310(5746), pp. 278–280.

Hässig, M., Altwegg, K., Balsiger, H., Bar-Nun, A., Berthelier, J. J., Bochsler, P., Briois, C., Calmonte, U., Combi, M., De Keyser, J., Eberhardt, P., Fiethe, B., Fuselier, S. A., Galand, M., Gasc, S., Gombosi, T. I., Hansen, K. C., Jäckel, A., Keller, H. U., Kopp, E., Korth, A., Kührt, E., Le Roy, L., Mall, U., Marty, B., Mousis, O., Neefs, E., Owen, T., Rème, H., Rubin, M., Sémon, T., Tornow, C., Tzou, C.- Y., Waite, J. H., and Wurz, P., 'Tie variability and heterogeneity in the coma of 67P/Churyumov-Gerasimenko,' Science, 2015, 347(6220), p. aaa0276.

Kelley, M. S. P., Woodward, C. E., Bodewits, D., Farnham, T. L., Gudipat, M. S., Harker, D. E., Hines, D. C., Knight, M.W., Kolokolova, L., Li, A., de Pater, I., Protopapa, S., Russel, R. W., Sitko, M. L., and Wooden, D. H., 'Cometary science with the James Webb Space Telescope,' Publications of the Astronomical Society of the Pacific, 2016, 128(959), p. 018009.

Le Roy, L., Altwegg, K., Balsiger, H., Berthelier, J.-J., Bieler, A., Briois, C., Calmonte, U., Combi, M. R., De Keyser, J., Dhooghe, F., Fiethe, B., Fuselier, S. A., Gasc, S., Gombosi, T. I., Hässig, M., Jäckel, A., Rubin, M., and Tzou, C.-Y., 'Inventory of the volatiles on comet 67P/Churyumov-Gerasimenko from Rosetta/ROSINA,' Astronomy & Astrophysics, 2015, 583, p. A1.

Levison, H. F., Morbidelli, A., Tsiganis, K., Nesvorny, D., and Gomes, R., 'Late orbital instabilities in the outer planets induced by interaction with a self-gravitating planetesimal disk,' The Astronomical Journal, 2011, 142(5), p. 152.

Lippi, M., Villanueva, G. L., DiSanti, M. A., Böhnhardt, H., Mumma, M. J., Bonev, B. P., and Prialnik, D., 'A new model for the ν_1 vibrational band of HCN in cometary comae, with application to three comets,' Astronomy & Astrophysics, 2013, 551, p. A51.

Luspay-Kuti, A., Hässig, M., Fuselier, S. A., Mandt, K. E., Altwegg, K., Balsiger, H., Gasc, S., Jäckel, A., Le Roy, L., Rubin, M., Tzou, C. Y., Wurz, P., Mousis, O., Dhooghe, F., Berthelier, J. J., Fiethe, B., Gombosi, T. I., and Mall, U., 'Composition-dependent outgassing of comet 67P/Churyumov-Gerasimenko from ROSINA/DFMS. Implications for nucleus heterogeneity?' Astronomy &Astrophysics, 2015, 583, p. A4.

Magee-Sauer, K., Mumma, M. J., DiSanti, M. A., and Dello Russo, N., 'Hydrogen cyanide in comet C/1996 B2 Hytakutake,' Journal of Geophysical Research (Planets), 2002b, 107(E11), p. 5096.

Magee-Sauer, K., Mumma, M. J., DiSanti, M. A., Dello Russo, N., Gibb, E. L., Bonev, B. P., and Villanueva, G. L., 'The organic composition of comet C/2002 A2 (LINEAR). i. evidence for an unusual organic chemistry,' Icarus, 2008, 194(1), pp. 347–356.

Magee-Sauer, K., Mumma, M. J., DiSanti, M. A., Dello Russo, N., and Rettig, T. W., 'Infrared spectroscopy of the v3 band of hydrogen cyanide in comet C/1995 O1 Hale-Bopp,' Icarus, 1999, 142(2), pp. 498–508.

McKay, A. J., Cochran, A. L., DiSanti, M. A., Villanueva, G., Dello Russo, N., Vervack, R. J. J., Morgenthaler, J. P., Harris, W. M., and Chanover, N. J., 'Evolution of H_2O, CO, and CO_2 production in comet C/2009 P1 Garradd during the 2011-2012 apparition,' Icarus, 2015, 250, pp. 504–515.

McKay, A. J., DiSant, M. A., Cochran, A. L., Bonev, B. P., Dello Russo, N., Vervack, R. J., Jr. Gibb, E., Roth, N. X., Saki, M., Khan, Y., Kawakita, H., 'Quantifying the Hypervolatile Abundances in Jupiter-family Comet 46P/Wirtanen,' The Planetary Science Journal, 2021, 2, P. 21.

Morbidelli, A., Levison, H. F., Tsiganis, K., and Gomes, R., 'Chaotic capture of Jupiter's Trojan asteroids in the early solar system,' Nature, 2005, 435(7041), pp. 462–465.

Mumma, M. J. and Charnley, S. B., 'The chemical composition of comets – emerging taxonomies and natal heritage,' Annual Review of Astronomy and Astrophysics, 2011, 49(1), pp. 471–524.

Mumma, M. J., DiSanti, M. A., Dello Russo, N., Fomenkova, M., Magee-Sauer, K., Kaminski, C. D., and Xie, D. X., 'Detection of abundant ethane and methane, along with carbon monoxide and water, in comet C/1996 B2 Hyakutake: Evidence for interstellar origin,' Science, 1996, 272(5266), pp. 1310–1314.

Mumma, M. J., DiSanti, M. A., Dello Russo, N., Magee-Sauer, K., Gibb, E., and Novak, R., 'Remote infrared observations of parent volatiles in comets: A window on the early solar system,' Advances in Space Research, 2003, 31(12), pp. 2563–2575.

Mumma, M. J., Weaver, H. A., Larson, H. P., Davis, D. S., andWilliams, M., 'Detection of water vapor in Halley's comet,' Science, 1986, 232, pp. 1523–1528.

Mumma, M. J., McLean, I. S., DiSanti, M. A., Larkin, J. E., Dello Russo, N., Magee-Sauer, K., Becklin, E. E., Bida, T., Chaffee, F., Conrad, A. R., Figer, D. F., Gilbert, A. M., Graham, J. R., Levenson, N. A., Novak, R. E., Reuter, D. C., Teplitz, H. I., Wilcox, M. K., and Xu, L. H., 'A survey of organic volatile species in comet C/1999 H1 (Lee) using NIRSPEC at the Keck Observatory,' The Astrophysical Journal, 2001, 546 (1183).

Paganini, L., Mumma, M. J., Boenhardt, H., DiSanti, M. A., Villanueva, G. L., Bonev, B. P., Lippi, M., Käufl, H. U., and Blake, G. A., 'Ground-based infrared detections of CO in the Centaur-comet 29P/Schwassmann-Wachmann 1 at 6.26 au from the Sun,' The Astrophysical Journal, 2013, 766(2), p. 100.

Radeva, Y. L., Mumma, M. J., Bonev, B. P., DiSanti, M. A., Villanueva, G. L., Magee-Sauer, K., Gibb, E. L., and Weaver, H. A., 'The organic composition of comet C/2000 WM1 (LINEAR) revealed through infrared spectroscopy,' Icarus, 2010, 206 (2), pp. 764–777.

Radeva, Y. L., Mumma, M. J., Villanueva, G. L., Bonev, B. P., DiSanti, M. A., A'Hearn, M. F., and Dello Russo, N., 'High-resolution infrared spectroscopic measurements of comet 2P/Encke: Unusual organic composition and low rotational temperatures,' Icarus, 2013, 223(1), pp. 298–307.

Rayner, J., Bond, T., Bonnet, M., Jaffe, D., Muller, G., and Tokunaga, A., 'iSHELL: a 1-5 micron cross-dispered R=70,000 immersion grating spectrograph for IRTF,' Proceedings of the SPIE, 2012, 8446, p. 84462C.

Rayner, J., Tokunaga, A., Jaffe, D., Bonnet, M., Ching, G., Connelley, M., Kokubun, D., Lockhart, C., and Warmbier, E., 'iSHELL: a construction, assembly and testing,' Proceedings of the SPIE, 2016, 9908, p. 990884.

Rickman, H., Marchi, S., A'Hearn, M. F., Barbieri, C., El-Maarry, M. R., Guttler, C., Ip, W. H., Keller, H. U., and Lamy, P., Marzari, F., Massironi, M., Naletto, G., Pajola, M., Sierks, H., Koschny, D., Rodrigo, R., Barucci, M. A., Bertaux, J. L., Bertini, I., Cremonese, G., Da Deppo, V., Debei, S., De Cecco, M., Fornasier, S., Fulle, M., Groussin, O., Gutierrez, P. J., Hviid, S. F., Jorda, L., Knollenberg, J., Kramm, J. R., Kuhrt, E., Kuppers, M., Lara, L. M., Lazzarin, M., Lopez Moreno, J. J., Michalik, H., Sabau, L., Thomas, N., Vincent, J. B., Wenzel, K. P., ' Comet 67P/Churyumov-Gerasimenko: Constraints on its origin from OSIRIS observations, AAP, 2015, 583, PP. A44.

Roth, N. X., Gibb, E. L., Bonev, B. P., DiSanti, M. A., Dello Russo, N., McKay, A. J., Vervack, J., Ronald J., Kawakita, H., Saki, M., Biver, N., Bockelée-Morvan, D., Feaga, L. M., Fougere, N., Cochran, A. L., Combi, M., and Shou, Y., 'Probing the evolutionary history of comets: An investigation of the hypervolatiles CO, CH_4, and C_2H_6 in the Jupiter-family comet 21P/Giacobini-Zinner,' The Astronomical Journal, 2020, 159, p. 42.

Roth, N. X., Gibb, E. L., Bonev, B. P., DiSanti, M. A., Dello Russo, N., Vervack, R. J. J., McKay, A. J., and Kawakita, H., 'A tale of "two" comets: The primary volatile composition of comet 2P/Encke across apparitions and implications for cometary science,' The Astronomical Journal, 2018, 156, p. 251.

Saki, M., Gibb, E. L., Bonev, B. P., Roth, N. X., DiSanti, M. A., Dello Russo, N., Vervack, R. J. J., McKay, A. J., and Kawakita, H., 'Carbonyl Sulfide (OCS): Detections in Comets C/2002 T7 (LINEAR), C/2015 ER61 (PanSTARRS), and 21P/Giacobini-Zinner and Stringent Upper Limits in 46P/Wirtanen,' The Astronomical Journal, 2020a, 160(4), p. 184.

Saki, M., Gibb, E., Bonev, B., Roth, N., DiSanti, M., Dello Russo, N., Vervack, R., McKay, A., Khan, Y., Kawakita, H., 'An Investigation of the Abundances of Hypervolatiles CO, CH_4, and C_2H_6 in Jupiter-family Comet 46P/Wirtanen,' AAS/Division for Planetary Sciences Meeting Abstracts, 2020b, 52, P. 212.04.

Saki, M., Gibb, E., Bonev, B., Roth, N., DiSanti, M., Khan, Y., Dello Russo, N., Vervack, R., McKay, Kawakita, H., 'An Investigation of the Abundances of Hypervolatiles CO, CH_4, and C_2H_6 in Jupiter-family Comet 46P/Wirtanen,' Astronomical Journal, 2021, in pres.

Saki, M., Gibb, E., Bonev, B., Roth, N., DiSanti, M., Khan, Y., Dello Russo, N., Vervack, R., McKay, Kawakita, H., 'Chemical Compostion of Long-period Oort cloud comet C/2002 T7 (LINEAR),' in preparation for the Astronomical Journal.

Schleicher, D. and Bair, A., Asteroids, Comets, Meteors, Book of Abstracts, chapter Chemical and physical properties of comets in the Lowell database: Results from 35 years of narrow-band photometry, p. 475, University of Helsinki, 2014.

Stern, S. A., 'The evolution of comets in the Oort cloud and Kuiper belt,' Nature, 2003, 424(6949), pp. 639–642.

Villanueva, G. L., DiSanti, M. A., Mumma, M. J., and Xu, L. H., 'A quantum band model of the ν_1 fundamental of methanol (CH_3OH) and its application to fluorescence spectra of comets,' The Astrophysical Journal, 2012a, 747(1), p. 3.

Villanueva, G. L., Magee-Sauer, K., and Mumma, M. J., 'Modeling of nitrogen compounds in cometary atmospheres: Fluorescence models of ammonia (NH_3), hydrogen cyanide (HCN), hydrogen isocyanide (HNC) and cyanoacetylene (HC_3N),' Journal of Quantitative Spectroscopy and Radiative Transfer, 2013, 129, pp. 158–168.

Villanueva, G. L., Mumma, M. J., Bonev, B. P., DiSanti, M. A., Gibb, E. L., Boehnhardt, H., and Lippi, M., 'A sensitive search for deuterated water in comet 8P/Tuttle,' The Astrophysical Journal Letters, 2009, 690(1), pp. L5–L9.

Villanueva, G. L., Mumma, M. J., Bonev, B. P., Novak, R. E., Barber, R. J., and DiSanti, M. A., 'Water in planetary and cometary atmospheres: H_2O/HDO transmittance and fluorescence models,' Journal of Quantitative Spectroscopy and Radiative Transfer, 2012b, 113(3), pp. 202–220.

Villanueva, G. L., Mumma, M. J., DiSanti, M. A., Bonev, B. P., Gibb, E. L., Magee-Sauer, K., Blake, G. A., and Salyk, C., 'The molecular composition of comet C/2007 W1 (Boattini): Evidence of a peculiar outgassing and a rich history,' Icarus, 2011a, 216(1), pp. 227–240.

Villanueva, G. L., Mumma, M. J., and Magee-Sauer, K., 'Ethane in planetary and cometary atmospheres: Transmittance and fluorescence models of the ν_7 band at 3.3 um,' Journal of Geophysical Research, 2011b, 116(E8), p. E08012.

Villanueva, G. L., Mumma, M. J., Novak, R. E., and Hewagama, T., 'Identification of a new band system of isotopic CO_2 near 3.3 um: Implications for remote sensing of biomarker gases on Mars,' Icarus, 2008, 195(1), pp. 34–44.

Villanueva, G. L., Bonev, B. P., Mumma, M. J., Magee-Sauer, K., DiSanti, M. A., Salyk, C., and Geoffrey, A., 'The volatile composition of the split ecliptic comet 73P/Schwassmann-Wachmann 3: A comparison of fragments C and B,' The Astrophysical Journal, 2006, 650(1), pp. L87–L90.

Zolensky, M. E., Zega, T. J., Yano, H., Wirick, S., Westphal, A. J., Weisberg, M. K., Weber, I., Warren, J. L., Velbel, M. A., Tsuchiyama, A., Tsou, P., Toppani, A., Tomioka, N., Tomeoka, K., Teslich, N., Taheri, M., Susini, J., Stroud, R., Stephan, T., Stadermann, F. J., Snead, C. J., Simon, S. B., Simionovici, A., See, T. H., Robert, F., Rietme.er, F. J. M., Rao, W., Perronnet, M. C., Papanastassiou, D. A., Okudaira, K., Ohsumi, K., Ohnishi, I., Nakamura-Messenger, K., Nakamura, T., Mostefaoui, S., mikouchi, T., Meibom, A., Matrajt, G., Marcus, M. A., Leroux, H., Lemelle, L., Le, L., Lanzirotti, A., Langenhort, F., Krot, A. N., Keller, L. P., Kearsey, A. T., Joswiak, D., Jacob, D., Ishii, H., Harvey, R., Hagiya, K., Grossman, L., Grossman, J. N., Graham, g. A., Gounelle, M., Gillet, P., Genge, M. J., Flynn, G., Ferroir, T., Fallon, F., Ebel, D. S., Dai, Z. R., Cordier, P., Clark, B., Chi, M., Butterworth, A. L., Brownlee, D. E., Bridges, J. C., Brennan, S., Brearley, A., Bradley, J. P., Bleuet, P., Bland, P. A., and Bastien, R., 'Mineralogy and petrology of comet 81P/Wild 2 nucleus samples,' Science, 2006, 314(5806), p. 1735.

VITA

Mohammad Saki was born in Kermanshah, Iran. He received his B.S. in Physics from Kharazmi Unversity in 2011. He went on to receive his M.S. in Computational Physics at the AmirKabir University of Technology (Tehran Polytechnic) in 2014. He received his second M.S. in Astrophysics from the University of Missouri–St. Louis in 2017. He received his Doctor of Philosophy in Physics from the Missouri University of Science and Technology and the University of Missouri–St. Louis in August 2021.